TECHNISCHE UNIVERSITÄT WIEN
Vienna | Austria

Diploma Thesis

Influence of Passive Tip-Injection on the Excitation Forces in Axial Turbines with Shrouded Blades

carried out for the purpose of obtaining the degree of
Master of Science (MSc or Dipl.-Ing. or DI)
submitted at Technische Universität Wien
Faculty of Mechanical and Industrial Engineering

by

Lukas KRISMER

Mat.Nr.: 0926915
Dr. Ambros Giner Weg 5a, 6065 Thaur, Austria

under the supervision of
Ao.Univ.Prof. Dipl.-Ing. Dr.techn. Reinhard Willinger
and
Dipl.-Ing. Dr.techn. Pouya Ghaffari, BSc

Institute for Energy Systems and Thermodynamics

October, 2017

Affidavit

I declare in lieu of oath, that I wrote this thesis and performed the associated research myself, using only literature cited in this volume. If text passages from sources are used literally, they are marked as such.

I confirm that this work is original and has not been submitted elsewhere for any examination, nor is it currently under consideration for a thesis elsewhere.

Vienna, Month, Year

Signature

Abstract

In turbomachinery the leakage of mass flow through the clearance between the rotor blade tips and the casing is one of the main sources of loss. In order to reduce this form of loss, the flow resistance of the blade tip clearance can be increased geometrically by winglets, squealers and shrouds or aerodynamically by a fluidic jet barrier. At the department of Fluid-Flow Machinery of the Institute for Energy Systems and Thermodynamics at the Technische Universität Wien passive tip-injection has been presented as a method of increasing the flow resistance of blade tip clearances in turbomachinery. This method extracts mass flow at the rotor blade leading edge which is then guided through the blade and injected into the blade tip clearance. Research shows, that passive tip-injection has the potential of significantly reducing the tip-leakage mass flow and improving the mixing conditions of the leakage mass flow with the main flow considerably.

The term tip excitation labels aerodynamically induced cross forces acting on the rotor of turbomachinery depending on the tip-leakage mass flow. These forces have the potential of inducing an instable whirling motion of the rotor above a limiting power level of the turbomachine, which renders further operation impossible. Two effects are known to be the main reasons of tip excitation in turbomachinery: The variable tip-leakage mass flow of an eccentric rotor leading to a variation in tangential forces on the rotor blades and the pressure variation in the tip gap of an eccentric rotor under swirled flow conditions. Both result in a cross force perpendicular to the direction of displacement of the rotor.

This thesis investigates the influence of passive tip-injection on the tip excitation in shrouded axial turbine stages. Therefore an analytical model for the tip-leakage mass flow and the pressure in the tip gap of a shrouded turbine rotor with passive tip-injection under swirled flow conditions is developed and evaluated numerically. Subsequently the resulting cross forces on the rotor are calculated. It is shown, that passive tip-injection has the potential of decreasing the tip excitation cross forces by reducing the tip-leakage mass flow and positively influencing the flow angles and the pressure distributions in the tip clearance.

Keywords: tip-leakage, fluidic jet barriers, passive tip-injection, tip excitation, rotordynamic instability in turbomachinery

Contents

Nomenclature

Latin Symbols

A	cross-sectional or surface area	[m^2]
A'	surface of the labyrinth fin sidewall	[m^2]
$C^{\times}_{AM}$	discharge coefficient for angular momentum	[-]
$C^{\times}_{E}$	relative inlet kinetic energy	[-]
c	mainstream flow velocity	[m/s]
D	damping force	[N]
d	diameter	[m]
d	external damping	[Ns/m]
e	eccentricity of the rotor	[m]
F_s	tangential blade force	[N]
f_L	shroud geometry control parameter	[-]
f_r	rotational frequency of the rotor	[1/s]
g	correction factor for stage efficiency	[-]
h	fin height	[m]
j	imaginary unit / number of support points in circumferential direction	[-]
L	channel length	[m]
l	streamtube length between subsequent support points	[m]
$M^{\times}$	dimensionless mass flow rate	[-]
$\dot{m}$	mass flow rate	[kg/s]
m	mass of lumped rotor	[kg]
m_N	Neumann constant	[-]
n	number of support points in axial direction	[-]
$P^{\times}$	dimensionless pressure force on the rotor surface	[-]
P	pressure force on the control volume side walls	[N]
p	pressure	[N/m^2]
p'	pressure on the labyrinth fin sidewall	[N/m^2]
Q	cross force	[N]
q	cross force coefficient	[N/m]
Re	Reynolds number	[-]
R	friction force	[N]
R_m	mean blade radius	[m]
r	radius	[m]
$\tilde{s}$	local radial clearance width	[m]
s	nominal radial clearance width	[m]

s	rotor shaft rigidity	[N/m]
T	characteristic angular momentum (torque)	[Nm]
t	distance between labyrinth fins	[m]
v	rotor displacement in lateral direction	[m]
w	rotor displacement in vertical direction	[m]
w	tip gap flow velocity	[m/s]

Greek Symbols

α	flow angle	[°]
γ	dimensionless injection channel diameter	[-]
$\Delta\varphi$	circumferential streamtube width	[°]
Δa	axial distance between support points	[m]
ΔH	total enthalpy drop of the stage	[J/kg]
δ	inclination angle	[°]
ζ	loss coefficient	[-]
η	efficiency	[-]
λ	eigenvalue of the characteristic equation	[rad/s]
μ	contraction coefficient	[-]
ν	kinematic viscosity	[m^2/s]
ξ	pressure loss coefficient	[-]
$\bar{\xi}$	momentum loss coefficient	[-]
ρ	fluid density	[kg/m^3]
φ	position in circumferential direction	[°]
Ω	angular velocity of the rotor rotation	[rad/s]
ω_{eig}	critical angular velocity of the rotor rotation	[rad/s]
ω_s	angular velocity of the rotor oscillation	[rad/s]

Vectors and Tensors

$\mathbf{D}$	damping tensor	[Ns/m]
$\mathbf{F_{tl}}$	tip excitation force	[N]
$\mathbf{\Lambda}$	tensor for characteristic equation	[rad/s^2]
$\mathbf{M}$	inertia tensor	[kg]
$\mathbf{S}$	stiffness tensor	[N/m]
$\mathbf{u}$	rotor displacement	[m]

Subscripts

A	tip gap exit
a	axial
B	theoretic maximum
C	relative to mainstream flow velocity c

Ch	labyrinth chamber
cl	tip clearance
E	tip gap entry
H	hydraulic
I	control volume inlet
II	control volume outlet
i	support point position in axial direction
id	ideal
inj	injection
k	support point position in circumferential direction
lim	limit
m	mean
max	maximum
n	normal/axial component
p	pressure force
R	friction force
s	blade force or Thomas-Alford force
$surf$	surface
t	total / turbulent
u	circumferential
v	pressure loss
W	relative to tip gap flow velocity w
0	main flow
$1, 2\,(x, y)$	component in direction 1,2 (x, y)
$\times$	relative to the theoretical maximum

Abbreviations

CFD	computational fluid dynamics
M.I.T.	Massachusetts Institute of Technology

1 Introduction

1.1 Motivation

With shortening natural resources and rising environmental concerns, the research in the field of fluid-flow machinery is continually striving to increase efficiency and reduce fuel consumption as well as green house gas emissions of turbomachinery. Turbomachines play a highly important role in current power generation in stationary power plants as well as in transportation and here especially in the propulsion of commercial aircrafts, which underlines the significance of these efforts. Two ways to reduce fuel consumption especially of aircraft engines are to reduce weight and to increase thermodynamic efficiency of the turbomachines. To increase the efficiency of a turbomachine, it is necessary to reduce its internal and external losses. Internal losses in turbomachinery are commonly clustered in profile loss, endwall loss and leakage loss. Although it is known today, that they are seldom completely independent. This work focuses on a method to reduce the leakage loss. Leakage loss accounts for the leakage flow over the tips of rotor blades and the hub clearances of stator blades and can make up approximately 30% of the total losses in turbomachinery.

At the department of Fluid-Flow Machinery of the Institute for Energy Systems and Thermodynamics at Technische Universität Wien fluidic jet barriers as a means of tip-leakage reduction have been studied for some time. Especially the method of passive tip-injection has been discussed at the department in detail. This method uses a mass flow extracted from the stage mass flow, which is injected into the tip gap cavity of a turbine blade row to increase its aerodynamic resistance. It is shown that this method has the potential of reducing the tip-leakage flow. Investigations have been carried out for shrouded and unshrouded turbine blades. In this work the focus lies on passive tip-injection for a shrouded turbine rotor.

One way to decrease weight of aircraft engines in order to reduce fuel consumption is to increase the power-density. This requires higher blade loading and rotational speeds of the turbomachinery components and could potentially allow a reduction of low pressure turbine stages especially in geared turbo fan engines. However this increase in power-density poses higher demands towards the operational safety and rotordynamic stability of the turbomachine.

In turbomachinery aerodynamically induced cross forces on the rotor have been described that can lead to rotordynamic instability above a limit power-output level. While increased external

damping and rigidity of the rotor shaft and bearings could reduce the magnitude rotor oscillation, the instability could not be eliminated. The generation of those aerodynamically induced cross forces shall be the focus of this thesis. It could be shown in earlier work, that instability, due to excitation forces on the rotor, occurs at a limit power rather than at a limit rotational speed of the rotor. Two cross force generating effects could be identified. One generating effect is the variation in stage efficiency, due to a variable leakage flow in circumferential direction of an eccentric rotor. This results in variable tangential blade forces in circumferential direction of a blade row and unbalanced torque. The resulting cross force acts perpendicular to the direction of displacement of the rotor and can cause an increasing whirling motion of the rotor. This whirling motion renders any operation impossible above a certain power level. The second effect is the variable pressure distribution in circumferential direction of the tip gap cavity for an eccentric rotor under swirled flow conditions. This pressure variation also leads to a cross force acting perpendicular to the direction of displacement of the rotor and a further destabilization of the oscillations of the rotor.

1.2 Scope and Outline of Thesis

It is the scope of this work to investigate the influence of passive tip-injection on the aerodynamically induced cross forces on the rotor analytically. It is the aim to elaborate if the influence of passive tip-injection on the rotordynamics of turbomachinery is to be taken into consideration for further numerical and experimental investigations. Earlier work [9–11] has shown, that passive tip-injection has the potential of reducing the overall tip-leakage mass flow and positively influencing the flow field downstream of the turbine stage by an increased turning of the tip-leakage flow. The overall tip-leakage mass flow and the flow direction in the tip gap are both of fundamental importance for the generation of tip excitation forces [1,23,27]. It is the aim of this thesis to establish if the positive impact of passive tip-injection on the overall tip-leakage reduction and the flow turning in the tip gap also has an advantageous effect on the reduction of tip excitation force generation. Therefore in the first part of this work (Ch. 2), the available literature on both fluidic jet barriers and especially passive tip-injection and on tip excitation forces in turbomachinery is reviewed. Subsequently in Ch. 3, an existing model describing the swirled flow through the tip gap of an eccentric rotor is modified as to include passive tip-injection into the tip gap cavity. The obtained model is applied to several exemplary turbine geometries and evaluated numerically. The obtained values for the pressure distribution in the tip gap as well as for the leakage mass flow and flow angles are used to calculate the resulting cross forces described above. The cross force generation for a turbine with passive tip-injection is compared with the cross force generation of the same turbine without passive tip-injection in order to evaluate the impact of the injection (Ch. 4). Finally in Ch. 5 the results are interpreted, the limitations of the developed model discussed and fields of further research on the topic suggested.

2 Literature Overview

In this chapter the available literature and previous work done on passive tip-injection as well as on tip excitation in axial turbine stages is presented. First the state of research on passive tip-injection and fluidic jet barriers in general is shown. Subsequently the available literature concerning tip excitation and flow induced cross forces on axial turbine blade rows is presented. Lastly the work done on the influence of passive tip-injection on the tip excitation is shown and its significance for this work is discussed.

2.1 Fluidic Jet Barriers

Tip-leakage over the blade tips in axial turbines and compressors is one of the three main loss mechanisms in turbomachinery and reduces the efficiency (see [6]). A reduction of those losses can be achieved by a number of different methods. It is possible to decrease the tip-leakage mass flow by increasing the flow resistance of the tip gap geometrically. Such geometrical modifications include squealers, winglets, shrouded blades, etc. which are described in great detail in common literature (see [24] for example).

Another method to decrease the tip-leakage is to increase the flow resistance aerodynamically in the form of fluidic jets injected into the tip clearance. Those jets are intended to block or disturb the tip-leakage flow and can be supplied externally or internally.
Several works have been published and patents granted for applications using an injection mass flow into the tip clearance of rotor blades of turbomachines in order to improve the sealing effect. Some of those publications, which are relevant for this work are presented in this section.

Auyer [3] was granted a patent for a fluidic sealing arrangement. It uses a fluidic jet from an external source (i.e. the compressor), which is injected through the casing into the tip clearance of an unshrouded turbine blade row. The injection slot is inclined against the main flow orientation by at least 45°. In the patent it is claimed that the arrangement minimizes leakage over the blade tips. It is further claimed, that the injection mass flow has an advantageous cooling effect on the casing.

A comprehensive analytical, experimental and computational investigation of the impact of an active injection on the tip-leakage flow over a shrouded turbine rotor is performed by Curtis et al. [5]. For a single stage low speed intermediate pressure air turbine a continuous circumfer-

ential injection nozzle in the casing, which is inclined by 45° against the leakage flow direction, is considered. The analytical investigation is performed in two ways. Firstly, it is considering that the over-shroud pressure gradient balances the momentum change of the leakage mass flow under influence of the injection mass flow. Secondly, the streamline curvature of the injection jet is considered. It could be shown that increasing the amount of injection mass flow decreases the leakage mass flow entering the tip gap by a similar amount. Thus the overall leakage flow reentering the mainstream flow after the shroud remains relatively constant at approximately 5 % of the mainstream mass flow. Further it could be shown, that the air curtain provided by an injection mass flow of approximately 3.5 % of the mainstream flow is able to perfectly seal the over-shroud leakage path. This leads to a decrease of 0.6 % in turbine efficiency though, due to the work the injection mass flow could ideally perform if not used for the sealing air curtain. A maximum increase in turbine efficiency of 0.4 % can be achieved for an injection mass flow of 1.2 %. In that sense it is stated, that the tip-injection method can yield substantial improvements in turbine efficiency if mass flows are used for the injection which are already accounted for in loss considerations (for example cooling flows).

Hogg et al. [15] investigate two different setups of active injection into the tip gap of a shrouded turbine numerically. It is stated that the increase in turbine efficiency due to improved sealing conditions provided by the injection, must be greater than the losses in turbine efficiency due to the extraction of the injection mass flow from the mainstream. First computations are carried out for a smooth clearance with the injection channel oriented perpendicular to the leakage flow direction. The numerical results are validated against an analytical model obtained from conservation equations for mass, momentum and energy for a compressible flow. It is shown, that injection with no inclination against the leakage flow has only limited potential of reducing the overall leakage mass flow and thus increasing the turbine efficiency. For the smooth clearance even an inclined injection channel shows no considerable improvement of the sealing capabilities. In the second part of their work Hogg et al. investigate a see-through labyrinth seal with three fins. Following the proposals of Turnquist et al. [26] the middle fin is inclined by 45° against the leakage flow direction and acts as a guiding nozzle for the injection mass flow. It is shown that the guided, inclined injection into a labyrinth seal has much greater potential of increasing the sealing capability of the seal. In the last part of the paper a method for harvesting the swirl kinetic energy of the main flow is presented. This is intended to provide the pressure gradients needed for the injection into the labyrinth chamber, although not much detail is given on the concept.

In [2] Auld et al. investigate active injection into the tip gap of a shrouded, small, high-speed, single stage axial turbine numerically. The parameters injection jet width, injection pressure ratio, injection inclination angle and axial position of the injection slot are varied in order to find the optimum in terms of turbine power output increase for the given turbine geometry. The overall leakage flow reduction, but also the influence of the injection on the shear forces

acting between the leakage and injection flow and turbine rotor are considered. It is stated that a pressure drop exists, that turns the momentum of the injection flow, which is oriented against the leakage flow into the direction of the main leakage flow. It is further stated that this pressure drop reduces the pressure gradient between the tip gap inlet and the injection position and thereby reduces the overall tip-leakage mass flow. It is shown that the fluidic seal has the potential of significantly improving the turbine efficiency. It is concluded, that for a maximum increase in turbine efficiency: The injection jet width has to be as narrow as possible in order to gain a high injection velocity for a constant injection mass flow. The injection jet has to be inclined against the leakage main flow direction. The injection position has to be positioned close to the tip gap outlet in order to reduce negative shear forces and improve mixing conditions of the leakage flow with the main flow downstream of the shroud.

Turnquist et al. [26] patented a variety of fluidic seal geometries, reducing the leakage flow by injecting a mass flow into the sealing gap. The patent covers both active injection where the necessary pressure gradient for the injection is provided externally and passive injection where the pressure gradient is obtained by connecting two sections in the turbomachinery with different pressure levels by an injection channel. The patent focuses on injection applications, where the injection channel leads through the casing into the sealing gap. Seal gaps with inclined and straight fins are considered as well as smooth clearances. In the patent it is claimed, that the injection mass flow is capable of disrupting and reducing the leakage flow through the seal.

Passive Tip-Injection

For some time passive tip-injection for uncooled turbine blades has been researched at the Technische Universität Wien. In contrast to other fluidic sealing applications, for passive tip-injection the pressure gradient necessary for driving an injection mass flow into a sealing gap is provided internally. Therefore the extraction point for the injection mass flow is located in the stagnation point at the turbine blade leading edge. The extraction point is chosen close to the turbine blade tip for loss reasons. The injection mass flow is guided through the injection channel from the blade leading edge, through the blade into the tip clearance between the rotor blade and the casing. Applications for unshrouded and shrouded turbine blades are covered and will be presented briefly.

Unshrouded Turbine Blades

In unshrouded axial turbines the tip-leakage flow is driven by the pressure difference between the pressure and suction surfaces of the blades. It enters the tip gap over the pressure side of the blade and passes over the blade tip towards the suction surface side of the blade where it mixes with the mainstream flow. Due to the velocity differences between the tip-leakage mass flow and the mainstream flow in both magnitude and direction a vortex is formed at their interface which moves downstream along the suction surface of the blade (see [6]). This causes entropy gener-

ation, which reduces the efficiency of the turbomachine. Passive tip-injection for unshrouded turbine blades aims at reducing this tip-leakage mass flow and the entropy generation associated with it.

In [13] Hamik presents analytical and simple 2D numerical investigations of a passive tip-injection application for an unshrouded turbine rotor. In this work the injection parameters are varied and the performance potential of passive tip-injection is shown. Substantial efficiency improvements are shown to be possible for specific injection parameters. The analytical and numerical work is followed up by more detailed simulations and experimental investigations on a linear cascade wind tunnel by Hamik in [14]. It is shown that passive tip-injection decreases the strength of the tip-leakage vortex as well as the under- and overturning of the flow next to the endwall. Additionally a reduction of the losses associated with the tip-leakage vortex through passive tip-injection could be shown.

In the second part of [8] Ghaffari presents a more detailed 2D numerical analysis of the setup described in [14]. Here the model also includes the injection channel leading from the extraction point at the blade leading edge to the tip gap. Different inclination angles and injection slot widths are examined and a reduction of the tip-leakage mass flow through passive tip-injection can be shown. Benoni [4] performs experimental investigations and an extensive 3D CFD simulation of the passive tip-injection model presented in [14]. It could be shown, that an inclined injection channel towards the pressure side of the turbine blade leads to a reduced leakage mass flow over the blade tip. The 3D CFD simulations could show that the passive tip-injection disrupts the forming of the characteristic tip-leakage vortex.

Shrouded Turbine Blades

As mentioned before it is possible to increase the flow resistance of tip gaps with aid of geometrical modifications of the blade tip. Here the use of shrouded turbine blades is considered. The shrouds can be equipped with circumferential fins, to form a labyrinth seal or have a smooth surface. For shrouded blades the driving pressure difference for the leakage mass flow is the pressure drop between the tip gap inlet and outlet. Literature on the combination of a shroud, which increases the flow resistance mechanically with methods which do so aerodynamically (i.e. tip-injection) is presented in this section.

Ghaffari [9] investigates such a combination of blade tip shroud and passive tip-injection. With a focus on aircraft engines with geared turbofans and aerodynamically highly loaded low pressure turbines operating at high rotational speed, relevant characteristic parameters are estimated. Those parameters are the basis for following analytical considerations and 2D CFD simulations. Different setups of turbine blade shrouds with fins are considered. The injection channel is in-

clined against the main tip gap flow direction and the injection position is varied from upstream of the first fin to positions between two fins. Investigations are also carried out for applications where the injection slot is located directly at the upstream edge of a fin and the injection mass flow is guided by the fin into the tip gap.
To characterize the effectiveness of the passive tip-injection a discharge coefficient is defined. It represents the ratio of the actual tip gap mass flow rate to its highest possible value. As the injection mass flow is extracted from the main flow it is added to the actual tip gap mass flow rate in those considerations. CFD simulations could show that flow separation occurs in the injection channel directly before the injection mass flow enters the tip clearance. This leads to an injection channel barricade, reducing the effective injection channel diameter. The flow separation also leads to a deflection of the injection mass flow in direction of the tip gap main flow direction. Both effects reduce the effectiveness of the passive tip-injection in terms of its tip-leakage reduction. It could be shown that the flow separation is minimized for applications with guided injection along the fin. It is concluded that a guided injection upstream of the first fin has the highest potential of reducing the overall tip-leakage mass flow.

In [11] Ghaffari et al. present the results of a 3D CFD simulation of an uncooled low pressure turbine stage with shrouded blades with passive tip-injection. Experimental data from a machine without tip-injection serve as boundary conditions for the simulation. The results are evaluated considering that any gain in turbine stage efficiency through a reduced tip-leakage mass flow has to be corrected by the losses due to changes in the profile pressure distribution in the vicinity of the injection mass flow extraction point at the blade leading edge. For the investigation a guided injection along the first fin on the turbine shroud is considered. It is shown that passive tip-injection has the potential of decreasing the mass flow entering the tip gap while the overall tip-leakage mass flow remains almost constant. It is reasoned that the injection mass flow contributes to the specific work of the stage and therefore increases the stage efficiency. As another beneficiary effect of passive tip-injection, its considerable influence on the flow conditions downstream of the stage could be identified.

In [10] Ghaffari investigates the impact of passive tip-injection on the low pressure turbine used in [11] experimentally and performs further 3D CFD simulations with special consideration of the downstream flow field in the tip section of the turbine stage. It is stated, that the mixing of the underturned tip gap flow with the main flow not only leads to a higher entropy production but also influences the incidence conditions of the subsequent blade row negatively. The effectiveness of the passive tip-injection can therefore be evaluated not only by the overall leakage mass flow reduction but also by the improved incidence angle of the subsequent blade row. Due to manufacturing restrictions and high mechanical stresses, no through-blade injection (with an injection channel from the blade leading edge to the tip gap) was feasible for the experiments. Instead a through-shroud injection between two fins, close to the pressure side of the turbine blades was realized. This has the advantage, that the injection mass flow is not extracted from

the main flow at the blade leading edge and therefore contributes to the stage work due to its turning, before it is injected into the tip gap cavity at the through-shroud injection position. It is shown that the passive tip-injection improves the uniformity of the flow field behind the blade row and reduces the angular momentum of the tip-leakage mass flow through stronger flow turning and reduction of the tip-leakage mass flow. In respect of flow turning the effectiveness of passive tip-injection can be improved further by a higher inclination angle of the injection jet against the rotational direction of the rotor.

2.2 Tip Excitation in Axial Turbine Stages

In turbines and compressors large amplitude oscillations in the form of a rotor whirl have been witnessed, rendering further operation impossible above a certain power level. In those cases the whirl frequency does not correspond with the rotor speed but is constant at the value of the fundamental natural frequency of the rotor. This form of rotordynamic instability could not be corrected by balancing. It could be reduced by increasing the rigidity of the rotor system, but not eliminated entirely. Thomas [23] identified the leakage flow over the blade tips and sealing glands as the reason for this effect. Therefore it is referred to as tip excitation in literature.

In [23] Thomas investigates this effect in steam turbines. It is stated, that an eccentric rotor leads to a circumferential variation in tip clearance. This leads to a variation of the local efficiency in circumferential direction. It is stated that in sections with a wider tip clearance a larger portion of the working gas leaks over the blade tip compared to sections with a narrower tip clearance. The leaking mass flow is not turned in the blade row, produces no tangential force on the blades and does not contribute to stage work. This leads to a variation of tangential force on the blades in circumferential direction and an unbalanced torque. The resulting force acts perpendicular to the direction of rotor displacement. It is stated, that this force can lead to a forward whirl of the rotor and rotordynamic instability if a certain power level is surpassed.

Alford [1] came to the same conclusions independently when investigating the instable rotordynamic behavior of aircraft turbines analytically and experimentally. In [1] Alford identifies a pressure force as a second disturbing aerodynamical force able to cause a whirling motion of the rotor alongside the force identified by Thomas. It is stated, that the misalignment of the rotor relative to the stator in combination with a radial motion of the rotor can lead to pressure forces acting perpendicular to the direction of rotor displacement. Dependent on how the rotor is misaligned relative to the stator, this pressure force can increase or decrease the whirling motion of the rotor.

The cross force due to the variable tangential force on the rotor blades will be referred to as Thomas-Alford force in the following sections.

The effect described by Thomas and Alford was studied in more detail in several experimental invetigations in the following years. Wohlrab [29] measured the cross forces and momenta acting on three typical steam turbine stages in order to gain information on the flow conditioned forces. The measurements were carried out for shrouded turbine blades and it could be shown that the tip excitation is of decisive significance to the rotordynamic stability. By modifying the bearing suspension of the rotor, it could be shown, that the anisotropy of bearing rigidity can have a stabilizing effect on the rotor.

A comprehensive study of the excitation forces due to tip-leakage was undertaken at the M.I.T., motivated by the rotordynamic issues that occurred with the liquid hydrogen turbopump system of the space shuttle. In experimental work by Martinez-Sanchez et al. in [17] and Song et al. in [22], shrouded and unshrouded turbines were investigated. A significant impact of the pressure forces as previously identified by Urlichs [27] especially for shrouded turbines could be shown alongside the impact of Thomas-Alford forces. It could be further shown, that the excitation forces increase considerable with a decreasing tip gap width.

The excitation force measured due to the pressure distribution in the tip clearance was first identified by Urlichs [27]. In [27] Urlichs performs a comprehensive analytical and experimental analysis of the tip gap leakage-flow of a shrouded turbine rotor with special consideration of the swirled inlet flow, entering the tip gap. The tip gap is discretized in individual stream tubes for which the leakage mass flow rate and pressure levels are calculated using semi-empiric loss coefficient models.
It could be shown that for an eccentric rotor under swirled inlet flow conditions, the pressure and leakage mass flow distributions in the tip gap vary asymmetrically in circumferential direction. For a purely axial flow through the tip gap, the maximum pressure occurs in the narrowest tip clearance section due to the inverse relation between the pressure loss coefficients and the radial clearance width. This is in good accordance with findings by Lomakin (quoted in [7]) and creates a restoring pressure force acting against the direction of displacement of the rotor. For a swirled flow through the tip gap of the eccentric rotor although, the pressure maximum occurs ahead of the narrowest clearance position in circumferential direction. One component of the resulting pressure force on the rotor shroud therefore acts perpendicular to the direction of displacement of the rotor, and adds energy to an assumed whirling motion of the rotor in rotational direction. Experiments by Urlichs on a single stage, impulse air turbine with shrouded and unshrouded blades confirm those findings.

The analytical model developed by Urlichs [27] is discussed in more detail in Sec. 3.2 and will be used as a basis to describe the flow through the tip gap of a shrouded turbine rotor with passive tip-injection (Sec. 3.4).

2.3 Influence of Passive Tip-Injection on Tip Excitation in Axial Turbine Stages

The influence of passive tip-injection on the tip excitation in an axial unshrouded turbine stage has been studied by aus der Wiesche et al. in [28]. The analytical work is focused on the generation of Thomas-Alford forces. First a model for the cross force generation of an unshrouded turbine rotor is obtained, using different models for the discharge coefficient, which describes the mass flow ratio between tip gap flow and main flow. Comparison to experimental data from Urlichs [27] supports the use of a discharge coefficient model, which takes viscous effects into consideration and depends non-linearly on the tip gap width.
To account for passive tip-injection, a model for the discharge coefficient for a setup with passive tip-injection obtained by Willinger et al. [4,8,13] is implemented into the cross force calculations. It could be shown, that passive tip-injection is capable of reducing the tip-leakage mass flow and also results in a slight decrease in Thomas-Alford forces on the rotor. Therefore it is shown, that passive tip-injection can increase the rotordynamic stability of turbomachinery.

Naljotov et al. [19] were granted a patent for a shrouded steam turbine setup with radial holes connecting the tip gap cavity with the mainstream blade channel. It is claimed that by varying the fin height of the labyrinth seal on the shroud it is possible to regulate the flow rate of steam passing through the shroud holes. It is claimed that this results in the relief of the pressure gradient on the surface of the shroud, which prevents the formation of metal oxide, salt and other deposits on the inner surfaces of the shrouds. This is claimed to prolong the period between repairs and the service life of the turbine. Further it is claimed that the method reduces Thomas-Alford forces on the rotor and thus decreases the vibration levels of the rotor. This in turn allows the reduction of the radial clearance width of the tip gap, leading to a reduction in tip-leakage mass flow and an increase of the turbine efficiency.

This method could be considered a form of passive tip-injection. The proposed flow direction from the tip gap cavity through the shroud into the turbine blade main channel is although opposite to the flow direction found in 3D CFD simulations by Ghaffari [10]. The claims made by Naljotov et al. should therefore be interpreted with a reasonable amount of suspicion.

To the author's knowledge, there is no literature available describing the influence of passive tip-injection on the tip excitation in shrouded axial turbine stages, especially considering the pressure excitation forces as described by Urlichs [27] and swirled flow conditions in the tip gap.

In the following chapters such an analytical model is developed and evaluated for an experimental turbine setup.

3 Theoretical Background and Methodology

3.1 Rotordynamics

In this work the influence of passive tip-injection on the tip excitation in shrouded axial turbine stages shall be investigated. To motivate and illustrate the necessity of such an investigation, first the influence of tip excitation on the dynamics and the stability of a turbine rotor (Fig. 3.1) shall be shown.

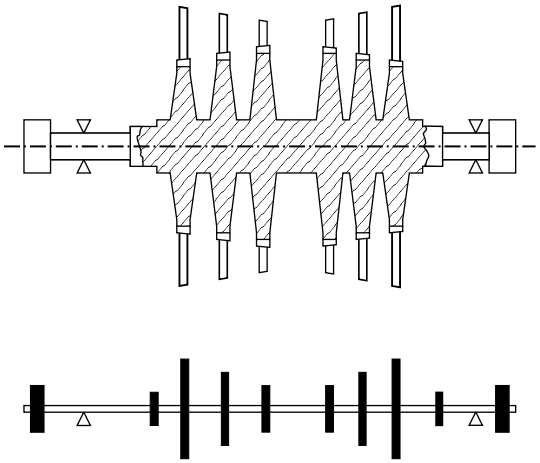

Figure 3.1: Top: Exemplary turbine rotor. Bottom: Simplified lumped-mass model. (adapted from [7])

3.1.1 Modeling

Literature describing the dynamics of a multi stage turbine rotor is readily available [7]. For this work the behavior of such rotors, especially in terms of stability in the face of self excited whirling motions, is of special interest. A general multi disc turbine rotor can be described in the simplified form as a series of discrete discs lined up on a massless, elastic shaft with the corresponding mass and inertia properties of the real rotor as shown in Fig. (3.1). It can be shown, that such a rotor, with an assumed unbalance, has a series of natural frequencies as shown in Fig. (3.2). Some of these frequencies lie in the operating range of the turbine and have to be avoided by all means due to the potential catastrophic resonance displacement of the rotor at the corresponding rotational frequencies.

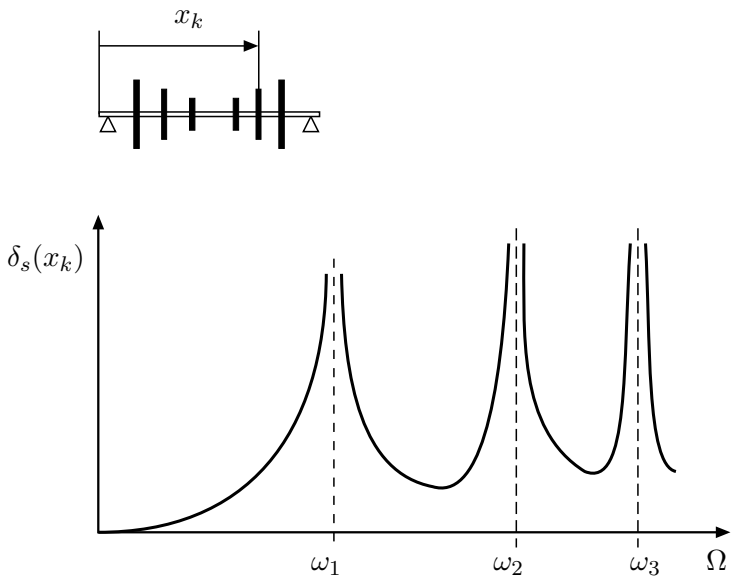

Figure 3.2: Shaft displacement δ_s at the position x_k against the rotational speed of the turbine rotor Ω. (adapted from [7])

3.1.2 Stability

Basically the multi disc rotor is a combination of a number of single disc elastic rotors also known as Laval rotors. The basic phenomenons of rotordynamics can be shown on such a simple Laval rotor as shown in Fig. (3.3).

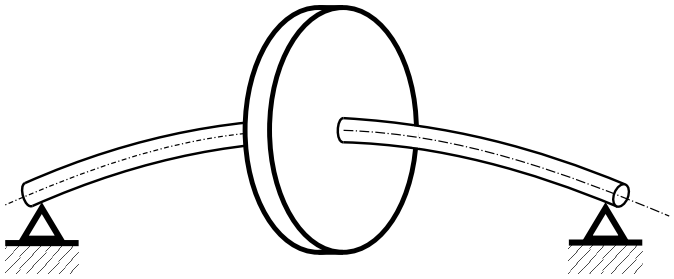

Figure 3.3: Single disc Laval rotor (adapted from [7])

By superposition of several single disc Laval rotors, the behavior of any multi disc rotor can be described. For a number of rotors, self excited oscillations occur beyond a certain limit rotational speed Ω_{lim}. For varying rotational speeds the behavior of such a rotor can be seen in Fig. (3.4).

With increasing rotational speed Ω, the rotor passes its eigenfrequency ω_{eig}, where for an appropriate run up speed and external damping, the oscillation amplitudes do not reach potentially catastrophic levels for the rotor. In the supercritical range of rotational speeds beyond ω_{eig}, stable operational points with relatively small oscillation amplitudes can be found. In this range the frequency of the oscillations are equal to the rotational frequency of the rotor, which runs

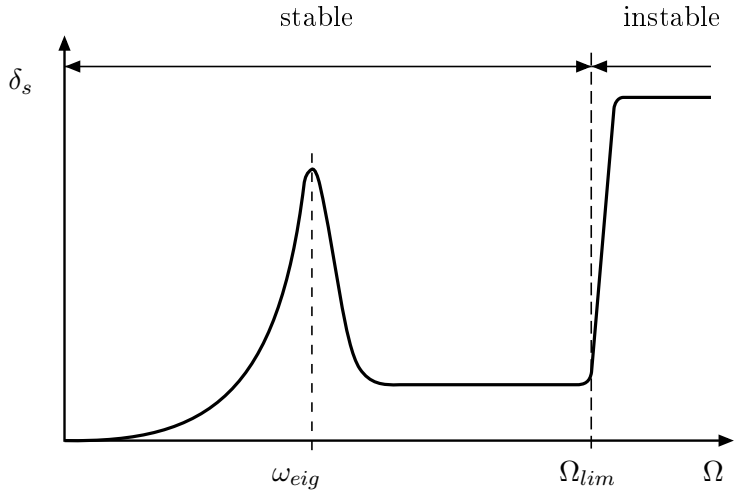

Figure 3.4: Shaft displacement δ_s against the rotational speed of the turbine rotor Ω. Instable operating range beyond Ω_{lim}. (adapted from [7])

along a cyclic or elliptical orbit once for every rotation. This changes drastically at the limit rotational speed Ω_{lim}. At this point the rotor no longer oscillates with its rotational frequency, but with its eigenfrequency with ever increasing amplitudes. Although in real rotors the oscillation amplitudes level off at a relatively high magnitude, no permanent operation beyond Ω_{lim} is possible. This shows the high importance of a comprehensive stability analysis of the rotor and the knowledge of the stability limits of the turbine.

There are numerous reasons for such an instability according to literature [7], as for example:

- friction mechanisms on rotating shafts
- journal bearing effects at high rotational speeds
- self excitation effects at seal clearances
- tip-leakage flows over shrouded turbine rotors

In this work the focus shall lie on the latter two effects.

Equation of Motion

For the excitation effects under investigation, the same basic form of differential equations describing the motion of the rotor in lateral and vertical direction in an inertial reference frame, can be used. For an exemplary single disc rotor (Fig. 3.5) the oscillation of a rotor without any unbalance can be described by the equation of motion

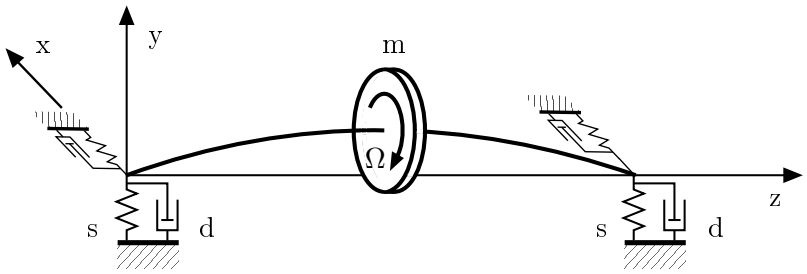

Figure 3.5: Single disc rotor on an elastic shaft in elastic and damped bearings. (adapted from [27])

$$\underbrace{\begin{bmatrix} m & 0 \\ 0 & m \end{bmatrix}}_{\mathrm{M}} \begin{pmatrix} \ddot{w} \\ \ddot{v} \end{pmatrix} + \underbrace{\begin{bmatrix} d & 0 \\ 0 & d \end{bmatrix}}_{\mathrm{D}} \begin{pmatrix} \dot{w} \\ \dot{v} \end{pmatrix} + \underbrace{\begin{bmatrix} s+q_1 & q_2 \\ -q_2 & s+q_1 \end{bmatrix}}_{\mathrm{S}} \begin{pmatrix} w \\ v \end{pmatrix} = 0 \tag{3.1}$$

$$\text{with} \qquad \ddot{\mathbf{u}} = \begin{pmatrix} \ddot{w} \\ \ddot{v} \end{pmatrix}, \qquad \dot{\mathbf{u}} = \begin{pmatrix} \dot{w} \\ \dot{v} \end{pmatrix}, \qquad \mathbf{u} = \begin{pmatrix} w \\ v \end{pmatrix} \quad .$$

Here the vector $\mathbf{u}$ describes the rotor displacement in lateral direction (component w) and vertical direction (component v). The mass of the rotor disc m constitutes the inertia tensor $\mathbf{M}$, the damping in the bearings of the rotor d constitute the damping tensor $\mathbf{D}$. While the tensors $\mathbf{M}$ and $\mathbf{D}$ are symmetric, the stiffness tensor $\mathbf{S}$ also has asymmetric components. The stiffness of the rotor shaft s as well as the restoring force component resulting from the leakage flow through the tip gap q_1 make up the symmetrical part of $\mathbf{S}$. The cross force coefficient q_2 makes up the asymmetric part of $\mathbf{S}$. The asymmetry of the stiffness matrix $\mathbf{S}$ occurs due to the nature of the cross forces generated by the tip gap leakage mass flow, acting perpendicular to the direction of displacement of the rotor, as will be shown later. The force acting on an eccentric rotor due to the tip gap leakage mass flow can be described in general by

$$\mathbf{F}_{tl} = \begin{bmatrix} q_1 & -q_2 \\ q_2 & q_1 \end{bmatrix} \begin{pmatrix} w \\ v \end{pmatrix} \tag{3.2}$$

The restoring force coefficient q_1 can add to the displacement of the rotor if negative. It is relatively small, compared to the cross force coefficient q_2 and is therefore not that important for the stability considerations for the rotor. The asymmetric part of $\mathbf{S}$ is the reason for instability of the rotor in the form of an increasing whirling motion. Therefore this work will focus on the determination of the cross force coefficients q_1 and q_2.

Figure (3.6) shows the forces acting on an eccentric rotor, oscillating on a circular orbit around the central position with the angular velocity $\dot{\varphi}_s = \omega_s$ and a rotational speed of the rotor disc

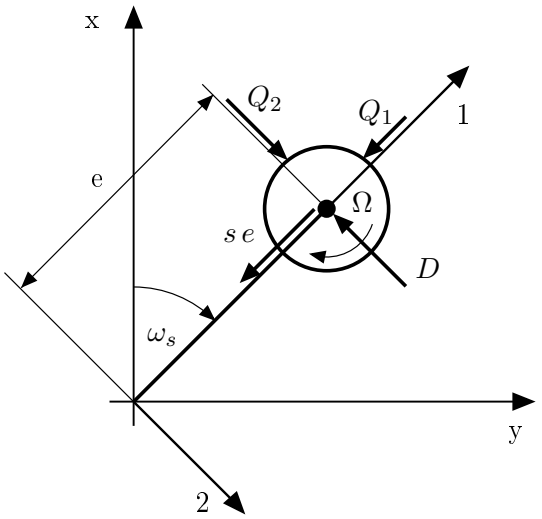

Figure 3.6: External forces acting on an eccentric turbine rotor. (adapted from [27])

of Ω. The rotor is deviated from the central position by w in lateral and v in vertical direction, resulting in an eccentricity of e. The restoring elastic force $s\,e$ in combination with the restoring force $Q_1 = q_1 e$ resulting from the tip gap leakage flow, act against the displacement of the rotor. The damping force D acts against the oscillation direction of the rotor, taking kinetic energy from the rotordynamic system. The cross force $Q_2 = q_2 e$ resulting from the tip gap leakage flow acts in direction of the oscillation, adding energy to the system and therefore increasing the whirling motion of the rotor.

Characteristic Equation and Stability Limit

The relation between the stability of the rotor motion and the cross force coefficient q_2 can be found by performing a stability analysis of the rotordynamic system described by Eq. (3.1). To find the homogeneous solution of the equation of motion the ansatz

$$\begin{pmatrix} w(t) \\ v(t) \end{pmatrix} = \begin{pmatrix} w_h \\ v_h \end{pmatrix} e^{\lambda t} \tag{3.3}$$

can be used. With Eq. (3.3) and its derivations, the equation of motion (3.1) can be transformed into the equation

$$\underbrace{\begin{bmatrix} \lambda^2 + \dfrac{d}{m}\lambda + \dfrac{s+q_1}{m} & q_2 \\ -q_2 & \lambda^2 + \dfrac{d}{m}\lambda + \dfrac{s+q_1}{m} \end{bmatrix}}_{\mathbf{\Lambda}} \begin{pmatrix} w_h \\ v_h \end{pmatrix} = 0 \quad , \tag{3.4}$$

which only has a nontrivial solution if the determinate of $\mathbf{\Lambda}$ is zero. This condition leads to the characteristic equation

$$a_4\lambda^4 + a_3\lambda^3 + a_2\lambda^2 + a_1\lambda + a_0 = 0 \quad , \tag{3.5}$$

with

$$\begin{aligned} a_4 &= 1 \\ a_3 &= 2\frac{d}{m} \\ a_2 &= \left(\frac{d}{m}\right)^2 + 2\frac{s+q_1}{m} \\ a_1 &= 2\frac{d}{m}\left(\frac{s+q_1}{m}\right) \\ a_0 &= \left(\frac{s+q_1}{m}\right)^2 + q_2^2 \quad . \end{aligned}$$

In order to find the stability limit of the rotor motion, the determination of the full set of eigenvalues λ can be skipped. It is known, that at the stability limit, the real part of the eigenvalues λ is zero and has a positive sign in the instable range. The eigenvalues at the stability limit are of the form

$$\lambda = 0 + j\omega_{lim} \quad , \tag{3.6}$$

where ω_{lim} is the frequency of oscillation at the stability limit. By inserting Eq. (3.6) into Eq. (3.5) and sorting in real and imaginary parts,

$$\begin{aligned} \text{Real part: } & a_4\omega_{lim}^4 - a_2\omega_{lim}^2 + a_0 = 0 \\ \text{Imaginary part: } & -ja_3\omega_{lim}^3 + ja_1\omega_{lim} = 0 \end{aligned} \tag{3.7}$$

is obtained. This allows the calculation of the frequency of oscillation at the stability limit

$$\omega_{lim} = \sqrt{\frac{a_1}{a_3}} \tag{3.8}$$

and when inserted into the real part of Eq. (3.7) this leads to the stability limit condition

$$a_4a_1^2 - a_1a_2a_3 + a_3^2a_0 = 0 \quad . \tag{3.9}$$

By evaluating this condition with the coefficients from Eq. (3.5), a condition for the cross force coefficient at the stability limit of the rotor motion can be found

$$q_{2,lim} = \frac{d}{m}\sqrt{\frac{s+q_1}{m}} \quad . \tag{3.10}$$

Equation (3.10) shows the maximum cross force coefficient for stable conditions for the rotor motion. It can be seen, that the external damping d, the rotor shaft stiffness s and the restoring force coefficient q_1 resulting from the tip-leakage flow, have an influence on the level of the maximum cross force coefficient $q_{2,lim}$. For cross force coefficients q_2 greater than $q_{2,lim}$, no stable operation point for the rotor can be found and a permanent operation becomes impossible as seen in Fig. (3.4). Therefore it is imperative that the cross force coefficient of the rotor is smaller than $q_{2,lim}$. As mentioned in literature [1, 23], the stability of the rotordynamic system for the effects under investigation depends on a limit power level of the turbomachinery rather than a limit rotational speed of the rotor. This will be shown in more detail in the following section.

3.1.3 Cross Forces

In order to calculate the cross force coefficient q_2 and the restoring force coefficient q_1 of the stiffness tensor $\mathbf{S}$ from Eq. (3.1), first the forces in direction of displacement of the rotor and the forces acting perpendicular to the direction of displacement of the rotor, will be calculated. To obtain the respective cross force coefficients those forces are then related to the displacement of the rotor. In general two different types of cross forces resulting from a swirled flow through the tip gap can be identified, Thomas-Alford forces and pressure forces.

Thomas-Alford Force

The cross forces due to a nonuniform tip gap leakage mass flow in circumferential direction of the rotor, were first described by Thomas [23] and several years later also by Alford [1]. In this work they will be referred to as Thomas-Alford forces.
For an eccentric turbine rotor the radial tip gap clearance and therefore the tip gap leakage mass flow varies in circumferential direction. The increased tip-leakage mass flow at positions with a greater radial tip clearance leads to a smaller mass flow through the meridional turbine blade channel and a reduced local stage work. This reduces the tangential force acting on the turbine blades at that position. For the narrower tip clearance on the opposite side of the rotor the conditions are reversed as seen in Fig. (3.7).
This results in a variable tangential force on the turbine blades in circumferential direction and a net force acting perpendicular to the direction of displacement as assumed for the stability considerations (Eq. 3.1). It will be shown that this force is proportional to the eccentricity e of the rotor.
For a centric rotor without losses, the thermal energy of the mass flow through the turbine row is transformed entirely into mechanical rotational energy

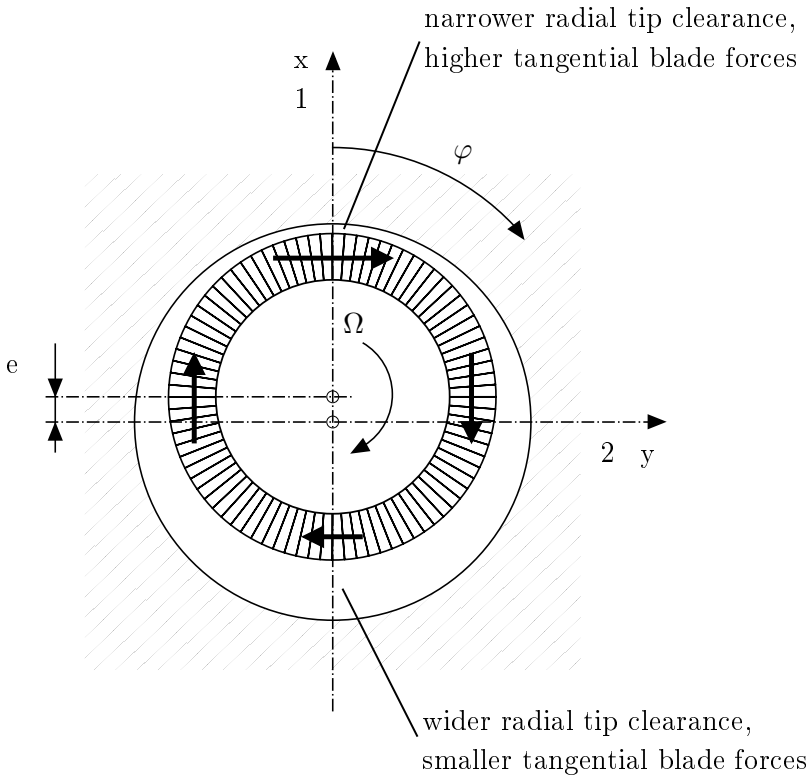

Figure 3.7: Variable tangential blade forces of an eccentric turbine rotor, leading to a net force acting perpendicular to the direction of displacement (Thomas-Alford force). (adapted from [7])

$$\dot{m}\Delta H = F_{s,id}\Omega R_m \quad . \tag{3.11}$$

$\dot{m}$	massflow through the turbine stage
ΔH	total enthalpy drop for the turbine stage
$F_{s,id}$	ideal tangential force on the turbine blades
Ω	angular velocity
R_m	mean blade radius

This leads to an ideal tangential force on the turbine blades of

$$F_{s,id} = \frac{\dot{m}\Delta H}{\Omega R_m} \quad . \tag{3.12}$$

Which leads to the tangential force on a section of the blades in circumferential direction $\mathrm{d}\varphi$ of

$$\mathrm{d}F_{s,id} = F_{s,id}\,\frac{\mathrm{d}\varphi}{2\pi} = \frac{\dot{m}\Delta H}{\Omega R_m}\,\frac{\mathrm{d}\varphi}{2\pi} \quad . \tag{3.13}$$

For the real tangential force, blade and tip gap losses have to be taken into consideration. With the circumferential efficiency η_u and the tip gap loss coefficient ζ this leads to

$$\mathrm{d}F_s = \mathrm{d}F_{s,id}\,(\eta_u - \zeta(\varphi)) \quad . \tag{3.14}$$

The dependency of the tip gap loss coefficient $\zeta(\varphi)$, on the position in circumferential direction φ, already takes the varying loss coefficients for an eccentric rotor into consideration.

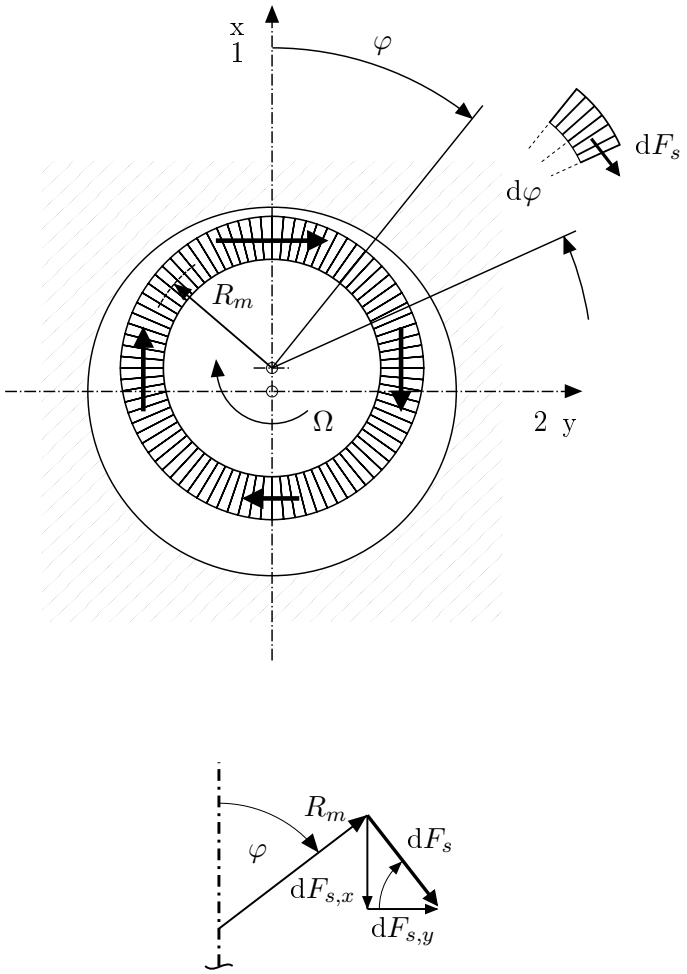

Figure 3.8: Thomas-Alford force components (adapted from [7])

According to Fig. (3.8), the tangential force $\mathrm{d}F_s$ can be split up in its components and integrated along the circumference of the rotor, in order to obtain the resulting cross forces $Q_{s,1}$ and $Q_{s,2}$

$$Q_{s,1} = \int \mathrm{d}F_{s,x} = -\int_0^{2\pi} \mathrm{d}F_s \sin\varphi = \frac{F_{s,id}}{2\pi} \int_0^{2\pi} \zeta(\varphi) \sin\varphi \,\mathrm{d}\varphi \quad . \tag{3.15}$$

$$Q_{s,2} = \int \mathrm{d}F_{s,y} = + \int_0^{2\pi} \mathrm{d}F_s \cos\varphi = -\frac{F_{s,id}}{2\pi} \int_0^{2\pi} \zeta(\varphi) \cos\varphi \, \mathrm{d}\varphi \quad , \tag{3.16}$$

The constant circumferential efficiency coefficients η_u disappear through the integration. It can be seen that the Thomas-Alford forces Q_s (Eq. 3.15 and Eq. 3.16) depend solely on the local tip gap loss coefficients $\zeta(\varphi)$ for a given ideal tangential force $F_{s,id}$ (Eq. 3.12). This dependence of the Thomas-Alford forces on the ideal tangential force shows that the stability limit of the rotordynamic system is defined by a limit power level of the turbomachine (limit ideal tangential force) rather than a limit rotational speed.
In general the loss in circumferential efficiency due to tip-leakage loss can be described by the ratio between the tip gap leakage mass flow $\dot{m}_{cl}$ and the main mass flow through the turbine stage $\dot{m}_0$

$$\zeta = \frac{\dot{m}_{cl}}{\dot{m}_0} \quad . \tag{3.17}$$

For an eccentric rotor with variable loss coefficients in circumferential direction this leads to the formulation

$$\zeta(\varphi) = \frac{\mathrm{d}\dot{m}_{cl}}{\mathrm{d}\dot{m}_0} \quad . \tag{3.18}$$

While there are models available for the tip gap leakage mass flow $\dot{m}_{cl}$ for axial flows and simple tip gap geometries, in this work the tip gap leakage mass flow will be considered in more detail, as shown below.

Pressure Force

Urlichs [27] could show, that for a swirled flow through the tip gap or seal gap of an eccentric rotor, additional cross forces to the Thomas-Alford forces act on the rotor. This is due to an asymmetric pressure distribution $p(\varphi)$ in the tip clearance relative to the location of the narrowest radial clearance width at φ=0° as seen in Fig. (3.9).
According to Urlichs and as proven later, the pressure maximum for a swirled flow occurs ahead of the narrowest clearance width position in circumferential direction. This leads to a net pressure force acting perpendicular to the direction of displacement w and in direction of rotation of the rotor.
In contrast to the Thomas-Alford forces this effect does not only occur in stages where the gap mass flow could potentially contribute to stage work as it is the case for tip gap of turbine rotors, but also at seal clearances. With knowledge of the pressure distribution the resulting pressure force can be easily calculated and split up in its components similar to Eq. (3.16) and Eq. (3.15),

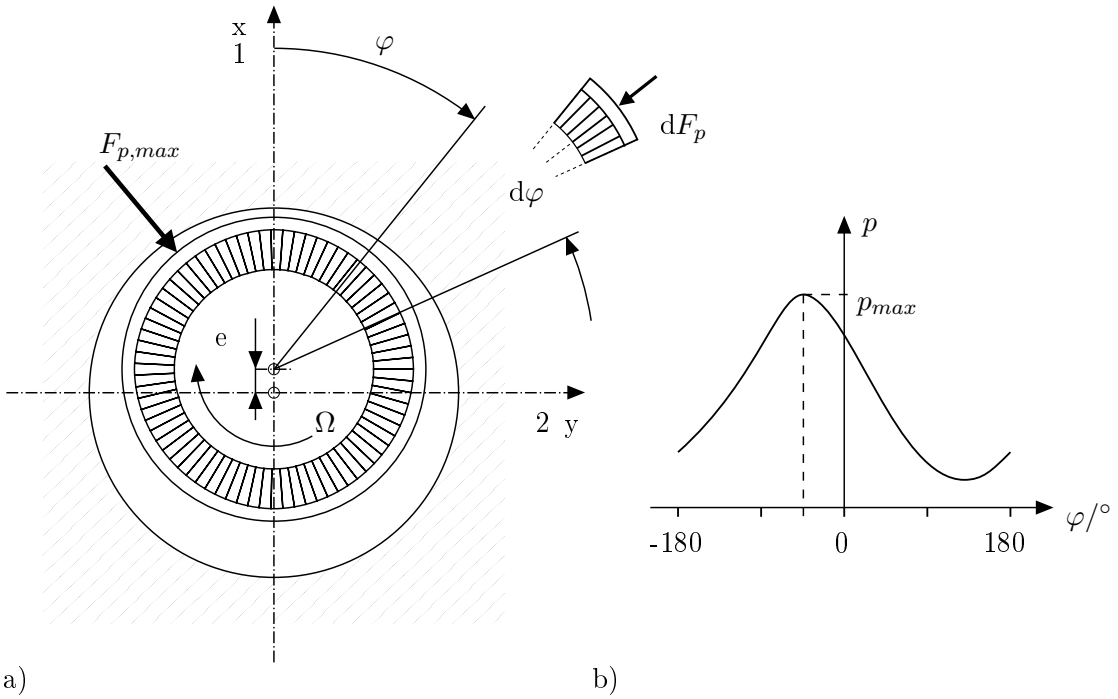

Figure 3.9: a) Pressure forces on an eccentric shrouded turbine rotor. b) Asymmetric pressure distribution in the rotor tip clearance for a swirled flow. (adapted from [27])

in order to calculate the resulting pressure cross forces $Q_{p,1}$ and $Q_{p,2}$

$$Q_{p,1} = \int \mathrm{d}F_{p,x} = -A_{surf} \int_0^{2\pi} p(\varphi) \cos\varphi \, \mathrm{d}\varphi \quad , \tag{3.19}$$

$$Q_{p,2} = \int \mathrm{d}F_{p,y} = -A_{surf} \int_0^{2\pi} p(\varphi) \sin\varphi \, \mathrm{d}\varphi \quad , \tag{3.20}$$

with the rotor surface of the tip gap or seal clearance A_{surf}.

As shown before, for both types of cross forces Q_s and Q_p the cross force coefficients q_1 and q_2 can be found by relating them to the displacement (in this case the eccentricity e) of the rotor. This shows, that in order to determine the cross force coefficients one possibility is to find the cross forces acting on the rotor first and then calculating the cross force coefficients by

$$q_1 = \frac{Q_1}{e} \quad , \tag{3.21}$$

$$q_2 = \frac{Q_2}{e} \quad . \tag{3.22}$$

In Fig. (3.10) the effect of cross forces perpendicular to the direction of displacement of a rotor is shown. For an assumed oscillation synchronous to the rotational direction of the rotor, the resulting cross force always points in the direction of oscillation. The force adds energy to the whirling motion of the rotor and increases with the growing eccentricity of the rotor. For cross force coefficients q_2 greater than the limit cross force coefficient $q_{2,lim}$ the excitation force perpendicular to the direction of displacement of the rotor can lead to catastrophic oscillation amplitudes of the rotor.

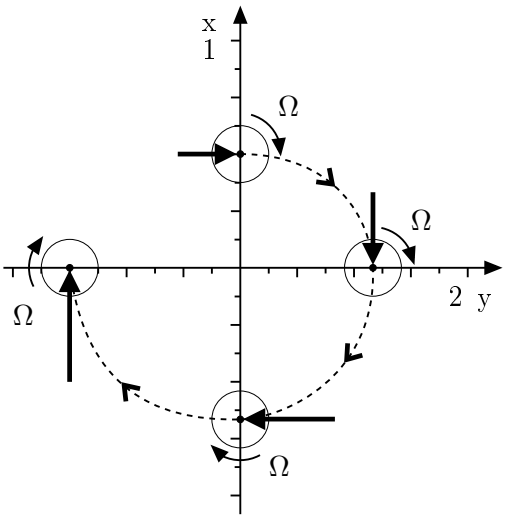

Figure 3.10: Orbit of an increasingly whirling rotor due to cross forces perpendicular to the direction of displacement. (adapted from [7])

In order to calculate the flow induced cross forces and subsequently the influence of passive tip-injection on those cross forces, it is necessary to find equations describing the tip-leakage mass flow and the pressure distribution in the tip gap.
In the following sections of this chapter, first the governing equations describing the flow through the tip gap of a shrouded turbine rotor in terms of pressure and mass flow will be obtained. Second the equations describing the passive tip-injection into the tip clearance will be built and combined with the equations of the tip gap. This yields a full set of equations, which describe the pressure and mass flow distributions in the tip gap, as well as the streamlines of the tip gap leakage mass flow for a shrouded turbine rotor with passive tip-injection.

3.2 Tip Gap Flow

The model to describe the tip gap flow of a shrouded turbine rotor (Fig. 3.11) developed by Urlichs [27] is used as a basis for the model of the flow through the tip gap of a shrouded rotor with passive tip-injection (Sec. 3.4). Therefore in this section Urlichs' model is presented in detail.

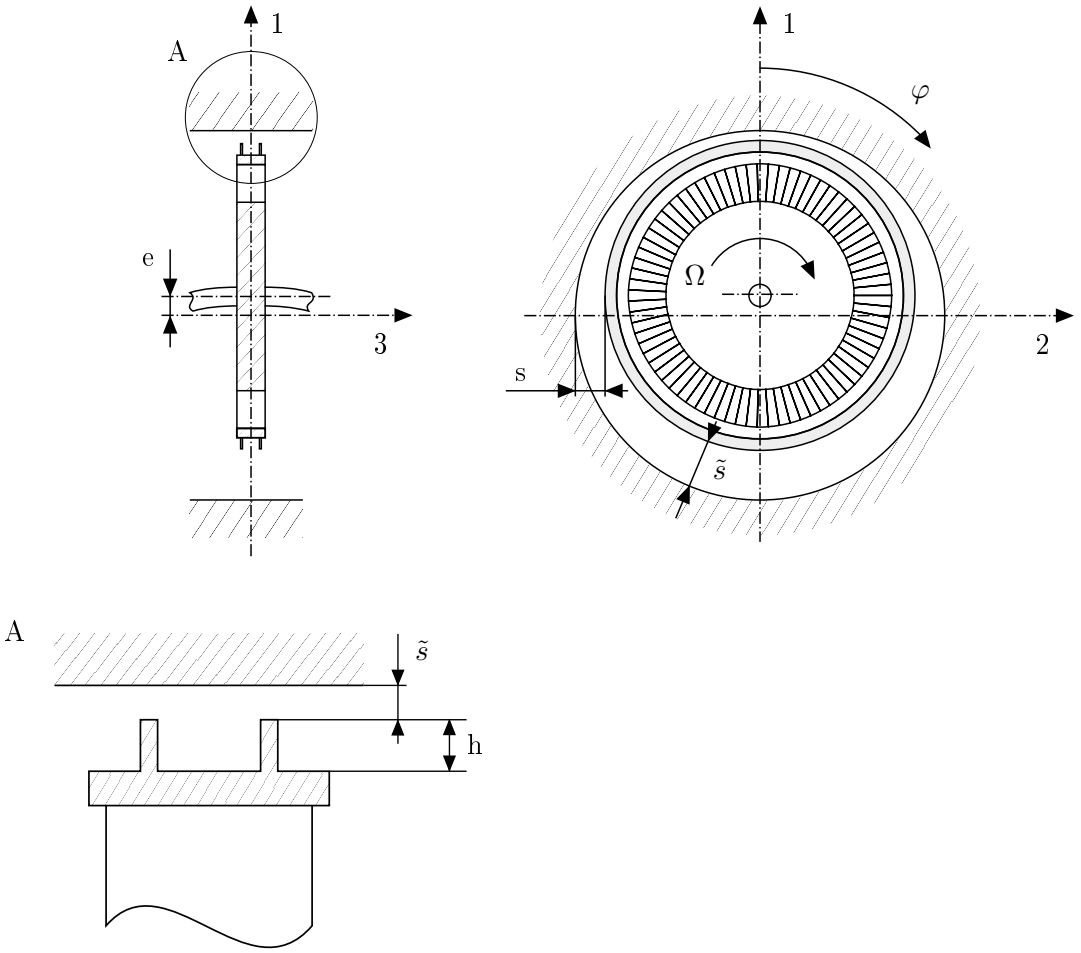

Figure 3.11: Geometry used to model an eccentric shrouded turbine rotor with two fins. With the eccentricity e, the nominal radial clearance width s, the local radial clearance width $\tilde{s}$ and the labyrinth fin height h. (adapted from [27])

By defining suitable control volumes the tip gap or any other radial clearance (for example shaft through housing etc.) can be modeled as a set of streamtubes with varying cross-sectional areas. In that way the mean velocity in the defined support points can be described by the continuity equation and the local stream tube cross-sectional areas.
The pressure drop and mass flow rate of such streamtubes can be calculated with the energy equation by using empiric loss coefficients.
The direction of the flow and thereby the orientation of the streamtubes is determined by momentum equations under special consideration of the inlet swirl.

The usage of energy and momentum equations enables the description of the gap flow without knowing the precise processes in the volume under investigation. This method depends strongly on the availability of empiric loss coefficients.
For the following calculations the separation of the tip gap mass flow from the main flow must be possible, which is only the case for shrouded blades. In the case of unshrouded blades an interaction of the main flow with the tip gap flow must be assumed and the loss mechanisms are more complex as shown in literature [6].
A stationary eccentricity of the rotor and the incompressibility of the flow is assumed in order to determine the cross force coefficients of the rotordynamic considerations in Sec. 3.1.

3.2.1 Discretization

For the building of the model a simple tip gap seal geometry is assumed similar to the one seen in Fig. (3.11). A geometry without radial inlets or outlets is chosen in order to make the obtained equations applicable not only to the tip gap of a shrouded turbine rotor but also to shaft seals and radial seal gaps in general.
By simple manipulations the obtained equations will be applicable to shrouded turbine blades with and without fins as well as to the tip gap of the stator.
A one dimensional description of the flow is possible by using control spaces, which vary according to the course of the respective streamlines.
The shape of the streamlines is described by the location of corresponding support points located on subsequent planes in axial direction perpendicular to the axis of rotation.
While the distance between the support points in axial direction is set to be constant, in circumferential direction the location of the support points is variable and determined by local flow angles i.e. angles of the tangents to the streamlines. The variable cross-sectional areas of the streamtubes are determined by the distance between the support points in circumferential direction and the local radial clearance width. In this way the flow angles can be determined iteratively from the basic equations and shall be assumed known for the following calculations.

The tip gap is divided in a number of j streamtubes marked by the index k in circumferential direction. While the distance of the support points in circumferential direction can be chosen arbitrarily, they shall be constant for the preliminary considerations for the support points at the tip gap entry and can be described by

$$\Delta\varphi_{E,k} = \frac{2\pi}{j}\,,\; k = (1, \dots j),$$

so the location of the support points in circumferential direction at the tip gap entrance can be determined by

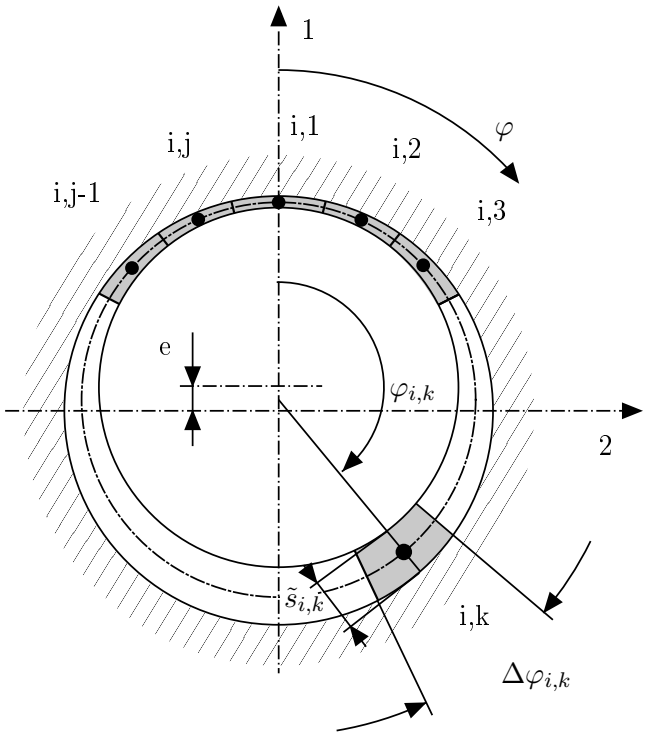

Figure 3.12: Discretization of the tip gap of a shrouded turbine rotor in circumferential direction. (adapted from [27])

$$\begin{aligned} \varphi_{E,1} &= 0\,, \\ \varphi_{E,k} &= \varphi_{E,k-1} + \Delta\varphi_{E,k}\,. \end{aligned} \tag{3.23}$$

Based on the location of the support points in plane $i{=}E$, the location of the subsequent support points in axial direction can be defined by using the local flow angles only. Thereby the support point angles φ and the streamtube widths $\Delta\varphi$ change in axial direction.
In axial direction the streamtubes are divided into a number of n support points marked by the index i. It is assumed that the streamlines are turned in axial direction passing through the tip gap as seen in Fig. (3.13). This is caused by the loss of kinetic energy of the flow due to wall friction and mixing in the case of shrouds with fins. The effect of flow turning is of great significance to the resulting cross force coefficients and is discussed in more detail later.
It is assumed that the streamlines between the support points can be approximated by aligning straight streamlines representing the tangents to the actual streamlines in the support points. Under this assumption the location of the support points can be constructed starting with the support points E,k at the entrance by

$$\begin{aligned} \varphi_{1,k} &= \varphi_{E,k} + \frac{\Delta a_{E,k}}{r_E}\left(0.5\cot\alpha_{E,k} + 0.5\cot\alpha_{1,k}\right) \qquad \text{for } j = 1, \\ \varphi_{i,k} &= \varphi_{i-1,k} + \frac{\Delta a_{i-1,k}}{r_i}\left(0.5\cot\alpha_{i-1,k} + 0.5\cot\alpha_{i,k}\right) \qquad \text{for } j = (2,\ldots n). \end{aligned} \tag{3.24}$$

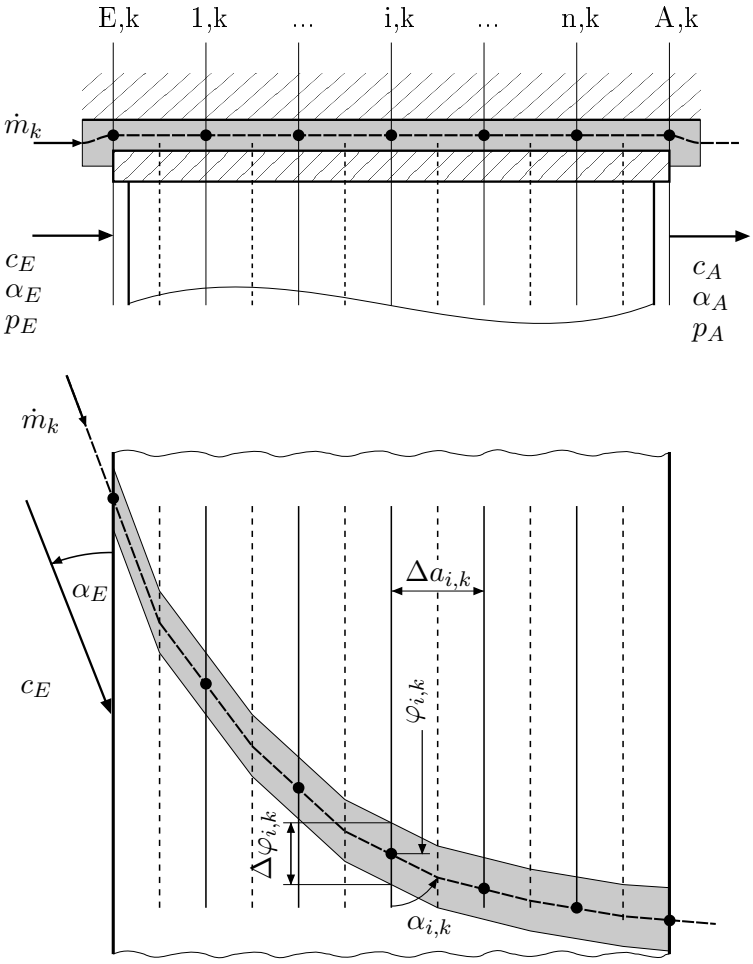

Figure 3.13: Discretization of the tip gap of a shrouded turbine rotor shown for the streamtube k. Assumed turning of the flow in axial direction due to friction losses as shown later. (adapted from [27])

In this formulation it is assumed, that the straight streamlines intersect each other in the middle of the labyrinth chamber.
By de definitions above, the flow path through the tip clearance is defined solely by the streamline angles and the axial distance between the support points (i.e. the labyrinth chamber axial length for shrouds with fins).

When assuming that the support points lie in the middle of their corresponding stream tube, the stream tube width $r\Delta\varphi$ can be defined by

$$\begin{aligned} \Delta\varphi_{i,1} &= \frac{1}{2}(\varphi_{i,2} - \varphi_{i,j} + 2\pi)\,, \\ \Delta\varphi_{i,k} &= \frac{1}{2}(\varphi_{i,k+1} - \varphi_{i,k-1})\,, \\ \Delta\varphi_{i,j} &= \frac{1}{2}(\varphi_{i,1} + 2\pi - \varphi_{i,j-1}) \end{aligned} \tag{3.25}$$

and the corresponding radii r_i of the support points.
For the eccentric rotor the local radial clearance width in the support points $\tilde{s}_{i,k}$ depends on the nominal radial clearance width s_i, the eccentricity e and the position in circumferential direction $\varphi_{i,k}$.

$$\tilde{s}_{i,k} = f(\varphi_{i,k}, s_i, e)$$

In the following considerations any inclination of the rotor against the axial direction is neglected. This can be done as the inclinations of the individual rows due to the bending of the oscillating rotor is rather small. The local radial clearance width in the support points can thus be approximated by

$$\tilde{s}_{i,k} = s_i - e\cos(\varphi_{i,k}), \tag{3.26}$$

while it is assumed that it represents the mean radial clearance width for the support point $\varphi_{i,k}$ over the streamtube width $\Delta\varphi_{i,k}$. The cross-sectional areas of the streamtubes can therefore determined by

$$A_{i,k} = r_i\,\Delta\varphi_{i,k}\tilde{s}_{i,k}\mu_{i,k}. \tag{3.27}$$

Here μ stands for the contraction coefficient for a flow passing over a sharp edge. μ describes the vena-contracta effect for the flow passing over a labyrinth fin, which reduces the effective cross-sectional area of the streamtubes. For further calculations the contraction coefficient is set constant at $\mu = 1$ and the vena-contracta effect is neglected.

For the calculations performed later in Ch. 4 a shroud with fins is assumed. The fins have the effect of a labyrinth seal atop the turbine shroud and reduce the tip gap leakage flow by increasing the blocking properties of the shroud.
As definitive statements about the flow velocity and pressure in a labyrinth seal can only be made at the tip of the labyrinth fin, the support points of a turbine shroud with fins are defined to be located accordingly at the tip of each labyrinth fin as seen in Fig. (3.14). By this definition, the number of labyrinth fins determines the number of support points in axial direction. This can lead to some numeric problems as shown later.

3.2.2 Governing Equations

By dividing the tip gap into a set of partially straight streamtubes, it is possible to describe the processes in the control volume by the one dimensional basic equations of fluid mechanics. In this way, known models for the loss coefficients in a labyrinth seal can be made use of. For the relatively low Mach-number and pressure drop in the exemplary calculations in Ch. 4, the

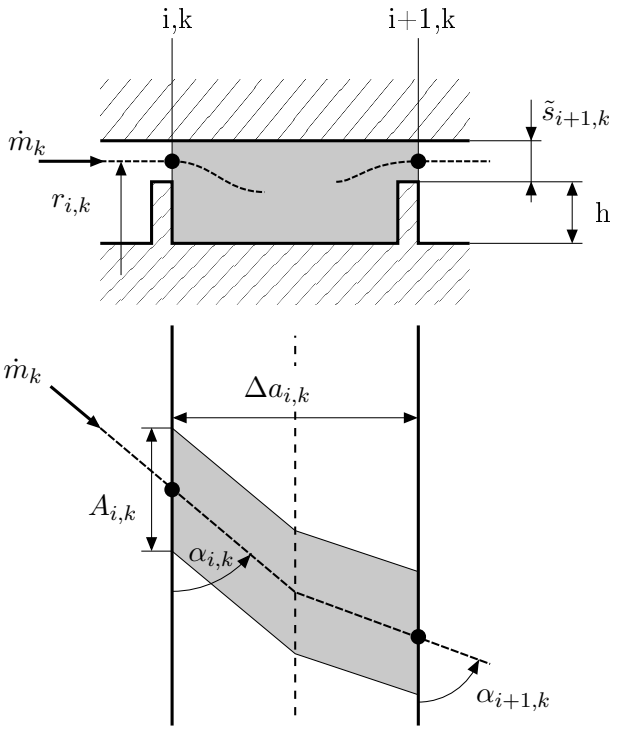

Figure 3.14: Location of the support points for a shrouded turbine rotor with fins. (adapted from [27])

assumption of incompressibility for the flow can be made.
At the tip gap entry it can be assumed that a streamtube exists which divides the tip gap mass flow of the main flow. Therefore the tip-leakage mass flow is not only determined by the static pressure drop, but also by the kinetic energy of the inlet flow field and its resulting momentum, which determines the flow direction in the tip gap. At the exit of the row the tip gap leakage flow mixes with the main flow. It is possible that as a cause of this some of the velocity energy of the tip gap flow or the main flow is recovered into pressure. It is assumed that only the static pressure behind the row acts on the exit tip gap flow.

Continuity Equation

For every support point i the continuity equation for the corresponding streamtube k is fulfilled. Under assumption of a mean flow velocity perpendicular to the cross-sectional area of the streamtube $A_{i,k}\sin(\alpha_{i,k})$ as seen in Fig. (3.15), using the mass flow rate of the streamtube $\dot{m}_k$ and the mean gas density ρ, the flow velocity in the support point $w_{i,k}$ can be determined by

$$w_{i,k} = \frac{\dot{m}_k}{\rho A_{i,k} \sin \alpha_{i,k}} \quad . \tag{3.28}$$

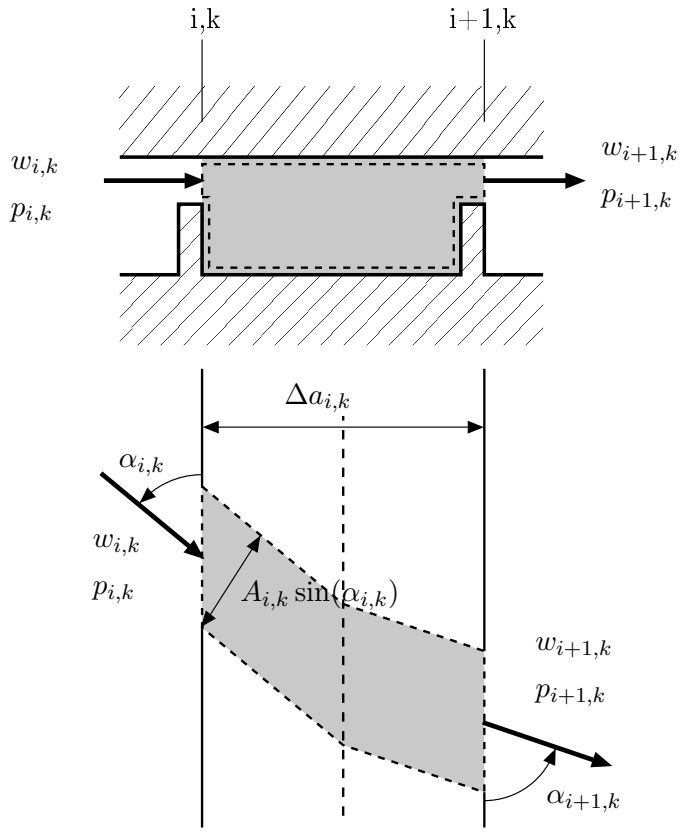

Figure 3.15: Boundaries of the control volume in the labyrinth chamber. (adapted from [27])

Energy Equation

In every streamtube k the energy equation from one support point to the next can be built. The pressure losses due to wall friction or mixing in the labyrinth chamber Δp_v can be defined proportional to the kinetic energy of the flow using a loss coefficient ξ,

$$\Delta p_v = \xi \frac{\rho}{2} w^2 \qquad . \tag{3.29}$$

The boundaries of the control volume for the energy equation are chosen as seen in Fig. (3.15), so that the velocities at the inlet and outlet can be determined by the continuity equation (3.28). The pressure loss is set proportional in part to the inlet velocity into the control volume $w_{i,k}$ and in part proportional to the outlet velocity of the control volume $w_{i+1,k}$. Under these assumptions the energy equation for the control volume can be written in the form

$$\frac{p_{i,k}}{\rho} + \frac{1}{2} w_{i,k}^2 (1 - \xi_{i,k}) = \frac{p_{i+1,k}}{\rho} + \frac{1}{2} w_{i+1,k}^2 (1 + f_L \xi_{i+1,k}) \qquad , \tag{3.30}$$

with f_L as a control parameter for different clearance shapes

$$\begin{aligned} f_L &= 0\,(labyrinth)\,, \\ f_L &= 1\,(smooth\,clearance)\,. \end{aligned} \tag{3.31}$$

The loss coefficients essentially depend on the local radial clearance width and the streamline length. In a labyrinth $\xi_{i,k}$ describes the incomplete mixing of the incoming mass flow. The coefficient $\xi_{i+1,k}$ stands for the pressure losses that occur when the flow accelerates from the labyrinth chamber to the subsequent labyrinth fin.
As the acceleration pressure losses are far smaller than those for the deceleration of the flow, $\xi_{i+1,k} = 0$ is used for the further calculations for a shroud with fins. In this way it is assumed, that the pressure loss in the labyrinth seal is caused solely by the mixing at fin i and the acceleration of the flow towards fin $i+1$ occurs loss free. In accordance with common labyrinth theory, the pressure in the labyrinth chamber is set constant to the pressure $p_{i,k}$.
For a smooth clearance the loss coefficients can be derived using classic hydraulics equations,

$$\xi = \lambda \frac{l}{d_H}$$

in dependence of the friction coefficient λ, the streamtube length l and the hydraulic diameter, which can here be set equal to $d_H = 2\tilde{s}$. For the inclined streamlines this leads to the formulation for the loss coefficient

$$\xi_{i,k} = \lambda(Re) \frac{\Delta a_{i,k}}{2\tilde{s}_{i,k} \sin \alpha_{i,k}} \quad . \tag{3.32}$$

$\lambda(Re)$ depends on the local Reynolds number and can be gained from literature [16].

As mentioned before, in the case of a labyrinth seal the loss coefficient $0 \leq \xi \leq 1$ describes the level of mixing in the labyrinth chamber, where a value of $\xi = 1$ corresponds to the ideal labyrinth seal and complete mixing of the inlet flow velocity into the labyrinth chamber. Neumann [20] derived a model to determine the loss coefficients for real- and see-through- labyrinths of the form

$$\xi = \frac{1}{\left(1 + m_N \frac{s}{t}\right)^2} \quad . \tag{3.33}$$

in dependence of the distance between labyrinth fins t and the radial clearance width s. Neumann found values for the constant m_N ranging from $m_N = 8.9$ to 16.6 [21]. Applied to the swirled flow through the tip clearance, where the longer streamlines between the labyrinth fins $t \cong \Delta a_{i,k} / \sin \alpha_{i,k}$ have to be taken into consideration, the loss coefficients are determined by

$$\xi_{i,k} = \frac{1}{\left(1 + m_N \frac{\widetilde{s}_{i,k} \sin \alpha_{i,k}}{\Delta a_{i,k}}\right)^2} \quad . \tag{3.34}$$

Using the general energy equation (3.30) the pressure drop along the tip gap can be described. By substituting the flow velocity with the continuity equation (Eq. 3.28), the pressure difference of two neighboring support points can be described in dependence of the mass flow rate, the local cross-sectional area and inclination of the streamtube and the empirical pressure loss coefficients. At the inlet and outlet of the tip gap loss coefficients ξ_C and ξ_W are introduced which describe the losses relative to the velocity c of the main flow and w of the tip gap flow.
Considering

$$\frac{1}{\sin^2 \alpha} = 1 + \cot^2 \alpha \quad ,$$

the pressure drops in a streamtube can be described as

$$p_E - p_{1,k} = \frac{1}{2}\frac{\dot{m}_k^2}{\rho}\left[\frac{1}{A_{1,k}^2}(1 + \xi_{WE})(1 + \cot^2 \alpha_{1,k})\right] - \frac{\rho}{2} c_E^2 (1 - \xi_{CE}) \quad , \tag{3.35}$$

for the first support point after the tip gap entry and

$$\begin{aligned} &\text{for } i = (1 \ldots n-1) \\ &p_{i,k} - p_{i+1,k} = \frac{1}{2}\frac{\dot{m}_k^2}{\rho}\left[\frac{1}{A_{i+1,k}^2}(1 + f_L \xi_{i+1,k})(1 + \cot^2 \alpha_{i+1,k}) - \frac{1}{A_{i,k}^2}(1 - \xi_{i,k})(1 + \cot^2 \alpha_{i,k})\right] \end{aligned} \tag{3.36}$$

for the subsequent support points along the streamtube. For the last support point before the tip gap flow exits the tip clearance and mixes with the main flow, the energy equation yields

$$p_{n,k} - p_A = \frac{\rho}{2} c_A^2 (1 - \xi_{CA}) - \frac{1}{2}\frac{\dot{m}_k^2}{\rho}\left[\frac{1}{A_{n,k}^2}(1 + \xi_{WA})(1 + \cot^2 \alpha_{n,k})\right]. \tag{3.37}$$

By adding the energy equations (3.35), (3.36) and (3.37) for all support points of one streamtube, in the form

$$p_E - p_1 + p_1 - p_2 + \ldots + p_{n-1} - p_n + p_n - p_A = p_E - p_A, \tag{3.38}$$

a single equation describing the mass flow rate of the streamtube can be obtained for the given total pressure drop, assuming the local streamtube cross-sectional areas, the flow angles and the

loss coefficients are known.

For the following calculations the total pressure drop Δp_B is defined

$$\Delta p_B = p_E - p_A + \frac{\rho}{2} c_E^2 \sin^2 \alpha_E (1 - \xi_{CE}) - \frac{\rho}{2} c_A^2 \sin^2 \alpha_A (1 - \xi_{CA}) \quad . \tag{3.39}$$

It describes the characteristic total pressure difference between the tip gap inlet and outlet which is the driving force for the tip gap leakage mass flow $\dot{m}_k$. The total pressure drop Δp_B takes into account the static and dynamic pressure upstream and downstream of the tip gap. As the kinetic energy of the circumferential components upstream and downstream of the clearance have no influence on the leakage mass flow rate, the total pressure drop is defined only with the axial components of those kinetic energies.
The equation for the mass flow rate of one streamtube then has the form

$$\begin{aligned} \Delta p_B = &- \frac{\rho}{2} c_E^2 \cos^2 \alpha_E (1 - \xi_{CE}) - \frac{\rho}{2} c_A^2 \cos^2 \alpha_A (1 - \xi_{CA}) \\ &+ \frac{1}{2} \frac{\dot{m}}{\rho} \sum_{i=1}^{n} \frac{1}{A_i^2} \xi_i (1 + \cot^2 \alpha_i) \quad . \end{aligned} \tag{3.40}$$

Due to the dependency of the flow angles on the leakage mass flow rate itself, further considerations have to be made in order to obtain a full description of the mass flow rate through the streamtubes.

Angular Momentum Equation

The change of momentum entering and exiting a control volume equals the sum of all external forces acting on the control volume. It is necessary to know those forces in order to calculate the change in momentum for the chosen control volume. In the case at hand, pressure forces $P_{i,k}$ at the boundaries of the volume and friction forces $R_{i,k}$ have to be considered while gravitational and centripetal forces are neglected (see Fig. 3.16). A formulation of the momentum equation perpendicular to the inlet and outlet planes of the control volume demands the knowledge of the pressures acting on those planes. Therefore, in order to reduce the unknowns in the equations, the momentum equation is formulated for the circumferential direction where only much smaller forces due to the variable pressure in circumferential direction are present.

Considering potentially variable radii $r_{i,k}$ at the control volume entry and outlet, the momentum equation can be formulated as

$$\begin{aligned} &\dot{m}_k \left(r_{i,k} w_{i,k} \cos \alpha_{i,k} - r_{i+1,k} w_{i+1,k} \cos \alpha_{i+1,k} \right) = \\ &r_{i,k} R_{i,k} \cos \alpha_{i,k} + f_L r_{i+1,k} R_{i+1,k} \cos \alpha_{i+1,k} - r_{i,k} P_{i,k} - f_L r_{i+1,k} P_{i+1,k}. \end{aligned} \tag{3.41}$$

The left hand side of Eq. (3.41) contains the change in momentum from the inlet to the out-

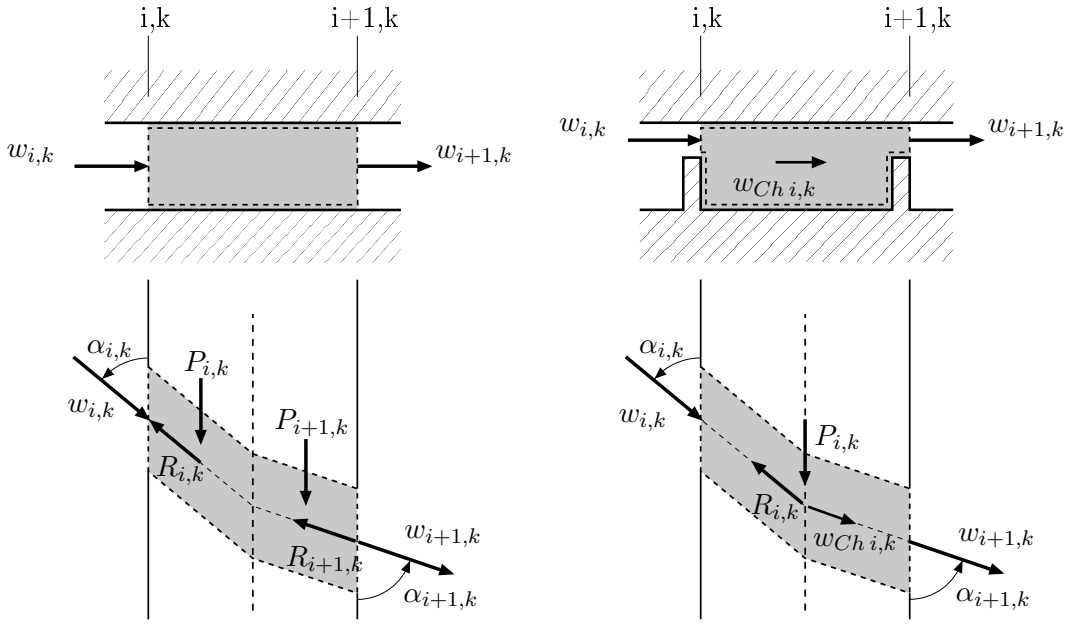

a) smooth shroud b) shroud with fins

Figure 3.16: Pressure and friction forces for a) smooth shroud b) shroud with fins. (adapted from [27])

let of the control volume. The right hand side shows the external forces acting on the control volume due to mixing or wall friction ($R_{i,k}$ and $R_{i+1,k}$) and the pressure forces acting on the sidewalls of the volume due to the variable pressure in circumferential direction ($P_{i,k}$ and $P_{i+1,k}$).

For a shroud with fins, the force $R_{i,k}$ acting on the control volume due to mixing effects in the labyrinth chamber, can be obtained making classic labyrinth seal assumptions. It is assumed that the pressure at the inlet fin defines the pressure in the labyrinth chamber. It is further assumed, that the entire pressure drop in the labyrinth chamber occurs due to the deceleration of the incoming flow, while the acceleration of the flow towards the outlet fin occurs loss free. Therefore the energy equation for the labyrinth chamber yields

$$\frac{1}{2}w_{i,k}^2(1-\xi_{i,k}) = \frac{1}{2}w_{Ch\,i,k}^2 \Rightarrow w_{Ch\,i,k} = w_{i,k}\sqrt{1-\xi_{i,k}}, \tag{3.42}$$

where $w_{Ch\,i,k}$ stands for the flow velocity in the labyrinth chamber (see Fig. 3.16 b). The momentum equation in circumferential direction for the labyrinth chamber for constant radii yields

$$\dot{m}_k[w_{i,k}\cos\alpha_{i,k} - w_{Ch\,i,k}\cos\alpha_{Ch\,i,k}] + R_{i,k}\cos\alpha_{R_{i,k}} = 0. \tag{3.43}$$

Assuming the flow does not change its direction during the mixing process in the chamber, the flow angle in the labyrinth chamber $\alpha_{Ch\,i,k}$ can be set equal to the flow angle of the incoming mass flow $\alpha_{i,k}$. Further it is assumed, that the external force $R_{i,k}$ is oriented against the flow velocity in the labyrinth chamber. This leads to $\alpha_{i,k} = \alpha_{Ch\,i,k} = \alpha_{R\,i,k}$.
With the relation found for the flow velocity in the labyrinth chamber (Eq. 3.42), the momentum equation (Eq. 3.43) transforms to

$$\dot{m}_k w_{i,k} \cos\alpha_{i,k} \left(1 - \sqrt{1-\xi_{i,k}}\right) + R_{i,k} \cos\alpha_{i,k} = 0.$$

Which can be written as

$$R_{i,k} = \dot{m}_k w_{i,k} \left(1 - \sqrt{1-\xi_{i,k}}\right),$$

or with the momentum loss coefficient $\bar{\xi}_{i,k}$

$$\bar{\xi}_{i,k} = 1 - \sqrt{1-\xi_{i,k}}. \tag{3.44}$$

as

$$R_{i,k} = \dot{m}_k w_{i,k} \bar{\xi}_{i,k}, \tag{3.45}$$

Equation (3.44) shows the relation between the momentum loss coefficient $\bar{\xi}$ to the pressure loss coefficient ξ.

With the knowledge of the external force $R_{i,k}$, the momentum equation in circumferential direction Eq. (3.41) can be written as

$$\begin{aligned} &\dot{m}_k[r_{i,k} w_{i,k} \cos\alpha_{i,k}(1-\bar{\xi}_{i,k}) - r_{i+1,k} w_{i+1,k} \cos\alpha_{i+1,k}(1+f_L\bar{\xi}_{i+1,k})] \\ &+ r_{i,k} P_{i,k} + f_L r_{i+1,k} P_{i+1,k} = 0. \end{aligned} \tag{3.46}$$

Assuming the external forces R and P acting on the control volume are known, Eq. (3.46) can be used to calculate the flow angle $\alpha_{i+1,k}$ in the support point $i+1,k$ for a given pressure at the inlet into the control volume $p_{i,k}$.
At the entry of the tip gap the flow angle is determined by the swirl of the meridional flow $c_E \cos\alpha_E$ and therefore all flow angles in the subsequent support points of one streamtube can be determined. Substituting the flow velocities in Eq. (3.46) with the continuity equation (3.28) the flow angles in the support points can be determined by

$$\cot\alpha_{1,k} = \frac{\rho}{\dot{m}_k} A_{1,k} c_E \cos\alpha_E \frac{1-\bar{\xi}_{CE}}{1+\bar{\xi}_{WE}}, \qquad \text{for} \quad i=1 \tag{3.47}$$

for the first set of support points after the tip gap entry and

$$\cot\alpha_{i+1,k} = \frac{A_{i+1,k} r_i}{A_{i,k} r_{i+1}} \frac{1-\bar{\xi}_{i,k}}{1+f_L \bar{\xi}_{i+1,k}} \cot\alpha_{i,k} + \frac{\rho}{\dot{m}_k^2} \frac{A_{i+1,k}}{1+f_L\bar{\xi}_{i+1,k}} (P_{i,k}\frac{r_i}{r_{i+1}} + f_L P_{i+1,k}), \tag{3.48}$$
$$\text{for} \quad i=(1\ldots n-1)$$

for all subsequent support points along the streamtube.
Due to the conditions at the gap inlet (Eq. 3.47), the flow angles in the support points depend on the leakage mass flow rate and the circumferential velocity component upstream of the gap. The momentum equations show that for a decreasing cross-sectional area A from one support point to the next, the flow angle increases. They also show that due to mixing or friction $\bar{\xi} > 0$, the angular momentum of the tip gap flow decreases even if the cross-sectional areas are constant.
By substituting the flow angles in the energy equation (3.40) with Eq. (3.47) and (3.48) a single equation for the mass flow rate $\dot{m}_k$ can be obtained, that only depends on the the total pressure drop Δp_B, the loss coefficients $\xi_{i,k}$ and the local streamtube cross-sectional areas $A_{i,k}$. This equation can then be solved iteratively.
Before the leakage mass flow rate can be calculated in this way, $A_{i,k}$ and $\xi_{i,k}$ have to be determined iteratively from the shape of the streamlines. The iterative procedure to determine all characteristic parameters of the tip gap flow will be discussed in more detail in Sec. 3.6.

Simplifications and Dimensionless Formulation

For a dimensionless description of the tip gap flow, the influence of the boundary conditions at the gap inlet and outlet have to be eliminated, while the influence of the seal geometry is preserved. Due to the dependency of the loss coefficients on the Reynolds number and the local flow angles, no complete similarity for different inlet pressures and velocities can be achieved. The total pressure drop Δp_B, which contains the static pressure drop between inlet and outlet alongside the axial velocity components of the flow, is used as a reference value for the inlet angular momentum. The dimensionless relative inlet kinetic energy is defined as

$$C_E^{\times} = \frac{\frac{\rho}{2} c_E^2 \cos^2\alpha_E}{\Delta p_B} \qquad . \tag{3.49}$$

$C_E^{\times}$ represents the ratio of the stagnation pressure of the circumferential flow velocity at the tip gap inlet $\frac{\rho}{2} c_E^2 \cos^2\alpha_E$ to the total axial pressure drop over the shroud Δp_B.

In order to obtain a reference value for the leakage mass flow rate, first a reference cross-sectional

area A_B has to be defined

$$A_B = 2\pi r_B s_B. \tag{3.50}$$

Here s_B is the minimal radial clearance width at a radius r_B for a centric rotor. With the total pressure drop Δp_B a leakage mass flow rate can be defined

$$\dot{m}_B = A_B \sqrt{2\rho \Delta p_B} \qquad , \tag{3.51}$$

which represents the maximum mass flow rate for the tip gap, assuming the kinetic energy is dissipated completely in the labyrinth chambers. In this way a reference value is obtained, which not only can be used to determine the effectiveness of a seal, but also to relate the variable mass flow rates of the single streamtubes.

For the following calculations a shrouded turbine rotor with a number of n fins shall be considered with constant radii of the support points $r_{i,k} = r_{i+1,k}$. For the pressure loss coefficients ξ_C and ξ_W, describing the losses at the tip gap inlet and outlet relative to the meridional flow velocity c and the tip gap flow velocity w, the following assumptions can be made: With $\xi_{CE} = 0$ it is assumed that the entire inlet kinetic energy of the mass flow into the tip gap is available. The main flow velocity in the meridional channel after the turbine rotor blade row has, by setting $\xi_{CA} = 1$, no influence on the tip gap flow. The coefficient ξ_{WE} describes the entry pressure loss related to the entry tip gap velocity $w_{1,k}$ and can be chosen $\xi_{WE} = 0$. The degree of mixing of the tip gap outlet velocity $w_{n,k}$ is described by the coefficient $\xi_{WA} \cong \xi_n$. Assuming that the pressure at the tip gap outlet has the constant value of p_A, $\xi_{WA} = 1$ can be set. This also means that the tip gap outlet velocity is dissipated entirely.
Under those assumptions and simplifications, the equations (3.35), (3.36) and (3.37) yield a general formulation for the pressure in the support points

$$p_{i,k} = p_A + \frac{1}{2}\frac{\dot{m}_k}{\rho}\left[\sum_{\nu=i}^{n}\left(\xi_{\nu,k}\frac{1+\cot^2\alpha_{\nu,k}}{A_{\nu,k}^2}\right) - \frac{1+\cot^2\alpha_{i,k}}{A_{i,k}^2}\right] \qquad . \tag{3.52}$$

It is assumed, that for a sufficiently fine discretization in circumferential direction (number of j streamtubes indicated by index k), the pressure forces $P_{i,k}$ acting on the sidewalls of the control volume, due to the variable pressure distribution in circumferential direction, are rather small and can be neglected. This leads to simplfied momentum equations (3.47), (3.48), describing the flow angles in the support points, which can be combined to

$$\cot\alpha_{i,k} = c_E \cos\alpha_E \frac{\rho}{\dot{m}_k} A_{i,k}\left(1-\bar{\xi}_{CE}\right)\prod_{\nu}^{i-1}\left(1-\bar{\xi}_{\nu,k}\right) \qquad . \tag{3.53}$$

Equation (3.53) shows, that for an ideal labyrinth, where the complete kinetic energy is dissipated in the labyrinth chamber ($\xi_{i,k} = 1 \Rightarrow \bar{\xi}_{i,k} = 1$), the flow through the tip gap is completely axial after the labyrinth chamber. This also means, that the flow is turned stronger in axial direction for higher $\xi_{i,k}$ values which leads to different streamtube shapes in areas with higher loss coefficients (for example at the narrowest tip gap at the φ=0°-position).
For complete dissipation of the kinetic energy at the last fin at the gap outlet $\xi_n = \xi_{WA} = 1$, Eq. (3.52) can be transformed, using the definition of the flow angles (Eq. 3.53), the momentum loss coefficients (Eq. 3.44) and the total pressure drop (Eq. 3.39) into an equation describing the mass flow rate of the streamtube k

$$\dot{m}_k = \sqrt{\frac{2\rho\Delta p_B}{\sum_{i=1}^{n} \frac{\xi_{i,k}}{A_{i,k}^2}}} \quad . \tag{3.54}$$

Due to the relation between the pressure loss coefficient ξ and the momentum loss coefficient $\bar{\xi}$ (Eq. 3.44), the leakage mass flow rate is independent of the inlet swirl. Considering the definition of the theoretical maximum mass flow rate for the tip gap $\dot{m}_B$ (Eq. 3.51), a dimensionless mass flow rate $M^\times$ can be defined

$$M_k^\times = \frac{\dot{m}_k}{\dot{m}_B} = \frac{1}{\sqrt{\sum_{i=1}^{n} \left(\xi_{i,k} \frac{A_B^2}{A_{i,k}^2} \right)}} \quad . \tag{3.55}$$

It is useful to additionally define a dimensionless total tip gap mass flow rate $\dot{m}^\times$

$$\dot{m}^\times = \frac{\sum_{k=1}^{j} \dot{m}_k}{\dot{m}_B} \quad . \tag{3.56}$$

For a concentric rotor ($e = 0$) the cross-sectional areas in the denominator of Eq. (3.55) are of equal size $A_{i,k} = A_B$. This means for an ideal labyrinth where the kinetic energy is dissipated entirely and the loss coefficients are therefore $\xi_{i,k} = 1$, the leakage mass flow rate is proportional to $\frac{1}{\sqrt{n}}$, which is in good accordance to known models for the labyrinth mass flow rate [24].

With Eq. (3.54) and (3.44) the equation for the flow angles in the support points (Eq. 3.53) can be written as

$$\cot^2 \alpha_{i,k} = C_E^\times A_{i,k}^2 (1 - \xi_{CE}) \prod_{\nu=1}^{i-1} (1 - \xi_{\nu,k}) \sum_{\nu=1}^{n} \frac{\xi_{\nu,k}}{A_{\nu,k}^2} \quad . \tag{3.57}$$

With the mass flow rate (3.54) and the flow angles (3.57), the pressure distribution in the tip gap (3.52) can be described in the form of a dimensionless pressure $P^{\times}$

$$P^{\times}_{i,k} = \frac{p_{i,k} - p_A}{\Delta p_B} = \frac{-\frac{1}{A^2_{i,k}} + \sum_{\nu=i}^{n} \frac{\xi_{\nu,k}}{A^2_{\nu,k}}}{\sum_{\nu=1}^{n} \frac{\xi_{\nu,k}}{A^2_{\nu,k}}} \quad . \tag{3.58}$$

Equation (3.58) shows that for a purely axial flow, where the cross-sectional areas of all individual streamtubes are constant, a constant pressure distribution in circumferential direction is obtained. This only holds true for constant loss coefficients. This would be the case for a concentric rotor with a purely axial inlet flow. In this case the dependence of the loss coefficients (Eq. 3.32) and (Eq. 3.34) of the local radial clearance width $\tilde{s}$, the maximum pressure occurs at the position with the narrowest clearance width at φ= 0° (see Fig. 3.11). This result is in good accordance with known theories for the pressure distribution in tip gaps (see Lomakin quoted in [7]).

For constant loss coefficients in circumferential direction it can be shown, that the pressure in streamtubes with converging cross-sectional areas is higher than in those with diverging cross-sectional areas. This is the reason for the characteristic pressure maximum ahead of the position with the narrowest clearance width for an eccentric rotor for swirled inlet conditions. This shift of the pressure maximum ahead of the narrowest position at φ=0° in rotational direction causes cross forces on the rotor, which excite an oscillating motion of the rotor perpendicular to the direction of displacement as described in Sec. 3.1.3 and seen in Fig. 3.9.

3.3 Passive Tip-Injection

The equations up to this point describe the model of the tip gap of a shrouded turbine blade row with and without fins. In order to implement passive tip-injection into this model, a formulation for the pressure and the flow angle in the corresponding support points has to be found. Later, those equations describing the passive tip-injection will be combined with the equations describing the flow through the tip clearance in order to obtain a complete model, describing the flow through a tip gap with passive tip-injection.

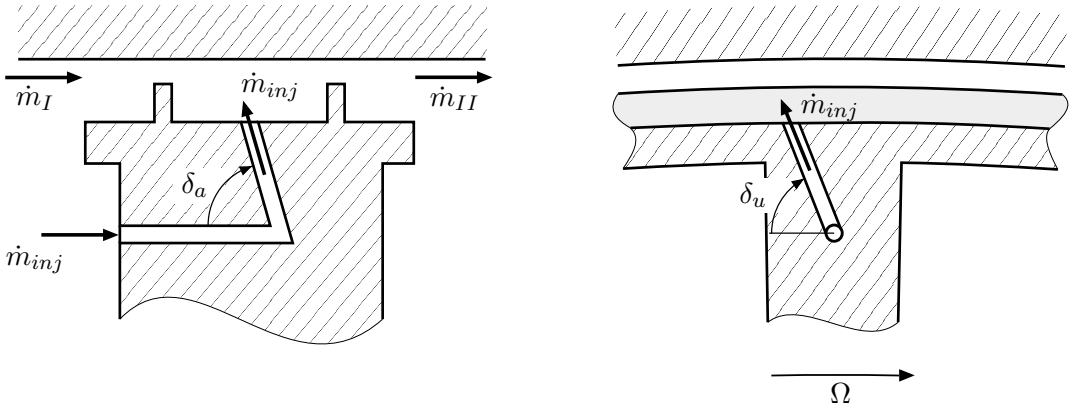

Figure 3.17: Shrouded turbine rotor with fins and with passive tip-injection. Injection channel inclined against the axial direction by δ_a and against the circumferential direction by δ_u.

3.3.1 Discretization

As the mass flow through the tip gap with passive tip-injection is different upstream and downstream of the injection chamber, the control volume of the tip gap is divided into three sections as seen in Fig. (3.18). Section I constitutes the tip gap upstream of the injection chamber section Ch, inj. Section II is the tip gap downstream of the injection chamber. Additionally the injection channel, running from the blade leading edge to the injection chamber, is treated as a separate control volume marked by the index inj. Upstream of the injection position in the section I, the tip gap mass flow $\dot{m}_I$ enters the tip clearance. Through the bore hole in the blade leading edge the injection mass flow $\dot{m}_{inj}$ enters the injection channel, driven by the pressure difference between the total pressure at the blade leading edge and the static pressure in the injection chamber. Through the injection channel, which is inclined against both, the axial direction and the circumferential direction, the injection mass flow enters the tip gap, where it mixes out with the tip gap flow $\dot{m}_I$ in the injection chamber. Downstream of the injection chamber the combined mass flow $\dot{m}_{II}$ exits the tip gap via the remaining labyrinth chambers into the main flow, where it is mixed out. The discretization of the tip gap into support points in axial direction and seperate streamtubes in circumferential direction shall be the same as in

section (3.2).

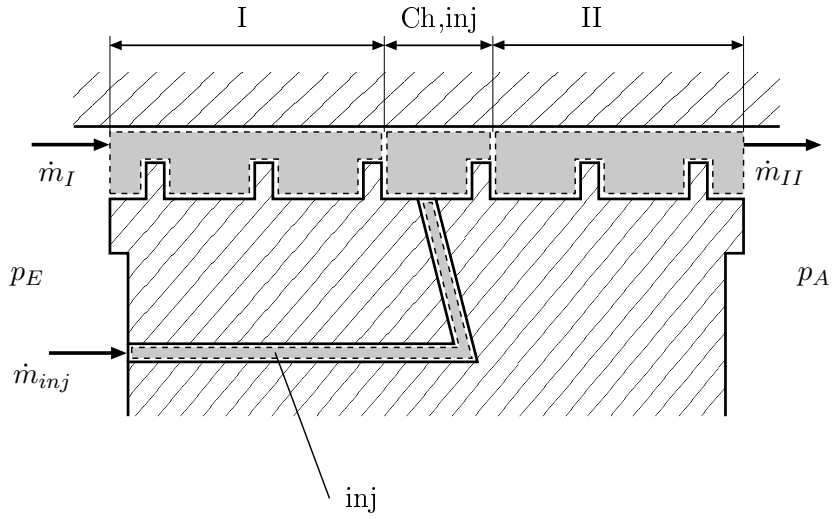

Figure 3.18: Seperation of the tip gap in different control volumes due to the changing mass flows.

3.3.2 Governing Equations

For a simple integration of the equations describing the passive tip-injection into the model for the tip gap flow, the same assumptions for incompressibility are made for the injection mass flow. This allows the use of the same basic fluid mechanical equations to describe the injection mass flow, as the ones used above to describe the tip gap flow.

Continuity Equation

In contrast to the tip gap flow without tip-injection, here the mass flow along the tip gap is not constant. Due to the additional injection mass flow, which is injected into the tip gap in the injection chamber, no continuous streamline can be defined and the tip gap is divided in the sections described above. For the relatively small pressure differences between the blade row inlet and outlet, used later for numerical calculations, the assumption of an incompressible flow can be made. For such a flow the flow velocities can be described by the mass flow, the local cross-section and the density of the fluid by

$$w_I = \frac{\dot{m}_I}{\rho A_I \sin \alpha_I} \quad ,$$

$$w_{inj} = \frac{\dot{m}_{inj}}{\rho A_{inj}} \quad , \tag{3.59}$$

$$w_{II} = \frac{\dot{m}_{II}}{\rho A_{II} \sin \alpha_{II}} \quad .$$

The mass balance for the injection chamber control volume yields

$$\dot{m}_{II} = \dot{m}_I + m_{inj} \quad , \tag{3.60}$$

for the mass flow through the tip gap downstream of the injection chamber.

Momentum Equation

Due to the mixing of the tip gap inlet mass flow $\dot{m}_I$ with the injection mass flow $\dot{m}_{inj}$, no single streamline passing all the way from the tip gap inlet to the tip gap outlet can be defined. Therefore the energy equation as used in section (3.2) is not applicable. This means in order to obtain an equation describing the pressure in the corresponding support points of the injection chamber, the momentum equation in axial direction has to be used. In axial direction the pressure drop between support points is much higher than that between the support points in circumferential direction. Therefore the pressure forces acting on the inlet and outlet walls of the control volume cannot be neglected. In addition to that the pressure forces acting on the inlet and outlet walls of the control volume, vary in radial direction. While it can be assumed that the pressure on the control volume wall-section between the casing and the fin tip is equal to the pressure in the respective support point, special considerations have to be made for the pressure along the fin sidewall.
As mentioned before, when defining the momentum loss coefficients (Eq. 3.44), the pressure in the control volume can only be considered constant on the value of the pressure at the volume inlet for an ideal labyrinth chamber. Due to the complex processes in the injection chamber, this assumption can no longer be made. In order to describe the pressure acting on the sidewall of the labyrinth fins p', the control volume is defined in such a way, that the control volume side walls A' are set off the labyrinth side walls. The offset is chosen in such a way, so that the areas in which the potential losses due to the dissipation of the kinetic energy of the incoming flow and due to the acceleration of the flow towards the following support point occur, are excluded from the control volume. This allows for a definition of the pressure at the labyrinth fin sidewalls as shown later. The form of the control volume also allows a formulation of the momentum

equation in axial direction without the friction force R. By using the momentum equation in axial direction and defining the control volume boundaries as seen in Fig. (3.19), the pressure in the injection channel does not occur in the equations.

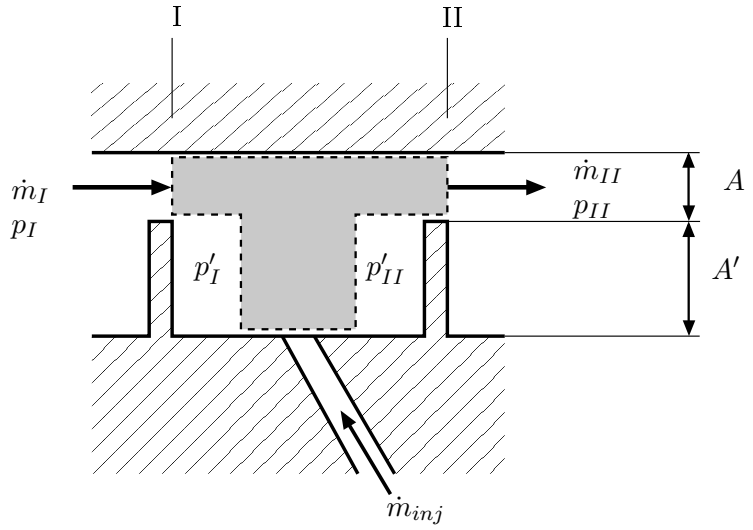

Figure 3.19: Control volume of the injection chamber.

Applying the momentum equation in axial direction for the control volume yields

$$\dot{m}_I w_{I,a} + p_I A_I + p'_I A'_I - \dot{m}_{inj} w_{inj,a} - p'_{II} A'_{II} - p_{II} A_{II} - \dot{m}_{II} w_{II,a} = 0 \quad , \tag{3.61}$$

where the index a indicates the axial components of the flow velocities $w_{I,a} = w_I \sin \alpha_I$.
It can be shown that the approximation

$$\frac{A'_I}{A_I}(p'_I - p'_{II}) = -\frac{1}{2} w_{II}^2 \rho$$

can be used if is assumed that $A_I = A_{II}$ [9]. The approximation was derived for an ideal labyrinth chamber with no injection, but shall be used for this case with tip-injection as well. This allows the transformation of Eq. (3.61) into

$$p_I - p_{II}\frac{A_{II}}{A_I} = \frac{\dot{m}_{II}}{\rho A_{II}}\left(\frac{1}{2}\frac{1+\cot^2\alpha_{II}}{A_{II}} + \frac{1}{A_I}\right) - \frac{\dot{m}_I^2}{\rho A_I^2} + \frac{\dot{m}_{inj} w_{inj,a}}{A_I} \quad . \tag{3.62}$$

Here the flow angle α_{II} and the incoming mass flow $\dot{m}_I$ as well as the injection mass flow $\dot{m}_{inj}$ are still unknown, and further calculations have to be made.

Angular Momentum Equation

In order to calculate the flow angle α_{II} at the support point downstream of the injection position, the angular momentum equation is applied to the injection chamber control volume. By choosing the momentum equation in circumferential direction, the relatively small pressure forces acting on the sidewalls of the control volume P_I and P_{II} can be neglected again, as they were in Eq. (3.41). Here the inclination of the injection channel in circumferential direction has to be considered especially. The angular momentum equation for the injection chamber yields

$$\dot{m}_I r_I w_I \cos\alpha_I \left(1-\bar{\xi}_I\right) - \dot{m}_{inj} r_{inj} \left(w_{inj,u} - r_{inj}\Omega\right) - \dot{m}_{II} r_{II} w_{II} \cos\alpha_{II} = 0 \quad , \tag{3.63}$$

when the pressure forces P_I, P_{II} are neglected, $f_L = 0$ for the labyrinth chamber and the friction force R_I is implemented proportional to the incoming momentum by the momentum loss coefficient $\bar{\xi}_I$. In Eq. (3.63) the absolute injection mass flow velocity is represented by $(w_{inj,u} - r_{inj}\Omega)$, which takes the rotational speed $r_{inj}\Omega$ of the rotor and thus of the injection slot into consideration. The index u indicates the circumferential velocity components.
By substituting the flow velocities with the continuity equations Eq. (3.59), Eq. (3.63) can be transformed into

$$\cot\alpha_{II} = \frac{\rho A_{II}}{\dot{m}_{II}^2}\left[\frac{\dot{m}_I^2}{\rho A_I}\cot\alpha_I\left(1-\bar{\xi}_I\right) - \dot{m}_{inj}\left(w_{inj,u} - r_{inj}\Omega\right)\right] \quad , \tag{3.64}$$

describing the flow angle in the downstream support point of the injection chamber. In Eq. (3.62) and Eq. (3.64) the mass flows $\dot{m}_I$ and $\dot{m}_{inj}$ are still unknown and shall be determined in the following section.

Injection Mass Flow

In this work a passive tip-injection shall be investigated. In contrast to the active tip-injection, the injection mass flow of the passive tip-injection depends on both, the total pressure at the blade leading edge and the static pressure in the injection chamber. The injection channel leads from the blade leading edge through the blade and the shroud into the tip gap. Here the injection channel leads into a labyrinth chamber. Experiments have shown, that this form of the injection channel leads to structural problems in the turbine blade and a through shroud injection is more feasible [10]. Although, in order to study the basic effects of passive tip-injection on the cross forces acting on a turbine rotor, the blade leading edge injection channel geometry shall be used. Applying the energy equation on the injection channel yields

$$p_{t,E} - p_{Ch,inj} = \frac{1}{2}\rho w_{inj}^2 \xi_{inj}, \tag{3.65}$$

where $p_{t,E}$ is the total pressure at the blade leading edge (i.e. total pressure upstream of the blade row) and $p_{Ch,inj}$ represents the pressure in the injection chamber. The pressure loss coefficient of the injection channel ξ_{inj} consists of the turbulent loss coefficient for the injection channel $\xi_{t,inj}$, the inlet loss coefficient at the bore hole in the blade leading edge $\xi_{E,inj}$ and the loss coefficient representing the losses due to the bends in the injection channel $\xi_{b,inj}$

$$\xi_{inj} = \xi_{E,inj} + \xi_{t,inj} + \xi_{b,inj} \quad .$$

While constant values for the given injection channel geometry for $\xi_{E,inj}$ and $\xi_{b,inj}$ can be found in literature [12], the turbulent pressure loss coefficient $\xi_{t,inj}$ depends on the injection channel length L_{inj}, diameter d_{inj} and Reynolds number $Re_{inj} = \frac{w_{inj} d_{inj}}{\nu}$ and therefore on the injection mass flow $\dot{m}_{inj}$ itself

$$\xi_{t,inj} = \frac{L_{inj}}{d_{inj}} \lambda_{t,inj} \quad \text{with} \quad \lambda_{t,inj} = 0.3164\, Re_{inj}^{-\frac{1}{4}} \quad . \tag{3.66}$$

With the continuity equations (3.59), the injection mass flow $\dot{m}_{inj}$ can be obtained from Eq. (3.65)

$$\dot{m}_{inj} = \rho A_{inj} \sqrt{\frac{2}{\rho} \frac{(p_{t,E} - p_{Ch,inj})}{\xi_{inj}}} \quad , \tag{3.67}$$

where A_{inj} is the injection channel cross-sectional area. A_{inj} can be calculated, assuming a circular cross section of the injection channel, by $A_{inj} = \frac{d_{inj}^2}{4}\pi$ with the injection channel diameter d_{inj}. The dimensionless injection channel diameter γ can be defined by

$$\gamma = \frac{d_{inj}}{s + h} \quad , \tag{3.68}$$

using the nominal clearance width s and the fin height h.
By relating the injection mass flow to the tip gap inlet mass flow the dimensionless relative injection mass flow can be obtained

$$\dot{m}_{inj}^{\times} = \frac{\dot{m}_{inj}}{\dot{m}_I} \quad . \tag{3.69}$$

3.4 Unified Model

Now that equations describing the tip gap flow of an eccentric rotor and equations describing the passive tip-injection are available, the tip gap flow of a shrouded turbine rotor with fins with passive tip-injection can be described. Therefore the equations describing the pressure and the flow angles in the support points forming the tip-injection control volume are implemented into the model for the tip gap flow from Sec. 3.2. The discretization is the same in both models, therefore the tip-injection equations can easily be inserted by substituting the respective indices I and II. For the following calculations a turbine shroud with n fins is considered. For the injection slots a variable position between the support points n_1 and n_2 is chosen. Therefore the indices in the tip-injection equations can be substituted by $I = n_1$ and $II = n_2$. The mass flow in streamtube k entering the tip gap is marked $\dot{m}_{1,k}$, mixes with the injection mass flow $\dot{m}_{inj,k}$ and exits the tip gap as $\dot{m}_{2,k} = \dot{m}_{1,k} + \dot{m}_{inj,k}$.
The injection slot is modeled to be a continuous injection gap in circumferential direction rather than a number of discrete injection slots. Therefore no special considerations are made for the index k, where k identifies the support point position in circumferential direction and the streamtube.

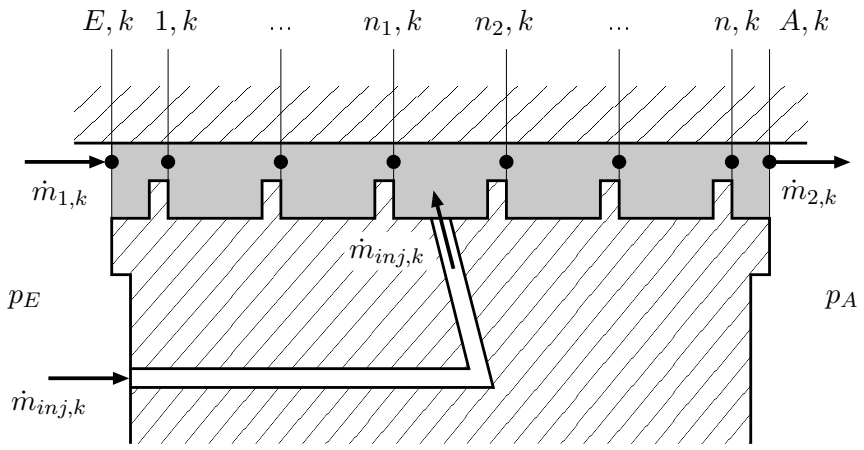

Figure 3.20: Geometry of tip gap of a shrouded turbine rotor with passive tip-injection.

For the unified model the same division of the tip gap in three different sections, identified by their corresponding indices is made. The model obtained here shall be valid for a labyrinth seal, therefore the control parameter f_L can be set to f_L=0. The pressure forces acting on the sidewalls of the injection control volume in circumferential direction P, shall be neglected.
In the following sections the complete set of equations describing the flow through the tip gap with tip-injection in terms of flow angles, pressure and leakage mass flow rate is shown.

3.4.1 Flow Angle

- Tip gap entry $i = 1$:

$$\cot \alpha_{1,k} = \frac{\rho}{\dot{m}_{1,k}} A_{1,k} c_E \cos \alpha_E \frac{1 - \bar{\xi}_{CE}}{1 + \bar{\xi}_{WE}} \tag{3.70}$$

- Tip gap upstream of the injection position $i = 1 \ldots n_1 - 1$:

$$\cot \alpha_{i+1,k} = \frac{A_{i+1,k}}{A_{i,k}} \frac{r_{i,k}}{r_{i+1,k}} \left(1 - \bar{\xi}_{i,k}\right) \cot \alpha_{i,k} \tag{3.71}$$

- Injection Position $i = n_2$:

$$\cot \alpha_{n2,k} = \frac{\rho A_{n2,k}}{\dot{m}^2_{2,k}} \left[\frac{\dot{m}^2_{1,k}}{\rho A_{n1,k}} \cot \alpha_{n1,k} \left(1 - \bar{\xi}_{n1,k}\right) - \dot{m}_{inj,k} \left(w_{inj,u,k} - r_{inj,k} \Omega\right) \right] \tag{3.72}$$

- Tip gap downstream of the injection position $i = n_2 \ldots n - 1$:

$$\cot \alpha_{i+1,k} = \frac{A_{i+1,k}}{A_{i,k}} \frac{r_{i,k}}{r_{i+1,k}} \left(1 - \bar{\xi}_{i,k}\right) \cot \alpha_{i,k} \tag{3.73}$$

3.4.2 Pressure

- Tip gap entry $i = 1$:

$$p_E - p_{1,k} = \frac{1}{2} \frac{\dot{m}^2_{1,k}}{\rho} \left[\frac{1}{A^2_{1,k}} (1 + \xi_{WE})(1 + \cot^2 \alpha_{1,k}) \right] - \frac{\rho}{2} c^2_E (1 - \xi_{CE}), \tag{3.74}$$

- Tip gap upstream of the injection position $i = 1 \ldots n_1 - 1$:

$$p_{i,k} - p_{i+1,k} = \frac{1}{2} \frac{\dot{m}^2_{1,k}}{\rho} \left[\frac{1}{A^2_{i+1,k}} (1 + \cot^2 \alpha_{i+1,k}) - \frac{1}{A^2_{i,k}} (1 - \xi_{i,k})(1 + \cot^2 \alpha_{i,k}) \right] \tag{3.75}$$

- Injection Position $i = n_2$:

$$p_{n_1,k} - p_{n_2,k}\frac{A_{n_2,k}}{A_{n_1,k}} = \frac{\dot{m}_{2,k}}{\rho A_{n_2,k}}\left(\frac{1}{2}\frac{1+\cot^2\alpha_{n_2,k}}{A_{n_2,k}} + \frac{1}{A_{n_1,k}}\right) - \frac{\dot{m}_{1,k}^2}{\rho A_{n_1,k}^2} + \frac{\dot{m}_{inj,k}w_{inj,a,k}}{A_{n_1,k}} \quad . \tag{3.76}$$

- Tip gap downstream of the injection position $i = n_2 \ldots n-1$:

$$p_{i,k} - p_{i+1,k} = \frac{1}{2}\frac{\dot{m}_{2,k}^2}{\rho}\left[\frac{1}{A_{i+1,k}^2}(1+\cot^2\alpha_{i+1,k}) - \frac{1}{A_{i,k}^2}(1-\xi_{i,k})(1+\cot^2\alpha_{i,k})\right] \tag{3.77}$$

3.4.3 Leakage Mass Flow Rate

The composition of the equations for pressure and flow angle in the support points to form a complete model of the tip gap with tip-injection could be done by simple combination of the corresponding equations. The leakage mass flow rate although has to be considered in more detail. By adding the equations (3.74) to (3.77) for the pressure in the support points of one streamtube similar to Eq. (3.38) in the form

$$\begin{aligned} &p_E - p_1 \; + \; p_1 - p_2 \; + \; \ldots \\ &+ \; p_{n_1-1} - p_{n_1} \; + \; p_{n_1} - p_{n_2} \; + p_{n_2} - p_{n_2+1} \; + \ldots \\ &+ \; p_{n-1} - p_n \; + \; p_n - p_A = p_E - p_A \quad , \end{aligned} \tag{3.78}$$

and assuming the simplifications $\xi_{CE} \approx 0$, $\xi_{WE} = 0$, $\xi_{CA} = 1$ and $\xi_{WA} \cong \xi_n = 1$, an equation for the pressure drop from tip gap inlet to tip gap outlet in the form

$$\begin{aligned} \Delta p_B = &-\frac{\rho}{2}c_E^2\cos^2\alpha_E + \frac{1}{2}\frac{\dot{m}_{1,k}^2}{\rho}\left[\sum_{\nu=1}^{n_1-1}\left(\frac{\xi_{\nu,k}}{A_{\nu,k}^2}\left(1+\cot^2\alpha_{\nu,k}\right)\right) + \frac{1}{A_{n_1,k}^2}\left(1+\cot^2\alpha_{n_1,k}\right)\right] \\ &+ \frac{\dot{m}_{2,k}^2}{\rho A_{n_2,k}A_{n_1,k}} - \frac{\dot{m}_{1,k}^2}{\rho A_{n_1,k}^2} + \frac{\dot{m}_{inj,k}w_{inj,a,k}}{A_{n_1,k}} \\ &+ \frac{1}{2}\frac{\dot{m}_{2,k}^2}{\rho}\left[\sum_{\nu=n_2}^{n}\left(\frac{\xi_{\nu,k}}{A_{\nu,k}^2}\left(1+\cot^2\alpha_{\nu,k}\right)\right)\right] \quad , \end{aligned} \tag{3.79}$$

can be obtained. Solving Eq. (3.79) for $\dot{m}_{1,k}$, yields a quadratic equation for the mass flow rate

of the respective streamtube. This quadratic equation can be solved with the simple quadratic formula

$$\dot{m}_{1,k} = \frac{-B \pm \sqrt{B^2 - 4AC}}{2A} \quad ,$$

$$\text{with} \quad A = \frac{1}{\rho A_{n_2,k} A_{n_1,k}} + \frac{1}{2\rho}\left[\sum_{\nu=n_2}^{n}\left(\frac{\xi_{\nu,k}}{A_{\nu,k}^2}\left(1+\cot^2\alpha_{\nu,k}\right)\right)\right]$$

$$+ \frac{1}{2\rho}\left[\sum_{\nu=1}^{n_1-1}\left(\frac{\xi_{\nu,k}}{A_{\nu,k}^2}\left(1+\cot^2\alpha_{\nu,k}\right)\right) + \frac{1}{A_{n_1,k}^2}\left(1+\cot^2\alpha_{n_1,k}\right)\right] - \frac{1}{\rho A_{n_1,k}^2} \quad ,$$

$$B = 2\dot{m}_{inj,k}\left[\frac{1}{\rho A_{n_2,k} A_{n_1,k}} + \frac{1}{2\rho}\left[\sum_{\nu=n_2}^{n}\left(\frac{\xi_{\nu,k}}{A_{\nu,k}^2}\left(1+\cot^2\alpha_{\nu,k}\right)\right)\right]\right] \quad ,$$

$$C = -\Delta p_B - \frac{\rho}{2} c_E^2 \cos^2\alpha_E + \frac{\dot{m}_{inj,k} w_{inj,a,k}}{A_{n_1,k}}$$

$$+ \dot{m}_{inj,k}^2\left[\frac{1}{\rho A_{n_2,k} A_{n_1,k}} + \frac{1}{2\rho}\left[\sum_{\nu=n_2}^{n}\left(\frac{\xi_{\nu,k}}{A_{\nu,k}^2}\left(1+\cot^2\alpha_{\nu,k}\right)\right)\right]\right] \quad . \tag{3.80}$$

With the equation for the leakage mass flow rate the model for the tip gap leakage flow with tip-injection is complete. In Eq. (3.80) the loss coefficients $\xi_{i,k}$ and the cross-sectional areas of the streamtubes $A_{i,k}$ have to be determined iteratively out of the shape of the streamtubes. The injection mass flow $\dot{m}_{inj,k}$ can be determined iteratively using Eq. (3.67) and the pressure equation in the injection chamber.
The iterative process to find solutions for the obtained tip gap model shall be discussed in more detail in the following section (3.6).

3.5 Cross Forces

With the model, developed above, the pressure distribution in the tip gap $p_{i,k}$ and the tip gap leakage mass flow $\dot{m}_{1,k}$ and $\dot{m}_{2,k}$ can be determined. As shown in Sec. 3.1.3, this allows the calculation of the cross forces due to the pressure distribution in circumferential direction of the tip gap Q_p and the variable tangential forces on the turbine rotor blades Q_s.

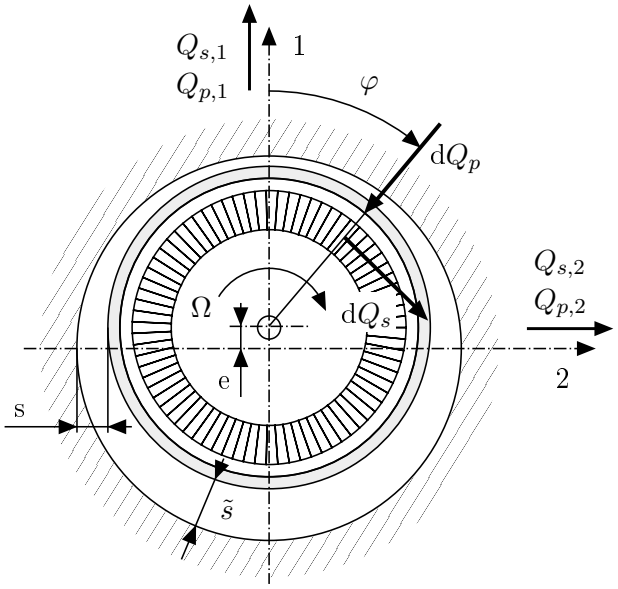

Figure 3.21: Cross forces acting on the eccentric turbine rotor. (adapted from [27])

Thomas-Alford Force

With the tip gap leakage mass flow $\dot{m}_{cl}(\varphi)$ the local tip loss coefficient $\zeta(\varphi)$ can be determined, which allows the calculation of the Thomas-Alford forces acting on the rotor. With Eq. (3.16), (3.15) and Eq. (3.18) the Thomas-Alford forces $Q_{s,1}$, $Q_{s,2}$ in the reference frame $\mathbf{e}_1$, $\mathbf{e}_2$ can be described in the form

$$Q_{s,1} = \frac{F_{u,id}}{2\pi} \int_0^{2\pi} g(\zeta) \frac{\mathrm{d}\dot{m}_{cl}}{\dot{m}_0} \sin\varphi \, \mathrm{d}\varphi \quad ,$$

$$Q_{s,2} = -\frac{F_{u,id}}{2\pi} \int_0^{2\pi} g(\zeta) \frac{\mathrm{d}\dot{m}_{cl}}{\dot{m}_0} \cos\varphi \, \mathrm{d}\varphi \quad .$$

Here $g(\zeta)$ is a correction factor, taking into account, that the drop in stage efficiency due to the tip-leakage mass flow is not directly proportional to the leakage loss coefficient ζ.
Here it is assumed, that $g(\zeta) = 1$, which leads with $\int_0^{2\pi} \mathrm{d}\varphi = 2\pi$ to the simplified equations for the Thomas-Alford forces

$$\begin{aligned} Q_{s,1} &= \frac{F_{u,id}}{\dot{m}_0} \int_0^{2\pi} \sin\varphi \, \mathrm{d}\dot{m}_{cl} \quad , \\ Q_{s,2} &= -\frac{F_{u,id}}{\dot{m}_0} \int_0^{2\pi} \cos\varphi \, \mathrm{d}\dot{m}_{cl} \quad . \end{aligned} \tag{3.81}$$

The total tip-leakage mass flow $\dot{m}_{cl}$ can be calculated by adding all discrete tip-leakage mass flows

$$\dot{m}_{cl} = \sum_{k=1}^{j} \dot{m}_k \quad . \tag{3.82}$$

Therefore the integrals can be written as sums, which leads to

$$\begin{aligned} Q_{s,1} &= \frac{F_{u,id}}{\dot{m}_0} \sum_{k=1}^{j} \dot{m}_k \sin\varphi_{1,k} \quad , \\ Q_{s,2} &= -\frac{F_{u,id}}{\dot{m}_0} \sum_{k=1}^{j} \dot{m}_k \cos\varphi_{1,k} \quad . \end{aligned} \tag{3.83}$$

Note that for set ups with passive tip-injection, in order to calculate the tip-leakage mass flow $\dot{m}_{cl}$, the mass flow $\dot{m}_2$ downstream of the injection position has to be used. In that way, it is taken into account that the injection mass flow $\dot{m}_{inj}$, extracted at the blade leading edge from the meridional flow, does not contribute to stage work.

It is assumed that the main flow downstream of the turbine stage is purely axial. This means the circumferential velocity downstream of the rotor blade row is zero. Therefore the ideal tangential force related to the meridional mass flow rate $\frac{F_{u,id}}{\dot{m}_0}$ can be set equal to the circumferential velocity upstream of the turbine rotor

$$\frac{F_{u,id}}{\dot{m}_0} = \Delta c_u = c_n \cot\alpha_E \quad . \tag{3.84}$$

Pressure Force

With the known pressure distribution in the discrete support points $p_{i,k}$ the equations (3.19) and (3.20) can be transformed, as to show the pressure forces acting on the rotor in the reference frame $\mathbf{e}_1$, $\mathbf{e}_2$

$$\begin{aligned} Q_{p,1} &= -\sum_{i=1}^{n}\sum_{k=1}^{j}(\Delta a_i\, r_i\, \Delta\varphi_{i,k}\, p_{i,k}\, \cos\varphi_{i,k}) \quad , \\ Q_{p,2} &= -\sum_{i=1}^{n}\sum_{k=1}^{j}(\Delta a_i\, r_i\, \Delta\varphi_{i,k}\, p_{i,k}\, \sin\varphi_{i,k}) \quad . \end{aligned} \tag{3.85}$$

A_{surf} here is substituted by the control volume rotor surface area $\Delta a_i\, r_i\, \Delta\varphi_{i,k}$.

Dimensionless Formulation

By defining a characteristic pressure force Q_B and relating the cross forces Q_s and Q_p to it, a dimensionless formulation for the cross forces can be obtained. This dimensionless formulation is needed, when two geometry set ups (for example a tip gap with and without passive tip-injection) or different operating points (different eccentricities e) are to be evaluated in respect to their cross force generating properties.
For a maximum eccentricity of $e{=}s$, the pressure drop from the tip gap inlet to the outlet can reach the maximum value of Δp_B. Hence the pressure difference in circumferential direction has a maximum value of $\frac{\Delta p_B}{2}$. For a linear pressure drop from the tip gap inlet to the outlet, the maximum pressure force can be defined as

$$Q_B = \frac{\Delta p_B}{2} r_B \pi \frac{b}{2}\frac{e}{s} \quad . \tag{3.86}$$

It is assumed that this maximum pressure force for a given eccentricity changes linearly with the eccentricity.
For a dimensionless description and comparability of the cross forces Q, relative, dimensionless cross forces $Q^{\times}$ of the form

$$\begin{aligned} Q_s^{\times} &= \frac{Q_s}{Q_B} \quad , \\ Q_p^{\times} &= \frac{Q_p}{Q_B} \quad , \end{aligned} \tag{3.87}$$

are formed.

3.6 Numerical Solution

The equations in the unified model for the flow angles in the support points $\alpha_{i,k}$ (Eq. 3.70-3.73), show that they depend on the streamtube cross-sectional areas $A_{i,k}$ (Eq. 3.27) as well as on the loss coefficients $\xi_{i,k}$ (Eq. 3.34), which themselves are derived from the flow angles. Therefore, the flow angles have to be determined iteratively. It can be also seen that the pressure in the support points $p_{i,k}$ (Eq. 3.74-3.77), the mass flow entering the tip gap $\dot{m}_{1,k}$ (Eq. 3.80) and the injection mass flow $\dot{m}_{inj,k}$ (Eq. 3.67) all depend on each other as well as on the flow angles. To find solutions for those parameters, further iteration loops are necessary.

Figure (3.22) shows the iterative procedure, which was solved numerically, to determine the flow angles, the pressure in the support points and the mass flow entering the tip gap as well as the injection mass flow for the tip gap of a shrouded turbine rotor with passive tip-injection. The knowledge of those parameters allows the determination of the cross forces Q_p and Q_s on the rotor. The first step of the procedure is to determine the initial values $\alpha_{i,k}^{(0)}$ and calculate $\varphi_{i,k}^{(0)}$, $\Delta\varphi_{i,k}^{(0)}$ and $A_{i,k}^{(0)}$. Subsequently, the initial values $\xi_{i,k}^{(0)}$, $\dot{m}_{1,k}^{(0)}$ and $\dot{m}_{inj,k}^{(0)}$ are set.

In the first iterative loop $\mathrm{M^I}$, the new values $\xi_{i,k}^{(1)}$ and $\alpha_{i,k}^{(1)}$ are calculated and improved iteratively until $|\xi_{i,k}^{(1)} - \xi_{i,k}^{(0)}|$ satisfies the precision ε^I. Those updated values are then used to calculate $\dot{m}_{1,k}^{(1)}$. This procedure is repeated in the loop $\mathrm{M^{II}}$ until $\dot{m}_{1,k}^{(1)}$ is determined to a precision of ε^{II}. Subsequently, the geometry of the streamtubes is updated ($\varphi_{i,k}^{(1)}$, $\Delta\varphi_{i,k}^{(1)}$, $A_{i,k}^{(1)}$) and the values of $\alpha_{i,k}^{(2)}$ and $\dot{m}_{1,k}^{(2)}$ are calculated to a precision of ε^{III} in loop $\mathrm{M^{III}}$. At this stage it is possible to calculate the pressure $p_{i,k}$ in the support points. The pressure in the injection chamber is then used to calculate the injection mass flow $\dot{m}_{inj,k}^{(1)}$. In the iteration loop $\mathrm{M^{IV}}$ the entire iterative procedure is restarted with the updated injection mass flow until a precision of $|\dot{m}_{inj,k}^{(1)} - \dot{m}_{inj,k}^{(0)}| < \varepsilon^{IV}$ is reached. This iterative procedure produces all the relevant values for the flow through the tip gap. Hence, it is possible to calculate the cross forces Q_p (Eq. 3.85) and Q_s (Eq. 3.83) on the rotor. For a given eccentricity e this further allows the determination of the cross force coefficients q_p and q_s (Eq. 3.21, 3.22) as well as the dimensionless parameters presented in Sec. 3.2.2.

Note that in the chosen discretization the number of support points in axial direction is given by the number of labyrinth fins on the shroud. Therefore the mesh of support points can not be refined arbitrarily in axial direction. This can lead to disadvantageous aspect ratios of the control volumes in the tip gap.
Further, the location of the support points and hence the control volume boundaries vary for every iteration step, that updates the flow angles $\alpha_{i,k}$ and therefore the geometry of the streamtubes. This leads to numerical problems in the form of divergence of the iterative procedure instead of the desired convergence. This is overcome by using a relaxation factor $\beta < 1$ for the update of the tip gap mass flow $\dot{m}_{1,k}$ in the iterative loop $\mathrm{M^{III}}$. Although, divergence issues still limit the range of some parameters in the parameter study, performed in Ch. 4.

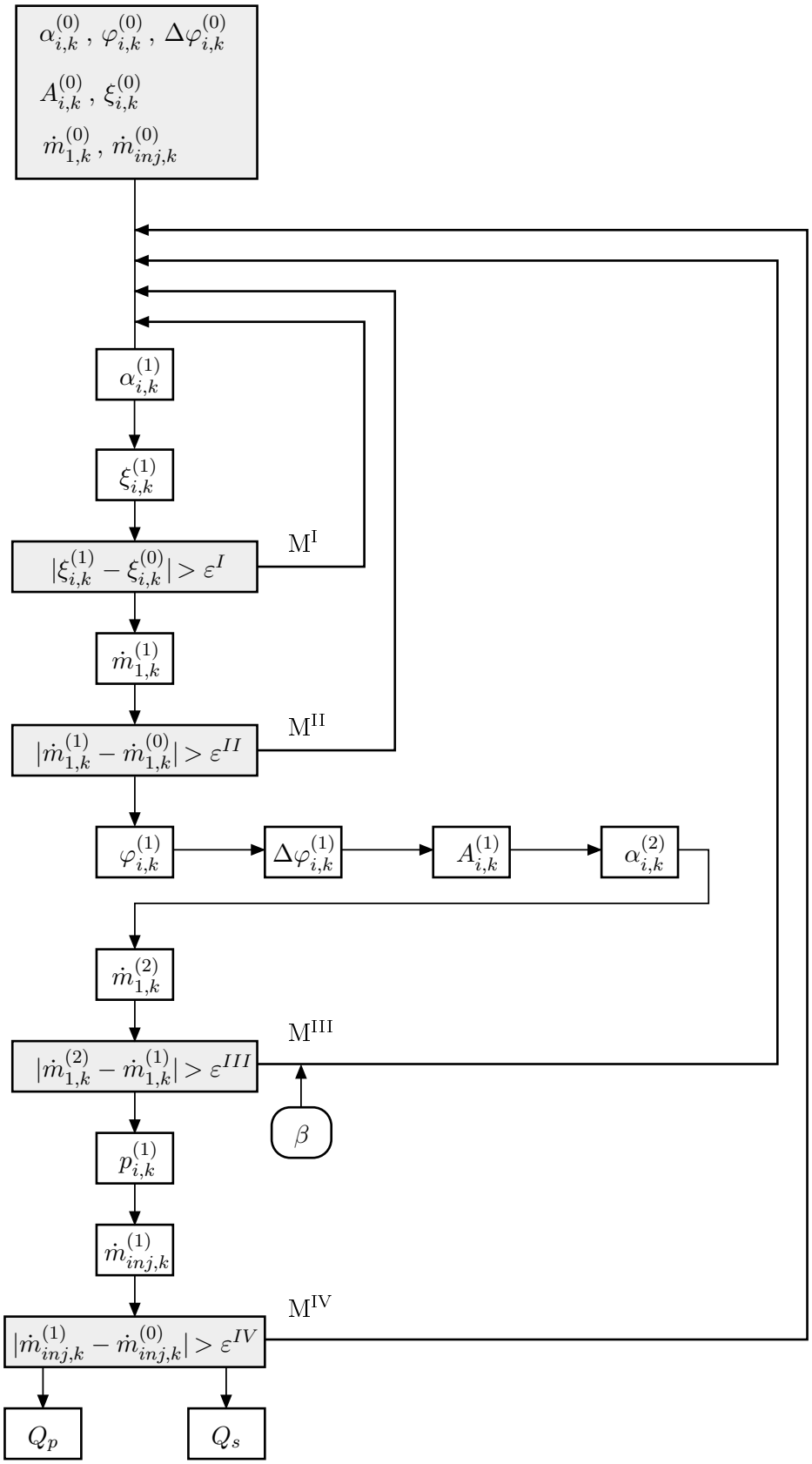

Figure 3.22: Iteration plan.

4 Results and Discussion

To learn which influence a passive tip-injection has on the cross force coefficients and the tip excitation of an eccentric rotor, in this chapter the model obtained in Ch. 3 shall be applied to an exemplary shrouded turbine rotor with fins. The relevant properties are calculated according to the iterative procedure described in Sec. 3.6.

To fully understand the results of such a calculation, first the fundamental effects of a swirled flow through a tip gap of an eccentric rotor have to be studied and fully understood. Therefore in the first part of this chapter, the model is applied to a simplified tip gap geometry without passive tip-injection.

After the underlying effects and correlations are established, in the second part of this chapter the full set of equations from Sec. 3.4 will be applied to tip gap setup with passive tip-injection. First, reference values for the flow and cross force properties will be obtained by applying the model to a setup with identical geometric properties, but without passive tip-injection.
An extensive parameter study will be performed and the results for the setups with and without passive tip-injection will be compared and evaluated. The focus lies especially on the tip gap pressure and leakage mass flow rate distribution in circumferential direction as well as on the resulting cross forces and excitation parameters for the rotor. The parameters studied in this work are:

- eccentricity e of the rotor
- radial clearance width s of the tip gap
- total pressure drop Δp_B
- relative inlet kinetic energy $C_E^{\times}$
- injection slot inclination angle in circumferential direction δ_u
- injection position in axial direction n_1

4.1 Shrouded Turbine Rotor with two Fins without Passive Tip-Injection

To demonstrate the fundamental principle of cross force generation by a swirled flow through a clearance as described by Urlichs [27], the model from Ch. 3 is applied to a simple shrouded turbine rotor with two fins without passive tip-injection (see Fig. 4.1).

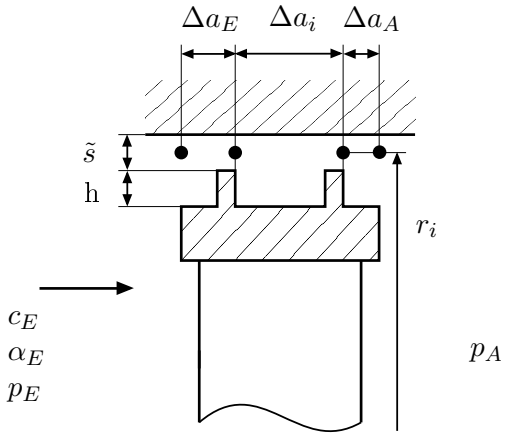

Figure 4.1: Geometry setup for a shrouded turbine rotor with two fins.

To apply the tip gap model obtained in Sec. 3.4 to the geometry depicted in Fig. (4.1) the number of labyrinth fins is reduced to two and the injection slot width is reduced to zero. This allows the generation of results for a setup without passive tip-injection. The operating point and geometry parameters for the exemplary calculations seen in Tab. (4.1) are chosen to resemble those used in literature [27] for an easier verification of the model and the obtained results.

Table 4.1: Parameters and constants for the chosen geometry and point of operation

geometry		point of operation and fluid properties	
$\Delta a_E = 4e\text{-}3$ m	$h = 4e\text{-}3$ m	$\rho = 1.2$ kg/m^3	$p_E = 1.04e5$ N/m^2
$\Delta a_i = 10e\text{-}3$ m	$e/s = 0.5$	$c_{E,n} = 41$ m/s	$p_A = 1e5$ N/m^2
$\Delta a_A = 4e\text{-}3$ m	$m_N = 9$	$\alpha_E = 20°$	
$s = 1e\text{-}3$ m	$n = 2$	$\Delta p_B = 5e3$ N/m^2	
$r_i = 104e\text{-}3$ m	$j = 20$	$C_E^{\times} = 1.52$	

4.1.1 Fundamental Effects

To demonstrate the effect of a swirled flow through the tip gap, the pressure in the support points $p_{i,k}$ and the mass flow rate of the streamtubes $\dot{m}_k$ are calculated. Figure (4.2) shows the

relative dimensionless pressure distribution $P^{\times}$ (Eq. 3.58) at the axial positions $i = 1$ and $i = 2$. Figure (4.3) shows the relative dimensionless mass flow $M^{\times}$ (Eq. 3.55) for the streamtubes in circumferential direction of the tip gap.

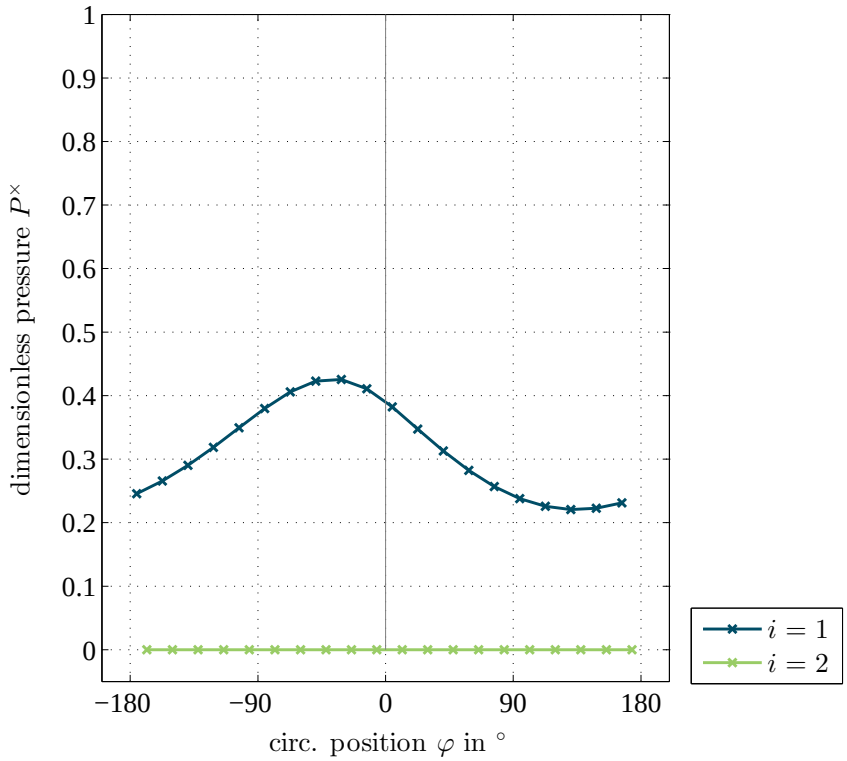

Figure 4.2: Dimensionless pressure $P^{\times}$ against the circumferential direction φ, for axial positions $i = 1$ and $i = 2$.

The characteristic peak of the relative pressure $P^{\times}$ ahead of the narrowest clearance at position φ=0° is clearly observable. As described in Sec. 3.2.2, ξ_{WA}=1 for complete mixing at the last fin of the shroud. Therefore the pressure at the last fin is equal to the outlet pressure and the relative pressure is equal to zero as displayed in Fig. (4.2).
Corresponding to the pressure distribution, the relative leakage mass flow rate $M^{\times}$ has its minimum in the streamtube with the highest relative pressure as seen in Fig. (4.3). The small off-set of the leakage mass flow minimum relative to the pressure maximum can be explained by the narrower streamtube width around the φ=0°-position compared to the streamtube width in the remaining positions in circumferential direction. $M^{\times}$ can be seen as an entity qualifying leakage mass flow and streamtube width at a given position and its curve should therefore only be considered in terms of shape and not absolute magnitude.

The pressure and momentum loss coefficients ξ and $\bar{\xi}$ are inversely correlated with the clearance width $\tilde{s}$ as can be seen in Eq. (3.34). Therefore the loss coefficients are higher for streamtubes

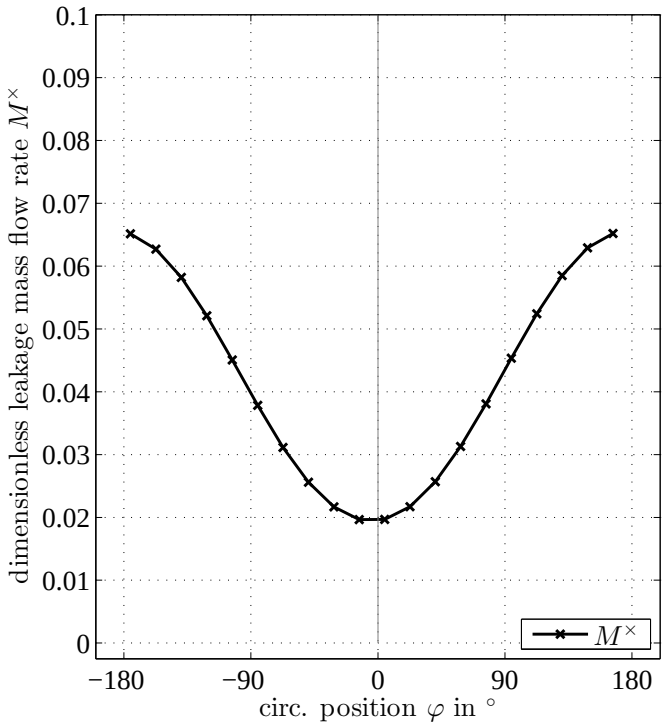

Figure 4.3: Dimensionless leakage mass flow rate $M^\times$ against the circumferential direction φ.

with smaller cross-sectional areas. This allows a higher pressure drop in such streamtubes from tip gap inlet to tip gap outlet. For a purely axial flow this effect causes a symmetric pressure distribution with a maximum pressure at the narrowest clearance. In that case, the resulting force acts solely against the direction of displacement and acts as a restoring force, reducing the eccentricity of the rotor as shown by Lomakin (quoted in [7]) and seen later in the parameter study.

As a result of the swirled flow through the clearance, the streamlines have the form of spirals. Along those spirals the cross-sectional area of the streamtubes vary, due to the eccentricity of the rotor and the changing radial clearance width $\tilde{s}$ of the tip gap. For the swirled flow, streamtubes ahead of the narrowest clearance in rotational direction have converging cross-sectional areas. Therefore the pressure maximum occurs ahead of the narrowest clearance in rotational direction. This leads to a pressure distribution asymmetric to φ=0°-position and a resulting cross force $Q_{p,2}$ perpendicular to the direction of displacement.

Corresponding to the pressure distribution the leakage mass flow also varies asymmetrically in circumferential direction. This varying leakage flow modifies the tangential forces acting on the turbine blades. The resultant of those tangential forces results in cross forces perpendicular to the direction of displacement ($Q_{s,2}$) and in the direction of displacement ($Q_{s,1}$).

The asymmetry in the pressure and leakage mass flow distribution in circumferential direction causes resulting cross forces Q_s and Q_p on the rotor. Note that cross forces perpendicular to the direction of displacement $Q_{p,2}$ and $Q_{s,2}$, potentially cause instability in the form of a whirling motion for an eccentric rotor.

By varying the eccentricity e of the rotor a better understanding of the effects under investigation can be gained.

4.1.2 Eccentricity

Figure (4.4) shows the impact of varying the relative eccentricity e/s on the cross forces and the relative pressure and leakage mass flow rate distributions. For a centric rotor at e=0, the cross-sectional areas are constant along the streamtubes. Therefore the pressure and momentum loss coefficients are constant in circumferential direction for the respective axial position i. As expected, the pressure distribution is constant in circumferential direction, as is the leakage mass flow as seen in Fig. (4.4). Therefore no cross forces act on the rotor despite the swirl of the flow.

With growing eccentricity of the rotor, the cross forces generated by the varying pressure and leakage mass flow rate distributions Q_p and Q_s increase linearly. Figure (4.4) shows that the components of the pressure force $Q_{p,1}$ and $Q_{p,2}$ are of the same magnitude. $Q_{p,1}$ acts against the direction of displacement and therefore as a restoring force on the rotor. $Q_{p,2}$ acts perpendicular to the direction of displacement and adds energy to the whirling motion of the rotor.

The cross forces resulting from the variable tangential force on the rotor blading, $Q_{s,1}$ and $Q_{s,2}$ (Thomas-Alford forces) differ considerably in magnitude. $Q_{s,2}$, acting perpendicular to the direction of displacement, is clearly higher than $Q_{s,1}$. As seen in the definition of the Thomas-Alford forces, $Q_{s,2}$ is the main effect of a variable tangential force on the rotor blading. $Q_{s,1}$ results only from the φ=0°–position shift of the leakage mass flow distribution minimum and acts as seen in Fig. (4.4) in direction of displacement due to its positive sign.

The overall behavior of the model for a shrouded turbine rotor with two fins agrees well with literature [27], what strengthens the confidence in the model and its use on a upscaled and modified shroud setup with and without passive tip-injection in the following sections.

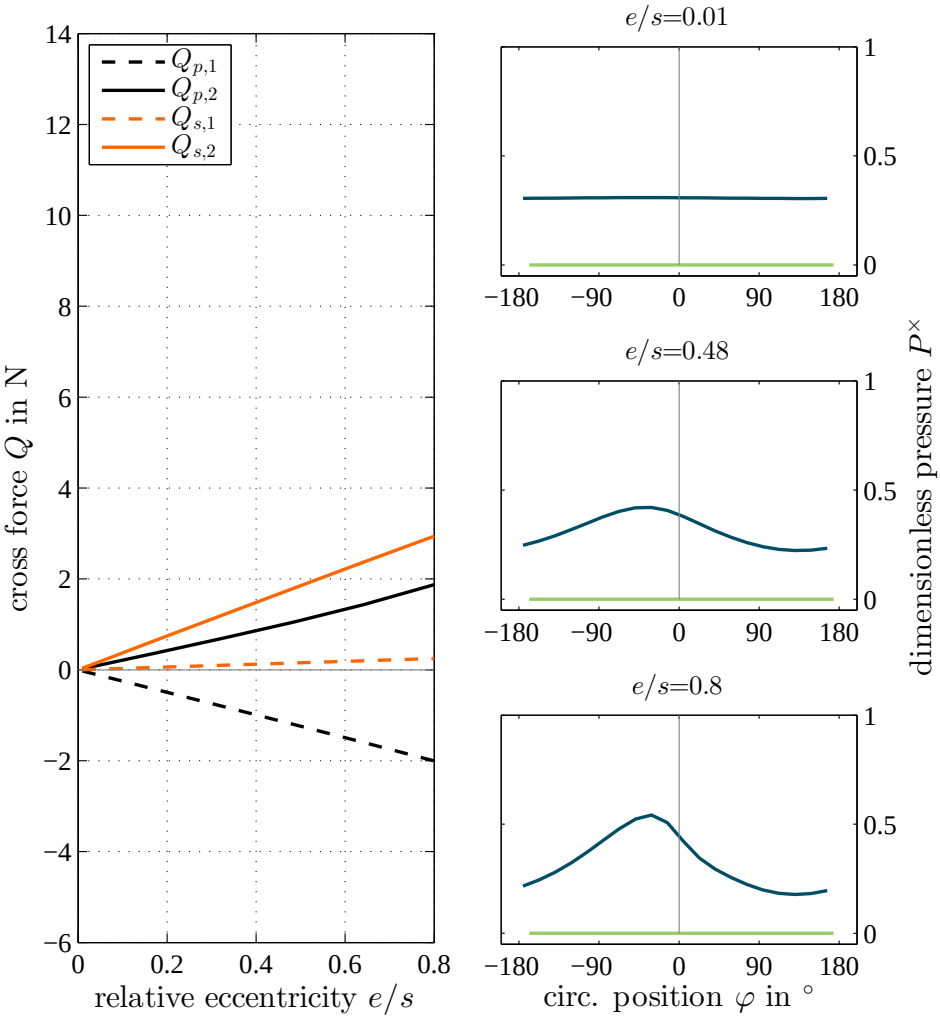

Figure 4.4: Cross forces Q against the relative eccentricity e/s and dimensionless pressure $P^{\times}$ for chosen relative eccentricities.

4.2 Shrouded Turbine Rotor with six Fins without Passive Tip-Injection

For a shrouded turbine rotor with fins and passive tip-injection (see Sec. 4.3) reference values for the tip gap flow have to be obtained. Therefore a geometry setup of the same geometric properties, but without passive tip-injection is considered. Except for the number of fins, which was increased to n=6, the point of operation and the geometry of the shrouded turbine rotor setup with two fins is kept the same (see Tab. 4.1), as seen in Fig. (4.5).
Due to the constant axial distance between the support points Δa_i (i.e. labyrinth chamber lengths), the overall tip gap length increases for the six finned model in comparison to the geometry with two fins. This has a significant impact on the results and is taken into consideration when interpreting the following, especially the pressure cross force Q_p and all parameters derived thereof.

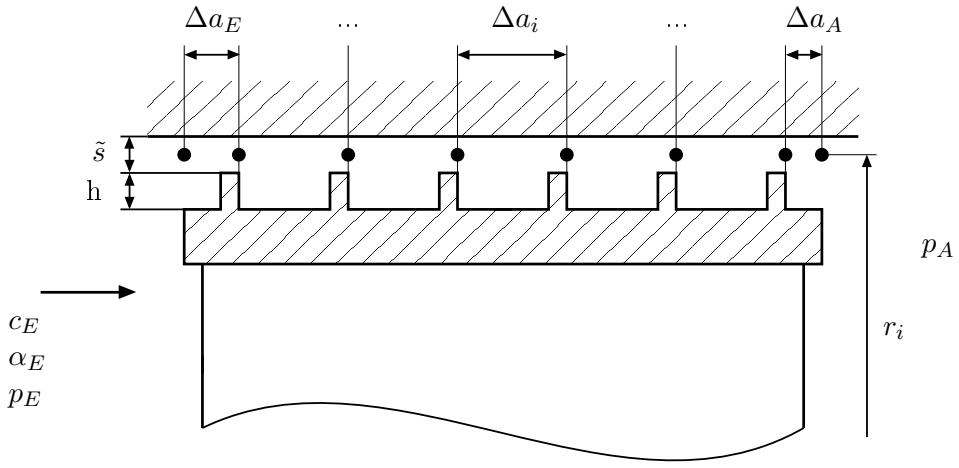

Figure 4.5: Geometry setup for a shrouded turbine rotor with six fins.

4.2.1 Fundamental Effects

Figure (4.6) shows the same characteristic curve shapes of the pressure distribution in circumferential direction as for the shroud with two fins (Fig. 4.2). Due to the increased number of fins, the pressure levels on the first and the subsequent fins are significantly elevated. The gradual pressure drop from fin to fin in axial direction is as expected from classic labyrinth seal theory [24]. The characteristic maximum pressure shift ahead of the narrowest clearance position at φ=0° is also clearly visible. Note that the pressure maxima move closer to the φ=0°-position with progressing fin number i in axial direction. It can be shown, that the pressure maximum occurs in the streamtube with the highest gradients of cross-sectional area convergence [27]. The same goes for minimum pressure streamtubes and the increase of the cross-sectional area respectively. Along a streamtube starting ahead of the narrowest clearance and crossing over

the φ=0°-position, the cross-sectional areas decrease before the narrowest clearance and increase directly after.

As expected for a labyrinth seal with multiple fins, the relative leakage mass flow rate $M^{\times}$ seen in Fig. (4.7) is considerably reduced in comparison to the two finned labyrinth seal. Due to the same parameters of operation used here as for the setup with two fins, the theoretical maximum leakage mass flow rate $\dot{m}_B$ is the same for the two setups investigated so far. Therefore a reduction in $M^{\times}$ indicates a reduced total tip-leakage flow $\dot{m}_{cl}$ for the setup with six fins compared to the setup with two fins. This reduction in tip-leakage mass flow results from the increased velocity dissipation, due to an increased number of labyrinth chambers.

To investigate the influence of operation point and geometry parameters on the tip gap flow and the resulting cross forces, in the following sections the computational results for a variable eccentricity e, radial clearance width s, total pressure drop Δp_B and relative inlet kinetic energy $C_E^{\times}$ are shown.

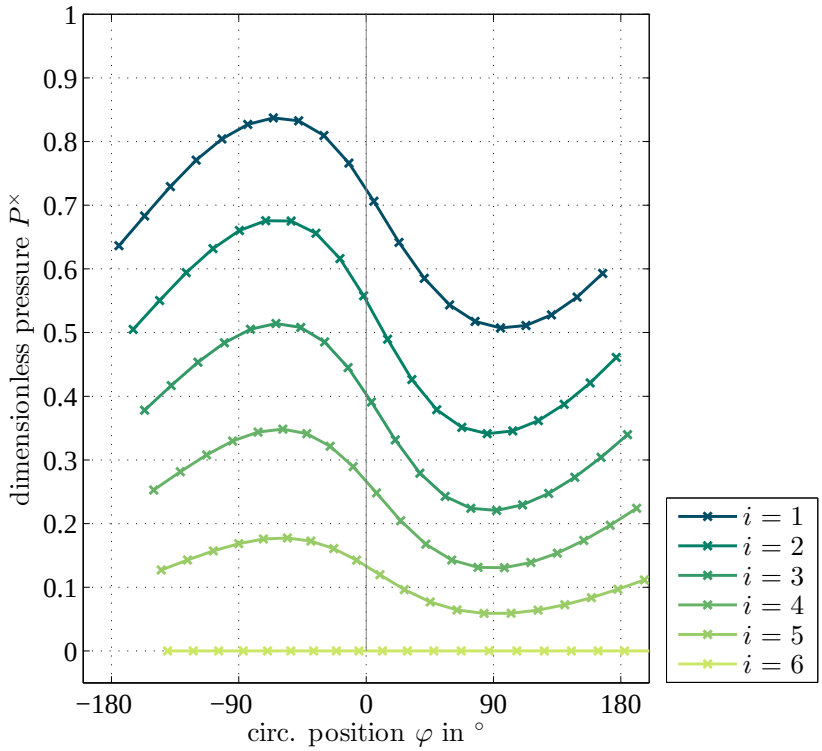

Figure 4.6: Dimensionless pressure $P^{\times}$ against the circumferential direction φ, for axial positions $i = 1 \ldots 6$.

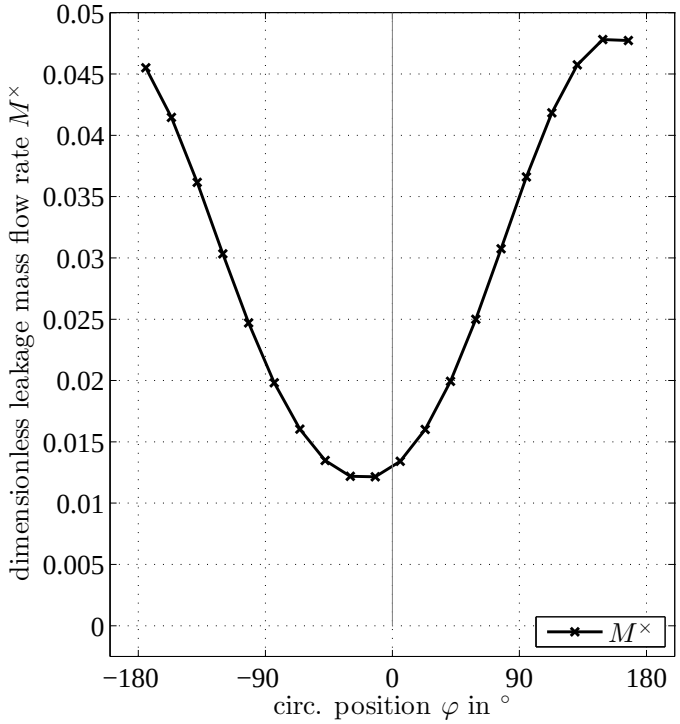

Figure 4.7: Dimensionless leakage mass flow rate $M^\times$ against the circumferential direction φ.

4.2.2 Eccentricity

Figure (4.8) shows the cross forces resulting from the asymmetrical pressure and leakage mass flow rate distribution for varying values of the relative eccentricity e/s. The linear relation between the forces and the eccentricity is clearly shown except for negligible deviations in the $Q_{p,1}$ curve.

The magnitude of the forces, resulting from the pressure distribution Q_p, clearly increases compared to the shroud with two fins. This is due to the larger rotor surface A_{surf}, the pressure acts on and the increased pressure levels along the tip gap.

The cross forces, which result from the variable leakage mass flow Q_s change too. As they solely depend on the overall leakage mass flow and the position of the minimum leakage mass flow streamtube in circumferential direction, they do not increase in the same way as the pressure forces. $Q_{s,2}$ acts perpendicular to the direction of displacement and is reduced, due to the reduced overall leakage mass flow. At the same time $Q_{s,1}$ is increased, due to the greater shift of the minimum leakage mass flow streamtube position from the φ=0°–position compared to the shroud with two fins. The shift increases, due to the increased streamline length in the longer tip gap with the same inlet flow angle α_E.

The cross forces increase linearly and therefore allow the definition of a constant increase factor in the form of $q = Q/e$. q which was introduced in Sec. 3.1, Eq. (3.21, 3.22) as cross force

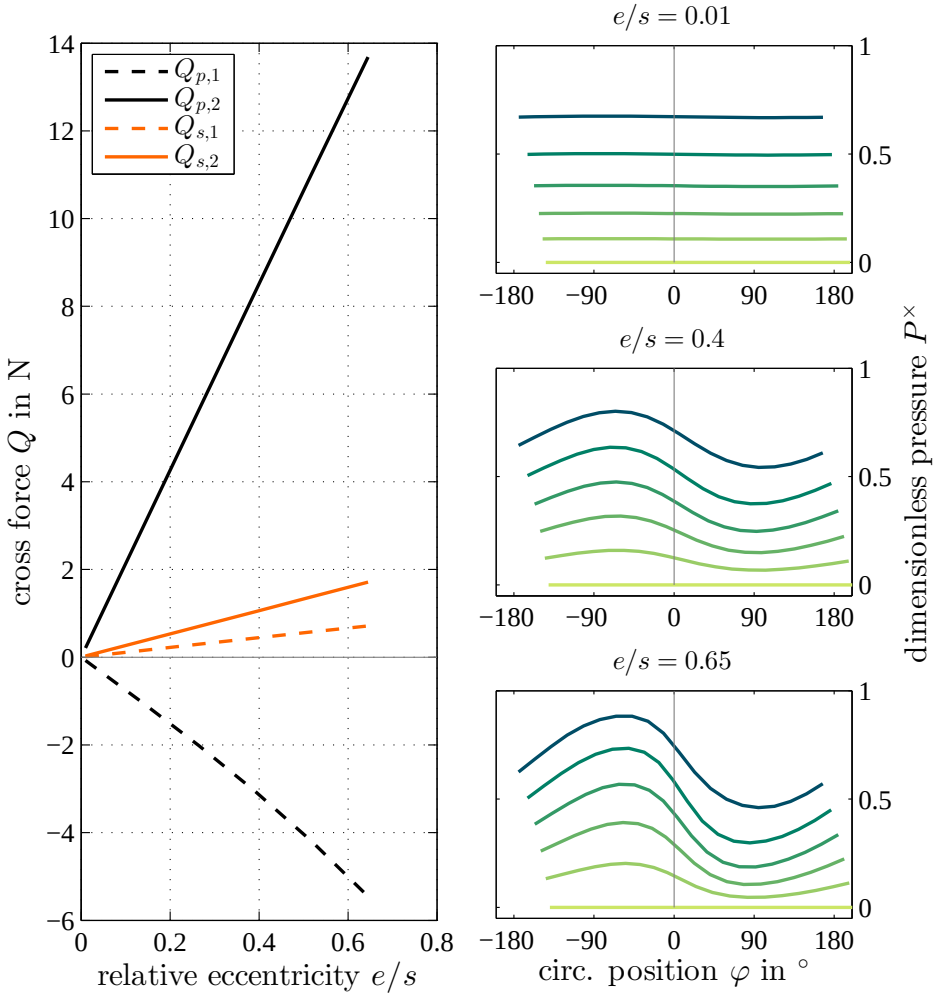

Figure 4.8: Cross forces Q against the relative eccentricity $\frac{e}{s}$ and dimensionless pressure $P^{\times}$ for chosen relative eccentricities.

coefficient and has the dimension of N/m. As shown in the stability analysis in Sec. 3.1.2, this factor is of fundamental importance for the stability of the rotor. Equation (3.10) shows, that small absolute cross force coefficients (given that q_1 has a negative sign) increase the stability of the rotor. Therefore the reduction of the cross forces and their respective coefficients is the desired behavior.

4.2.3 Radial Clearance Width

Figure (4.9) shows the cross force coefficients q_p and q_s for varying radial clearance widths s for a constant relative eccentricity of e/s=0.5. Note that for all further analysis the relative eccentricity is set to e/s=0.5. For this relative eccentricity the assumed linearity of the cross forces (see Fig. 4.8) is a good representation of the real cross force curve shape.

With decreasing radial clearance width s the cross force coefficients $q_{p,1}$ and $q_{p,2}$, which result from the pressure distribution, strongly increase. For smaller radial clearance widths the pressure and momentum loss coefficients ξ and $\bar{\xi}$ increase (Eq. 3.34). This in turn results in elevated pressure levels in the tip gap, which can be seen in Fig. (4.9). Although the leakage mass flow rate increases with a greater radial clearance width, the cross forces Q_s are independent of the total tip gap leakage flow according to Eq. (3.83) and only depend on the degree of variation of the leakage mass flow in circumferential direction. The increase of the $P^{\times}$ amplitudes in Fig. (4.9) can be explained by the reduced leakage flow turning in a wider tip gap.

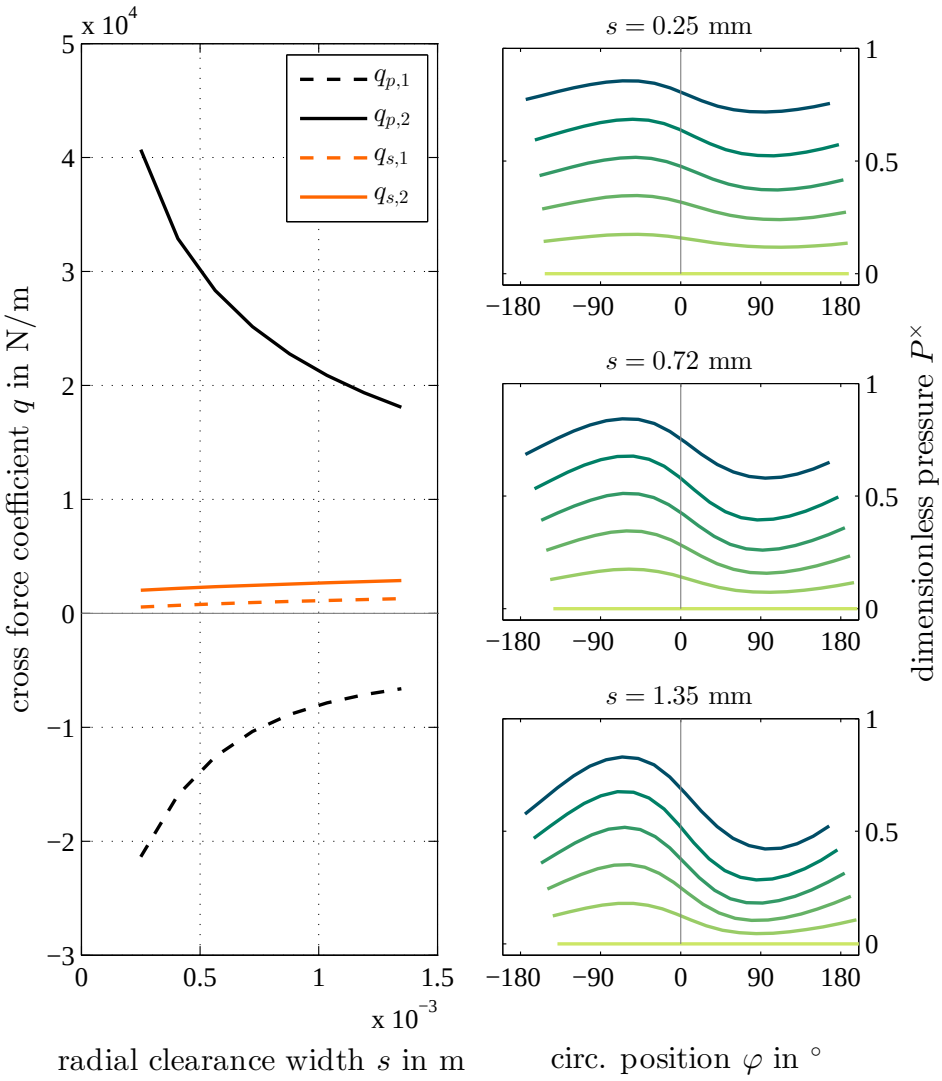

Figure 4.9: Cross force coefficient q against the radial clearance width s and dimensionless pressure $P^{\times}$ for chosen radial clearance widths.

4.2.4 Total Pressure Drop

For a varying total pressure drop in the tip gap Δp_B the forces, resulting from a varying tangential force on the turbine blades Q_s, change according to Eq. (3.83). In Eq. (3.83) it was shown that the cross force Q_s only depends on the local leakage mass flow $\dot{m}_k$, which itself contains the square root of Δp_B (see Eq. 3.80). The expected parabolic shape of Q_s can not be identified in Fig. (4.10). This is attributed to the relatively small range of Δp_B values for the parameter study, due to numerical reasons. While the restoring pressure force $-Q_{p,1}$ for a solely axial flow increases linearly with Δp_B (see Eq. 3.58), this is not the case for the swirled flow. Both, $Q_{p,1}$ and $Q_{p,2}$, depend nonlinearly on the total pressure drop Δp_B, as also the relative inlet kinetic energy $C_E^{\times}$ changes with changing Δp_B. The influence of the relative inlet kinetic energy $C_E^{\times}$ is shown in the subsequent calculations.

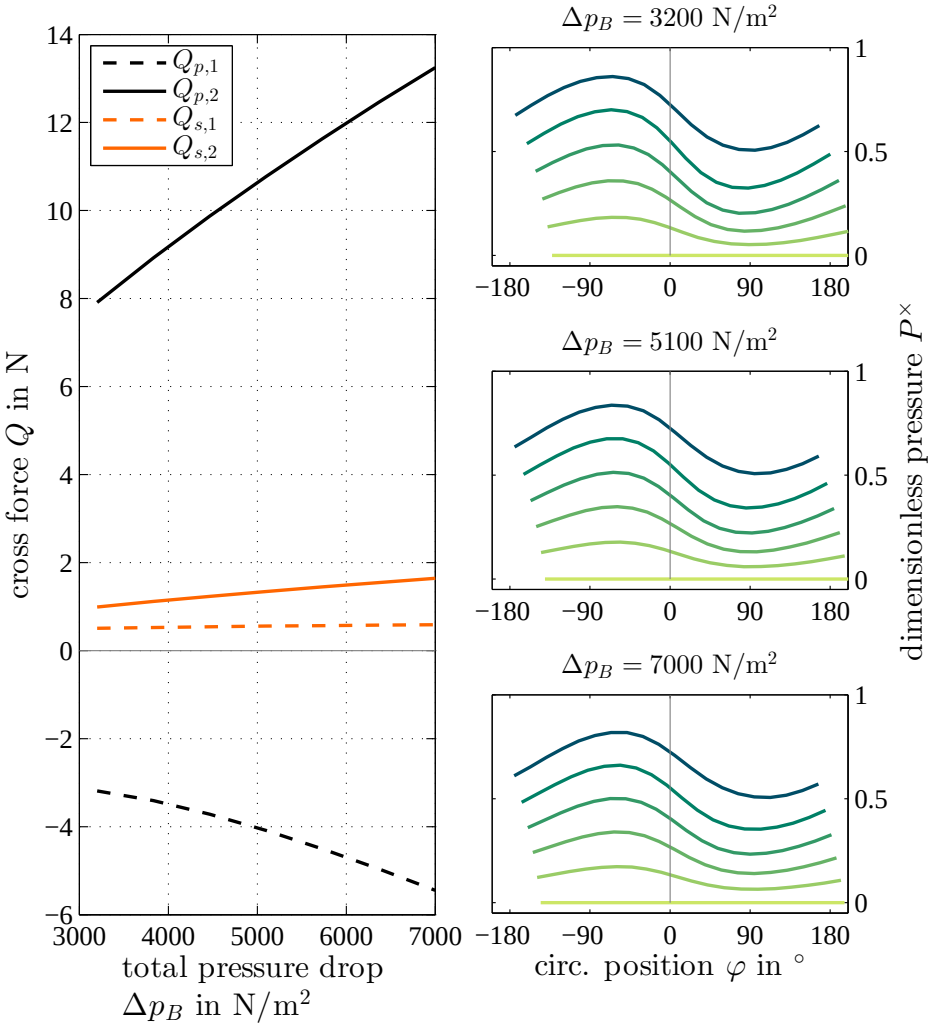

Figure 4.10: Cross forces Q against the total pressure drop Δp_B and dimensionless pressure $P^{\times}$ for chosen total pressure drops.

The linearity of the cross forces for different values of eccentricity as seen in Fig. (4.8) allows for the definition of a dimensionless increase $Q^{\times}$ across the displacement e. In contrast to the dimensioned cross force coefficient q, this dimensionless cross force is used to compare different operating points in terms of their rotor-dynamic relevance. The factor of the form $Q^{\times}$, according to Eq. (3.86) and Eq. (3.87), is defined using the cross forces at a relative eccentricity of $e/s = 0.5$ and the reference maximum cross force Q_B for a total pressure drop of Δp_B=5e3 N/m^2.

4.2.5 Relative Inlet Kinetic Energy

All the parameters in the relative maximum cross force Q_B have been varied and the dimensionless cross forces $Q_s^{\times} = Q_s/Q_B$ and $Q_p^{\times} = Q_p/Q_B$ can be plotted alongside the dimensionless relative tip gap mass flow rate $\dot{m}^{\times}$ on the same scale.
In Fig. (4.11) the relative inlet kinetic energy $C_E^{\times}$ (Eq. 3.49) is varied by changing the inlet flow angle α_E and therefore the swirl of the incoming flow into the tip gap. Note that in the chosen definition of α_E a value of α_E=90° stands for a completely axial flow, while values of $0° < \alpha_E < 90°$ characterize the swirled inlet flow. The pressure distributions illustrate the impact of the relative inlet kinetic energy, as the pressure peaks move against the rotational direction further ahead of the narrowest clearance position at φ=0° and their amplitudes rise with increasing inlet flow angle.

The relative tip gap mass flow rate $\dot{m}^{\times}$ also changes with $C_E^{\times}$. With a rising rotational component of the inlet flow (with decreasing α_E and increasing $C_E^{\times}$ values), the flow paths in the tip gap get longer. Therefore the pressure and momentum loss coefficients rise, resulting in a lower leakage mass flow rate. $\dot{m}^{\times}$ (Eq. 3.56) is displayed in the plot, for which no considerable changes were observable in the parameter variations up to this point.

$C_E^{\times}$ is also characteristic for the forming of cross forces on the rotor. Considering the equation for $C_E^{\times}$ (Eq. 3.49) and the dependence of $Q_{p,2}$ on the pressure maximum shift in circumferential direction, one can see, as stated by Urlichs in [27], that the excitation cross force $Q_{p,2}$ only manifests itself in turbine stages with a low degree of reaction, as high circumferential flow velocities and a low total pressure loss are required. The restoring force $Q_{p,1}$ on the other hand depends solely through the changed pressure and momentum loss coefficients on $C_E^{\times}$.

The excitation cross force $Q_{s,2}$ also rises with growing $C_E^{\times}$. By increasing the inlet swirl, the circumferential velocity component increases which, according to Eq. (3.84), leads to higher Thomas-Alford cross forces.

Figure (4.11) also shows the values for a purely axial flow. At $C_E^{\times}$=0, α_E has the value of 90°, which corresponds to an irrotational inlet flow. The pressure and leakage mass flow rate distributions show symmetric curves to the φ=0°–position. This leads to vanishing pressure cross forces perpendicular to the direction of displacement. Solely $Q_{p,1}$ remains nonzero, due to

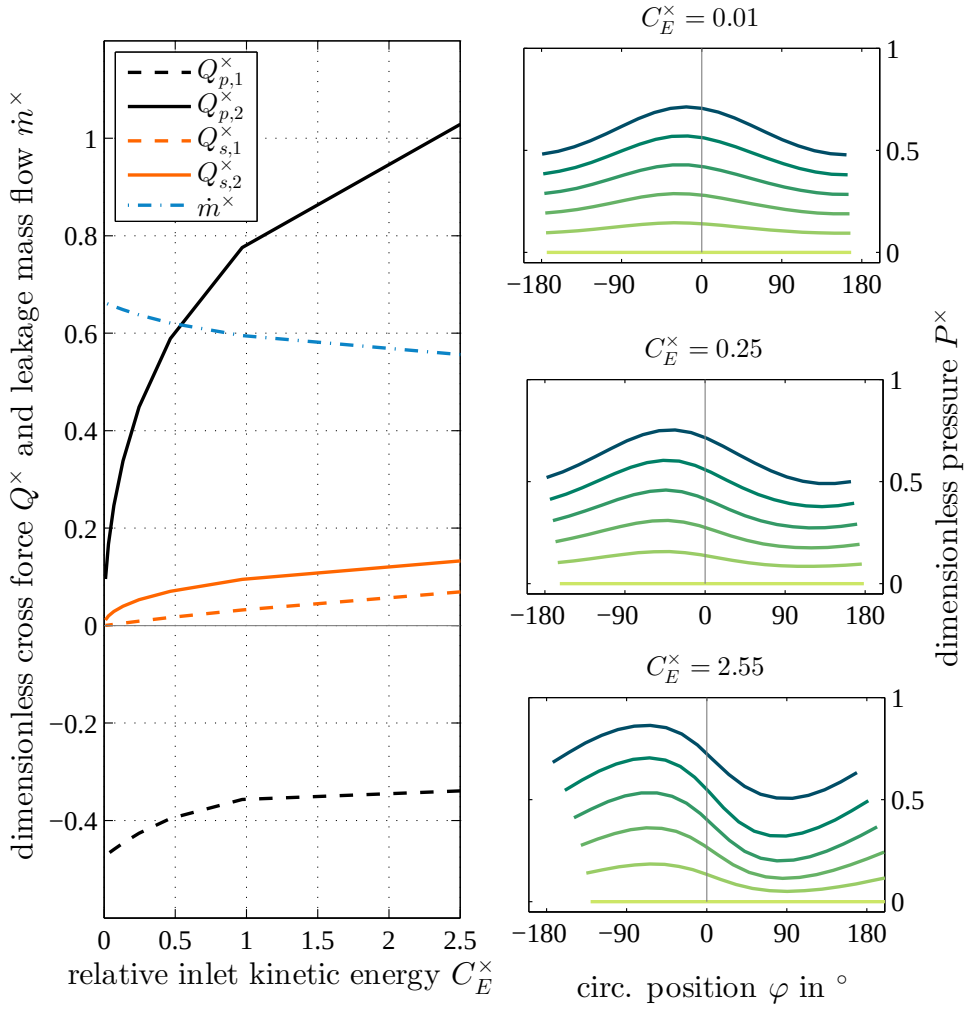

Figure 4.11: Dimensionless cross force $Q^\times$ and leakage mass flow rate $\dot{m}^\times$ against the relative inlet kinetic energy $C^\times_E$ and dimensionless pressure $P^\times$ for chosen relative inlet kinetic energies.

the existing eccentricity of the rotor (see Lomakin quoted in [7]). The cross forces resulting from a varying tangential force on the turbine blades $Q_{s,1}$, $Q_{s,2}$ disappear for $C^\times_E = 0$ as no tangential forces act on the turbine blades for $\alpha_E = 0°$.

4.3 Shrouded Turbine Rotor with six Fins and with Passive Tip-Injection

Now, that the fundamental effects of a swirled flow through the tip gap for an eccentric rotor are known, and reference values of essential parameters are available, the unified model, obtained in Sec. 3.4, can be applied to the geometry setup of a shrouded turbine rotor with six fins and tip-injection seen in Fig. (4.12). The geometry as described in Tab. (4.2) was chosen in order to clearly distinguish the effects resulting from the swirled flow and the ones resulting from the passive tip-injection. For a setup with a fin number of n=2 like in Sec. 4.1, this would no longer be possible, due to smearing effects on the pressure and leakage mass flow rate distributions. The results gained above for a six finned labyrinth seal without passive tip-injection in Sec. 4.2 act as a reference to evaluate the impact of passive tip-injection on the tip excitation of a turbine rotor.

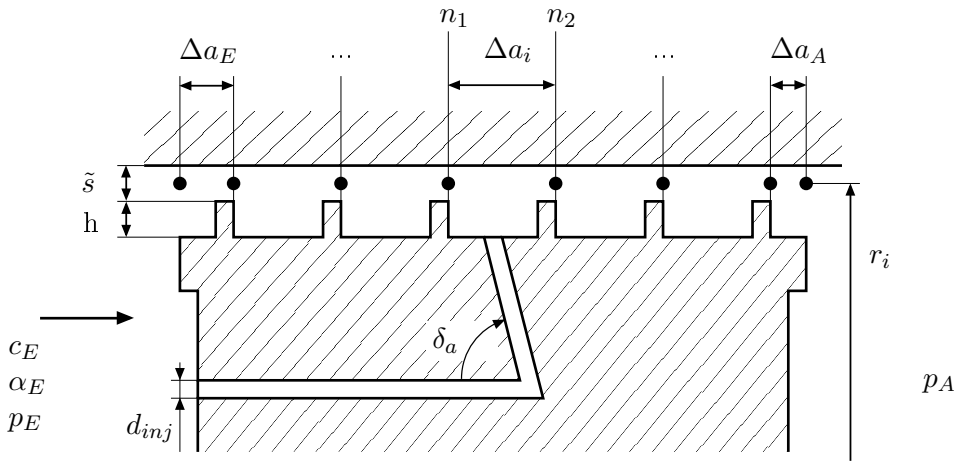

Figure 4.12: Geometry setup for a shrouded turbine rotor with six fins with passive tip-injection.

Table 4.2: Parameters and constants for the chosen geometry and point of operation

geometry			point of operation and fluid properties	
$\Delta a_E = 4e\text{-}3$ m	$e/s = 0.5$	$n_{inj} = 24$	$\rho = 1.2$ kg/m^3	$p_E = 1.04e5$ N/m^2
$\Delta a_i = 10e\text{-}3$ m	$m_N = 9$	$\delta_a = 70°$	$c_{E,n} = 41$ m/s	$p_A = 1e5$ N/m^2
$\Delta a_A = 4e\text{-}3$ m	$n_1 = 3$	$\delta_u = 45°$	$\alpha_E = 20°$	$f_r = 50$ Hz
$s = 1e\text{-}3$ m	$n_2 = 4$	$\gamma = 0.5$	$\Delta p_B = 5e3$ N/m^2	$\Omega = 2\pi f_r$
$r_i = 104e\text{-}3$ m	$n = 6$	$d_{inj} = 2.5e\text{-}3$ m	$C_E^{\times} = 1.52$	
$h = 4e\text{-}3$ m	$j = 20$			

4.3.1 Fundamental Effects

The pressure and leakage mass flow rate distributions seen in Fig. (4.13) differ drastically from the ones obtained so far. Some characteristic aspects are still observable though. The characteristic maximum pressure shift, due to the eccentricity of the rotor and the swirl of the flow, can still be seen.

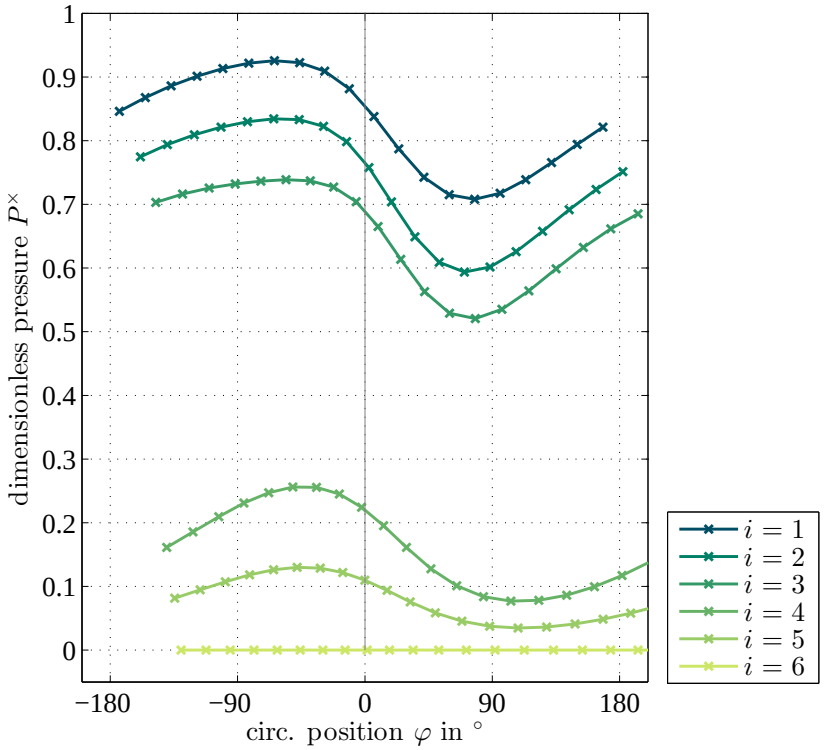

Figure 4.13: Dimensionless pressure $P^{\times}$ against the circumferential direction φ, for axial positions $i = 1 \ldots 6$.

The distinctive pressure drop at the injection cross section can be seen clearly. Note that the calculated pressures can only be observed in the support points at the downstream edge of each fin. In the theory for the ideal labyrinth seal (see [25]), the pressure in the labyrinth chamber is considered to be constant on the level of the pressure at the fin upstream of the chamber. This assumption is also made in order to calculate the resulting pressure forces on the rotor in this case. In the injection chamber the complex process of mixing and friction losses are combined with the effects of the injection mass flow into the injection chamber. Therefore with the model based on simplified conditions, no definitive statement can be made for the pressure distribution between the corresponding support points and the real pressure in the injection chamber. This has to be kept in mind when interpreting the following results.

As a result of the passive tip-injection, the pressure levels in the support points ahead of the

injection position in axial direction are clearly elevated, while the amplitudes of the pressure distributions shrink. The altered curve shape on the right hand side to the φ=0°-position indicates the influence of the injection channel inclination against the direction of rotation.
Compared to the pressure in the corresponding support points in the case without passive tip-injection, the pressure downstream of the injection position, seen in Fig. (4.13), is on a lower level. The slight shift of the pressure maximum points towards the φ=0°-position, compared to the setup without tip-injection occurs, due to the shorter streamtube length from the tip gap entry to the injection position.
Due to the mixing of the injection mass flow $\dot{m}_{inj}$ with the inlet tip-gap mass flow $\dot{m}_1$, the streamtubes starting at the tip gap inlet, end at the injection position, where the second set of streamtubes for the mixed flow and the outlet mass flow $\dot{m}_2$ begins.

Figure (4.14) illustrates the relative leakage mass flow rates upstream and downstream of the injection position $M_1^\times$ and $M_2^\times$ as defined in Eq. (3.55). The curves show a minimum mass flow rate for the streamtube with the maximum pressure levels and maximum mass flow rate for streamtubes with minimum pressure levels as seen before.

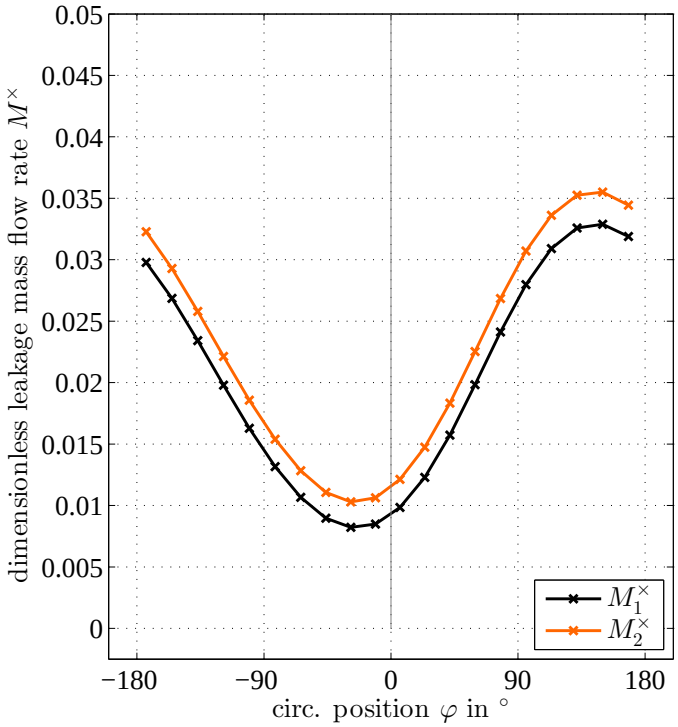

Figure 4.14: Dimensionless leakage mass flow rate $M^\times$ against the circumferential direction φ, upstream $M_1^\times$ and downstream $M_2^\times$ of the injection position.

In Tab. (4.3) the values for the relative leakage mass flow rates $\dot{m}_1^\times$ and $\dot{m}_2^\times$ as defined in Eq. (3.56) are shown alongside the relative leakage mass flow rate $\dot{m}^\times$ of the shroud setup with-

out tip-injection. The relative leakage mass flow rates can be interpreted as discharge coefficients for the theoretical maximum leakage mass flow rate $\dot{m}_B$ for the chosen shroud geometry and operation point parameters of the turbine. By comparing the values for the relative leakage mass flow rate $\dot{m}_2^\times$ and $\dot{m}^\times$, as seen in Tab. (4.3), one can see the reduced values for the application with passive tip-injection, compared to the setup without passive tip-injection. It should be mentioned that comparing $\dot{m}_2^\times$ (as opposed to $\dot{m}_1^\times$) with $\dot{m}^\times$ takes into account, that the injection mass flow $\dot{m}_{inj}$, which is extracted at the blade leading edge, does not contribute to stage work. $\dot{m}_{inj}$ has to be treated as part of the overall tip-leakage mass flow of the seal setup. The reduction in tip-leakage mass flow demonstrates the effectiveness of passive tip-injection method. The relative injection mass flow $\dot{m}_{inj}^\times$ as defined in Eq. (3.69) depends on the difference of the stagnation pressure at the blade leading edge and the pressure in the injection chamber. It further depends on the injection channel loss coefficient ξ_{inj} (Eq. 3.66) and the relative injection channel diameter γ. It is shown alongside the relative leakage mass flow rates in Tab. (4.3).

Table 4.3: Comparison of discharge coefficients and angular momentum for the shrouded turbine rotor with six fins, with and without passive tip-injection.

with passive tip-injection	without passive tip-injection
$\dot{m}_1^\times$=0.4037	-
$\dot{m}_2^\times$=0.4524	$\dot{m}^\times$=0.5767
$\dot{m}_{inj}^\times$=0.1206	-
$T_A = 0.089$ Nm	$T_A = 0.144$ Nm
$C_{AM}^\times$=0.0477	$C_{AM}^\times$=0.0773

The pressure loss coefficient ξ for the last labyrinth fin was set to one (see Sec. 3.2.2). Therefore, by definition, the outflow is purely axial and thus has no circumferential component or angular momentum. Nevertheless a characteristic angular momentum flow (torque) for each shroud setup T_A[1] is defined and shown in Table (4.3) alongside the discharge coefficients for the leakage mass flow. The passive tip-injection not only reduces the overall tip-leakage mass flow, but also the outlet angular momentum. This results from the reduced tip-leakage mass flow $\dot{m}_2$, and from improved turning conditions of the tip gap flow, due to the inclination of the injection mass flow against the rotational direction of the rotor.

This reduction in angular momentum is also one of the fundamental effects of tip-injection as identified by Ghaffari et al. in [10]. The fact, that the mixing process of the underturned leakage mass flow with the main flow behind the blade row is one of the main reasons for losses

[1] T_A is defined as the angular momentum at the last fin of the shroud. The axial flow caused by the complete mixing is established in the pseudo chamber between the last fin and the tip gap outlet as can be seen in Eq. (3.73).

associated with leakage [6], underlines the importance of reducing the angular momentum of the tip-leakage mass flow.

Besides the discharge coefficients $\dot{m}_1^{\times}$ and $\dot{m}_2^{\times}$ the effectiveness of the passive tip-injection can therefore also be measured by the characteristic angular momentum flow T_A. It will be considered in the following calculations in the form of a dimensionless discharge coefficient for angular momentum $C_{AM}^{\times} = \frac{T_A}{T_B}$[2].

Note that for the given boundary conditions the passive tip-injection yields relatively low $\dot{m}_{inj}^{\times}$ values and therefore small injection velocities. For the rotational frequency of the rotor chosen in the exemplary calculation of f_r=50 Hz and the inclination angle of the injection slot against the rotational direction δ_u, the absolute injection velocity in circumferential direction $w_{inj,u,abs} = (w_{inj,u} - r * \Omega)$ yields negative values. This means, the absolute injection velocity is oriented in direction of rotation. This means, the injection mass flow is oriented opposite to the intended direction, established by the injection slot inclination in circumferential direction. It still reduces the angular momentum of the tip gap flow, due to the lower circumferential velocity of the injection mass flow, compared to the tip gap mass flow.

4.3.2 Eccentricity

The variation of the eccentricity of the rotor shows similar effects as for the setup without tip-injection in respect of linear cross force increase and rise in amplitude for the pressure distribution with growing eccentricity (see Fig. 4.15). Nonetheless small differences can be made out.

The pressure differences between the support points located upstream of the injection position and downstream of the injection position are smaller, compared to the corresponding support points in the setup without tip-injection. Hence the amplitudes of the pressure distribution in circumferential direction are lower. This leads to smaller pressure cross forces Q_p. Due to the correlation of the pressure distribution and the leakage mass flow rate distribution described in Sec. 4.1.1, the amplitude of the leakage mass flow rate distribution also shrinks in the case of passive tip-injection, which leads to reduced Thomas-Alford forces Q_s on the rotor.

Figure (4.15) shows that the pressure maximum position shifts towards the φ=0°-position, but the minimum position does not move considerably with increasing eccentricity. Therefore the resulting pressure cross force moves towards the φ=0°-position. This again leads to a lower component acting in direction perpendicular to the direction of displacement ($Q_{p,2}$) and a potential

[2] $T_B = \frac{\dot{m}_B^2}{\rho A_B} \cot \alpha_E r_E$ ... Theoretic maximum angular momentum at the tip gap entry.

$T_A = \sum_{k=1}^{j} \frac{\dot{m}_{n,k}^2}{\rho A_{n,k}} \cot \alpha_{n,k} r_{n,k}$ ... Angular momentum at last fin $i = n$.

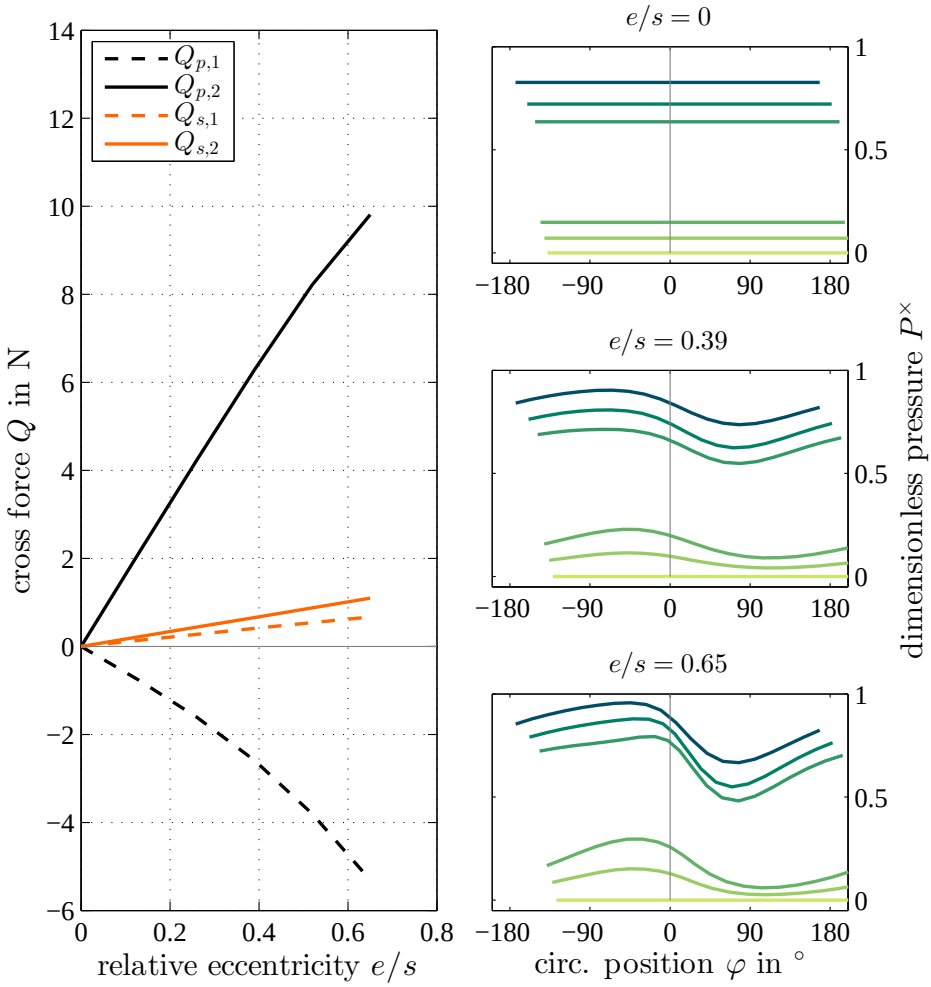

Figure 4.15: Cross forces Q against the relative eccentricity $\frac{e}{s}$ and dimensionless pressure $P^{\times}$ for chosen relative eccentricities.

increase in the component acting against the direction of displacement ($Q_{p,1}$). For $Q_{p,1}$ the two effects of a lower pressure drop and a changed position of the resulting pressure force cancel each other out, as the force stays on the same level as for the setup without passive tip-injection.

To express the pressure forces in the formulation of Eq. (3.85), the conservative assumption was made, that the pressure in the support point position upstream of the injection chamber acts on the entire rotor area of the injection chamber. Therefore the pressure forces calculated here lie at the upper limit of the uncertainty in respect to the acting pressure in the injection chamber.

Again, the linearity of the cross forces in dependence of the eccentricity allows the definition of linear increase factors (i.e. cross force coefficients) of the form $q = Q/e$ for the setup with

passive tip-injection.

4.3.3 Radial Clearance Width

In Fig. (4.16) the cross force coefficients show the same general behavior for the tip-injection setup as for the shroud without tip-injection. While the curve shapes are identical for q_p, the ones for passive tip-injection show lower levels, due to the lower levels of Q_p, as explained above. That means the pressure cross forces $Q_{p,1}$ and $Q_{p,2}$ are not only smaller for the setup with tip-injection, but also increase with a smaller gradient for increasing radial clearance widths s.
Note that due to numerical reasons, no value lower than 0.75 mm could be set for the radial clearance width s in this parameter study. Figure (4.16) still gives a good idea about the increasing cross force coefficients for smaller clearance widths.

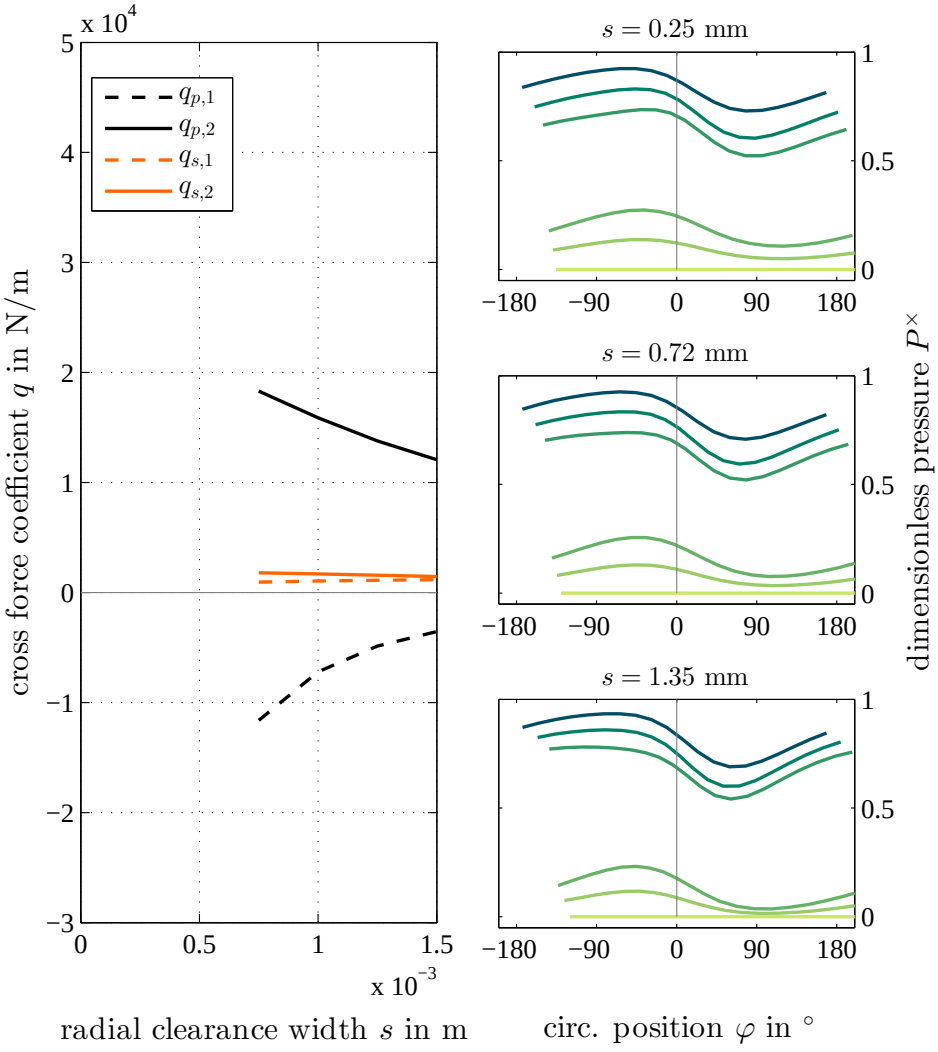

Figure 4.16: Cross force coefficient q against the radial clearance width s and dimensionless pressure $P^\times$ for chosen radial clearance widths.

4.3.4 Total Pressure Drop

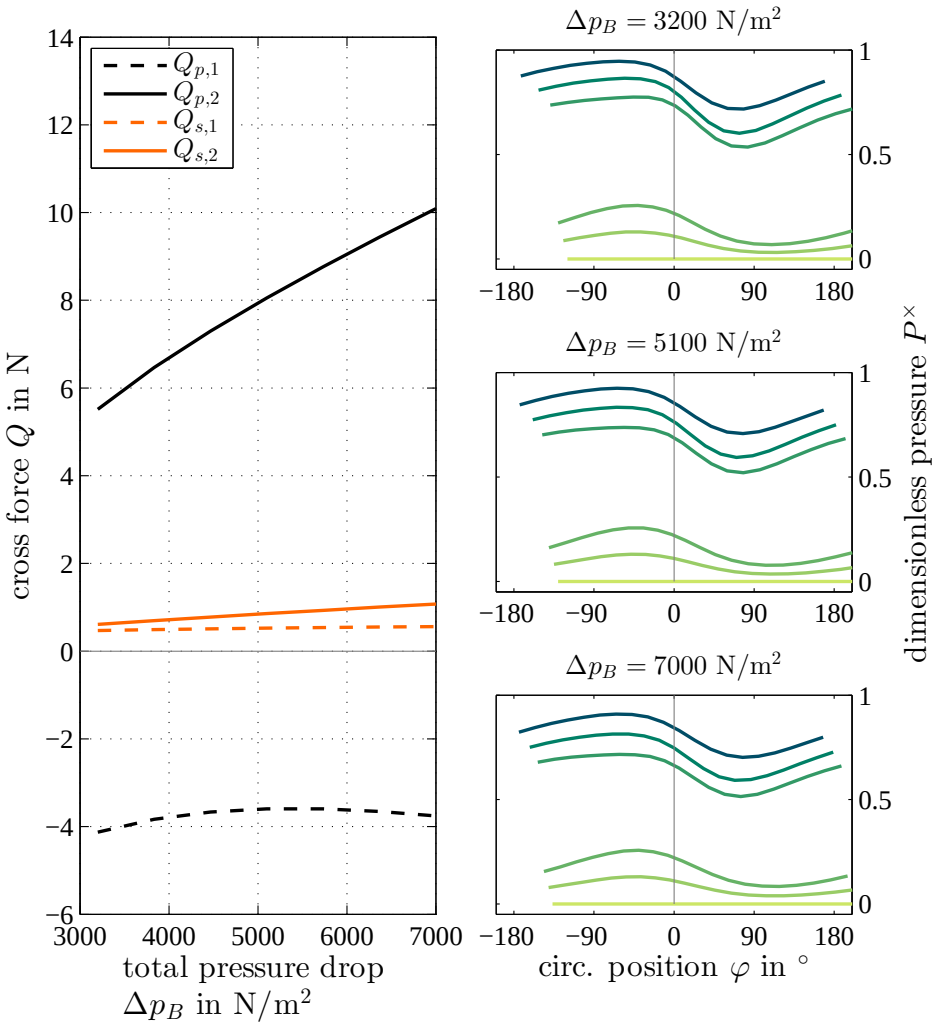

Figure 4.17: Cross forces Q against the total pressure drop Δp_B and dimensionless pressure $P^\times$ for chosen total pressure drops.

The curves for the cross forces as seen in Fig. (4.17) show the same parabolic shape for increasing values of total pressure drop Δp_B as seen in Fig. (4.10) for the setup without tip-injection, but on a lower level. Worth mentioning is the minimum for the $Q_{p,1}$ force at approximately $\Delta p_B = 55\,\text{mbar}$, a behavior that seems restricted to the passive tip-injection setup. In contrast to the dimensioned cross forces, the dimensionless values for $P^\times$ and $M^\times$ show no considerable change for increasing values of Δp_B. Their level, amplitude and φ=0°-position shift are constant across Δp_B as is expected, considering their definition, which takes Δp_B into account.

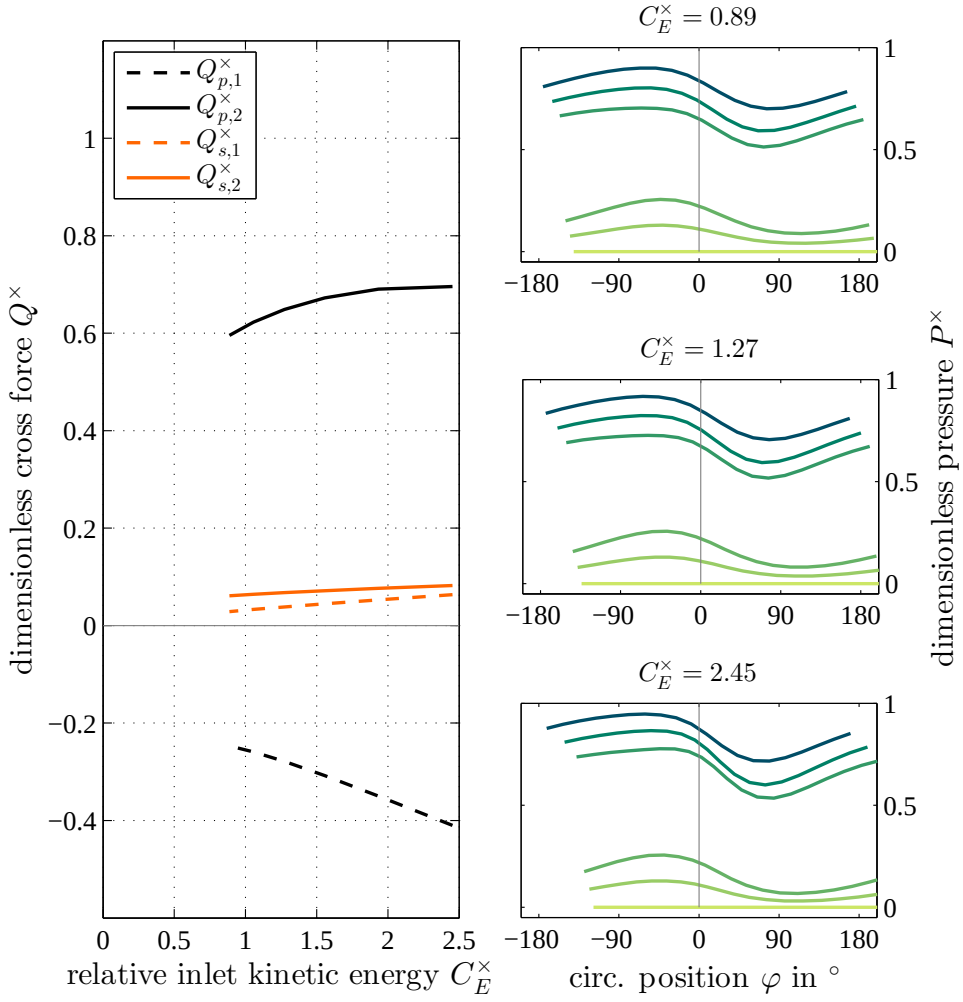

Figure 4.18: Dimensionless cross force $Q^\times$ against the relative inlet kinetic energy $C_E^\times$ and dimensionless pressure $P^\times$ for chosen relative inlet kinetic energies.

4.3.5 Relative Inlet Kinetic Energy

Figure (4.18) shows that the pressure maximum position shifts towards the φ=0°-position for increasing values of $C_E^\times$, while the minimum pressure positions do not move considerably. This contrasts the behavior of the pressure distribution for the setup without tip-injection. This counterintuitive behavior can be attributed to the increase in tip-injection mass flow as seen in Fig. (4.19). Up to this point, neither the variation of the eccentricity e, radial clearance width s, nor the variation of total pressure drop Δp_B had a considerable influence on the relative injection mass flow $m_{inj}^\times$. Figure (4.19) shows an increase in passive tip-injection effectiveness with growing inlet kinetic energy in terms of reducing the overall tip-leakage mass flow. This increase in effectiveness leads to the mentioned pressure peak shift and improved outflow conditions indicated by reduced $C_{AM}^\times$ values.

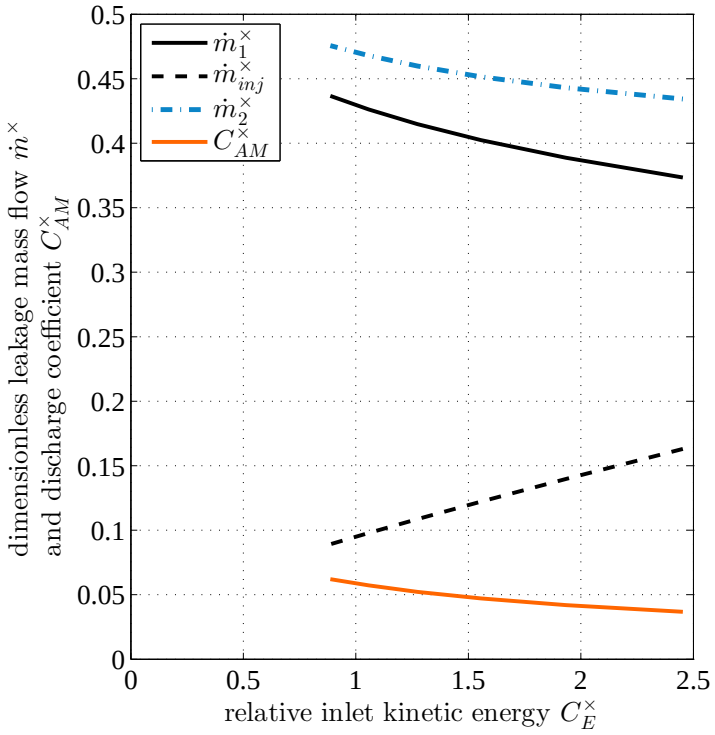

Figure 4.19: Dimensionless leakage mass flow $\dot{m}^\times$ and discharge coefficient for angular momentum $C_{AM}^\times$ against the relative inlet kinetic energy $C_E^\times$.

The shift of the pressure maximum towards the φ=0°-position causes a higher curvature of the $Q_{p,2}$ and $Q_{s,2}$ curves (see Fig. 4.18) for an increasing $C_E^\times$ in comparison to the setup without tip-injection. It is also responsible for the increase in $Q_{p,1}$ and $Q_{s,1}$, which decreases in the setup without tip-injection.

Up to this point, the parameters of operation have been varied and the reaction of two systems, one without and one with passive tip-injection, has been investigated. In the following sections the parameters of the passive tip-injection are varied in order to find the optimal set of parameters in respect of tip-leakage reduction and rotordynamic behavior. The parameters in question are the inclination in circumferential direction of the injection slot δ_u and the location of the injection position in axial direction.

4.3.6 Injection Slot Circumferential Inclination Angle

As suggested by Ghaffari et al. [10], passive tip-injection can improve the mixing conditions of the tip gap flow with the main flow considerably by reducing the angular momentum of the tip gap flow. To investigate this effect, in the following computations the injection slot inclination angle in circumferential direction δ_u as seen in Fig. (3.17) is varied. Note that small angles

δ_u indicate a strong inclination of the injection channel against the circumferential direction, while for δ_u=90° the injection channel is oriented perpendicular to the tip gap flow direction in circumferential direction.

The curves of the dimensionless cross forces seen in Fig. (4.20) differ from the expected results. It was expected, that a stronger inclination of the injection channel against the circumferential direction (i.e. smaller angles δ_u) would lead to an increased effectiveness of the passive tip-injection in terms of flow turning and cross force reduction. Figure (4.20) although shows an increase of the pressure force component $Q^{\times}_{p,1}$ and a decrease of the pressure excitation force $Q^{\times}_{p,2}$. This suggest a slight shift of the pressure maximum towards the φ=0°-position, which is confirmed by the pressure distributions seen in Fig. (4.20). This unexpected result can be explained by studying the relative tip gap and injection mass flows in Fig. (4.21).

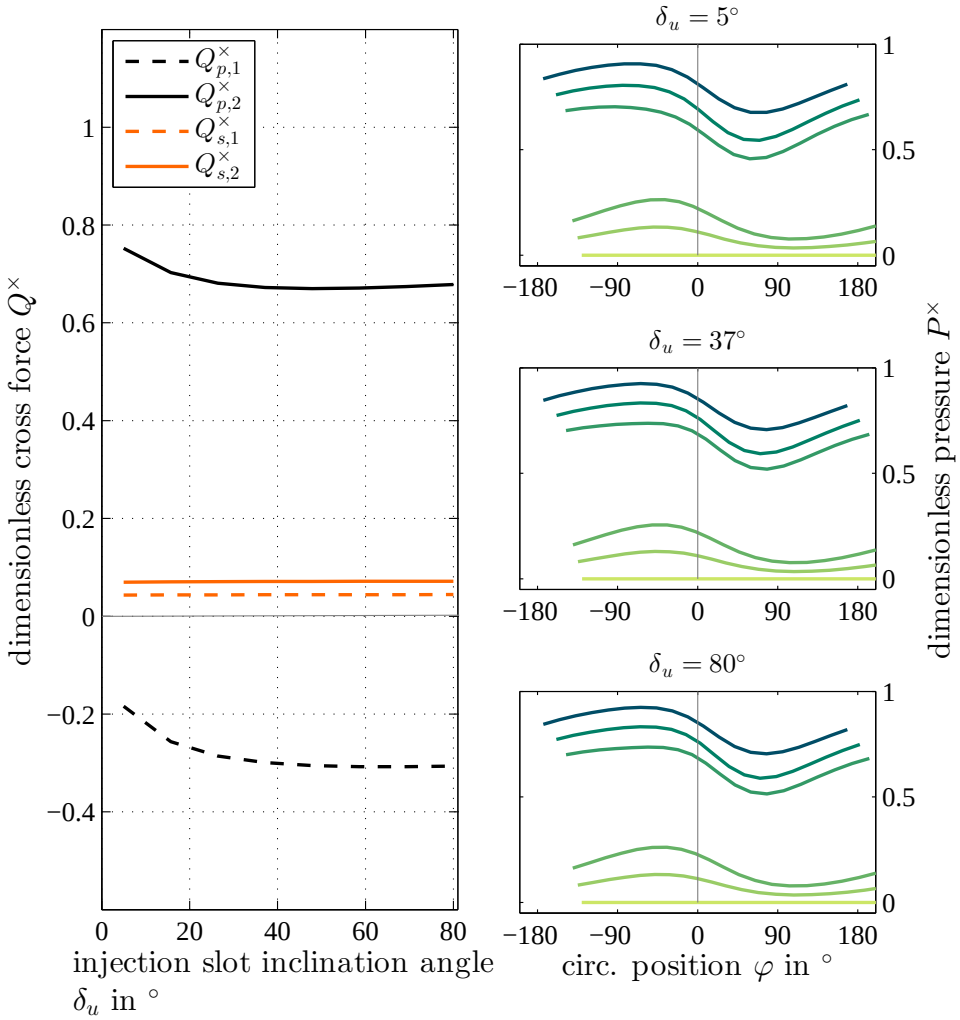

Figure 4.20: Dimensionless cross force $Q^{\times}$ against the injection slot inclination angle δ_u and dimensionless pressure $P^{\times}$ for chosen injection slot inclination angles.

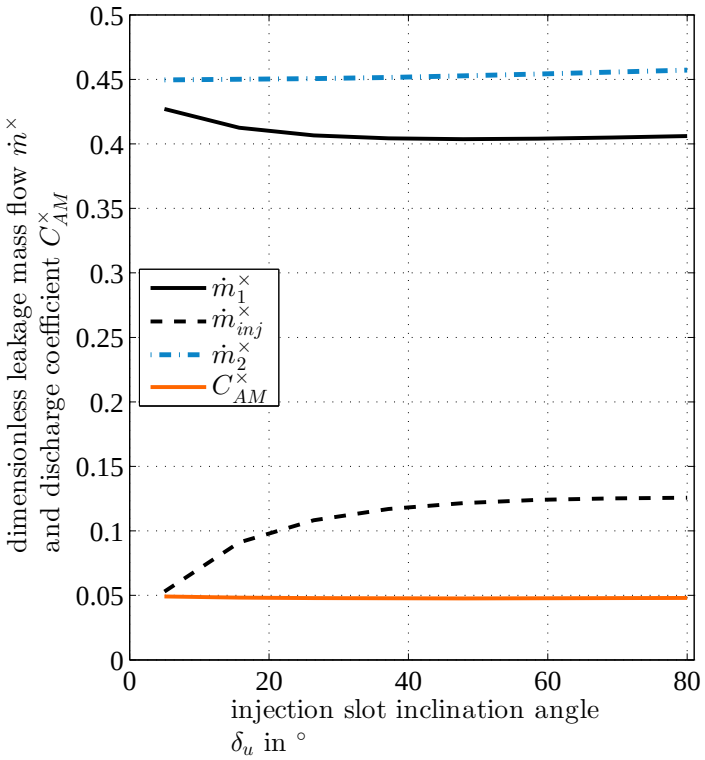

Figure 4.21: Dimensionless leakage mass flow $\dot{m}^\times$ and discharge coefficient for angular momentum $C^\times_{AM}$ against the injection slot inclination angle δ_u.

Figure (4.21) shows the tip gap inlet mass flow $\dot{m}^\times_1$ slightly decreasing before staying relatively constant for higher values of δ_u. This fading out of the δ_u-influence on the curves is also seen in Fig. (4.20). It is also shown, that the outlet tip gap mass flow $\dot{m}^\times_2$ is constant for the entire range of δ_u-values. This means, the injection mass flow increases by the same amount as the inlet tip gap mass flow is decreased. This can be explained by the increased injection channel length L_{inj} for smaller inclination angle values δ_u. An increase of L_{inj} in turn raises the flow resistance of the injection channel and reduces the injection mass flow. It can be shown, that this increase in injection channel flow resistance cancels out the benefits of an increased inclination of the injection channel against the circumferential direction.

4.3.7 Injection Position

In [10] and [2] it is shown, that the injection position in axial direction of the tip gap has a significant impact on the performance of the passive tip-injection. Here the injection position is moved from the labyrinth chamber number three between fin number i=3 and i=4 to labyrinth chamber number two upstream and labyrinth chamber number four downstream of this position respectively.

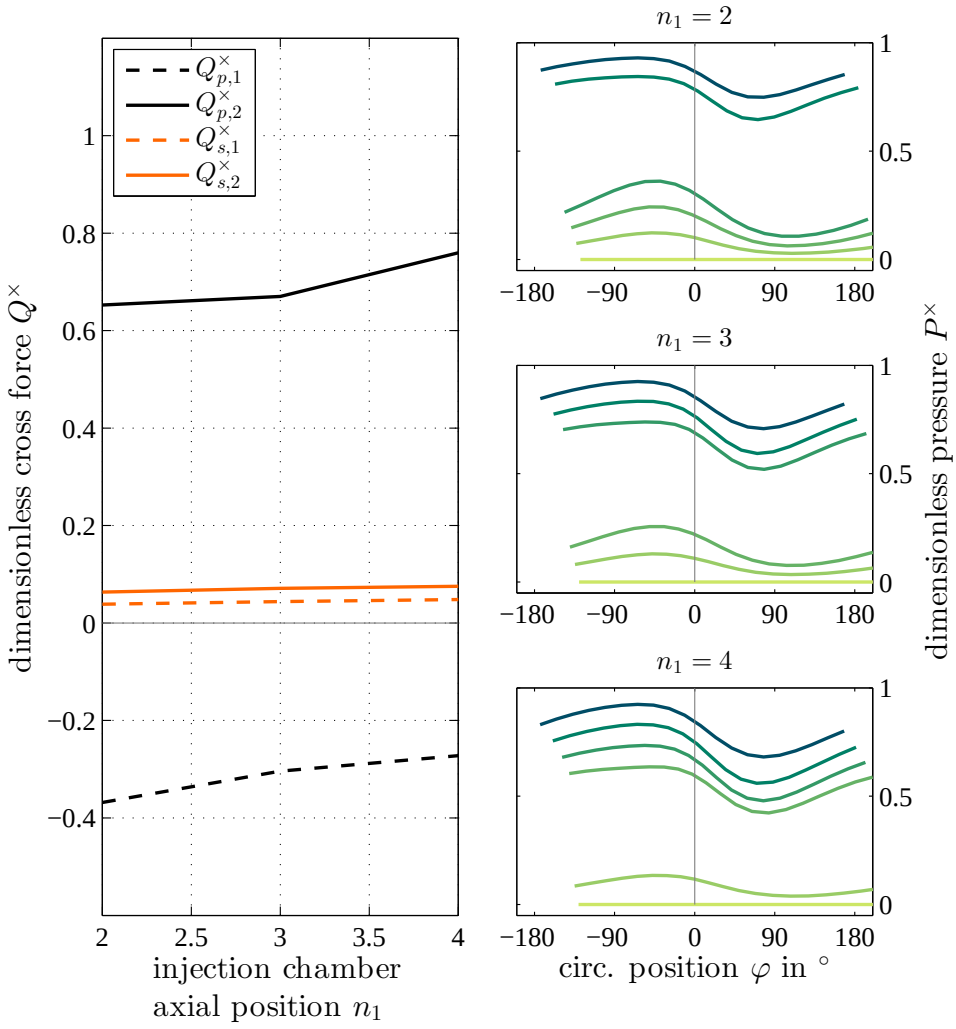

Figure 4.22: Dimensionless cross force $Q^{\times}$ against injection chamber axial position n_1 and dimensionless pressure $P^{\times}$ for chosen injection chamber axial positions.

In Fig. (4.22) the increase of $Q^{\times}_{p,2}$ with an injection position further downstream can be seen. This results from the increased number of support points on a higher pressure level. At the same time the pressure peaks on a lower level downstream of the injection position decline in number, as the injection position is moved further downstream. A slight shift of the pressure

peaks towards the φ=0°-position causes the $Q_{p,2}$ force to decline with growing injection chamber position in axial direction. The small increase in Thomas-Alford forces Q_s can be explained by the increase of tip-leakage mass flow as seen in Fig. (4.23).

Figure (4.23) shows, that an injection position further upstream in the tip gap is advantageous in terms of overall tip-leakage mass flow reduction. No significant change of the discharge coefficient for angular momentum $C^{\times}_{AM}$ with a more downstream position of the injection chamber is seen. It can be shown although, that higher flow turning is achieved by an injection in a position closer to the outlet of the tip gap. Although in this case this effect is compensated by the increased overall tip-leakage mass flow, which leads to the mentioned constant $C^{\times}_{AM}$ values.

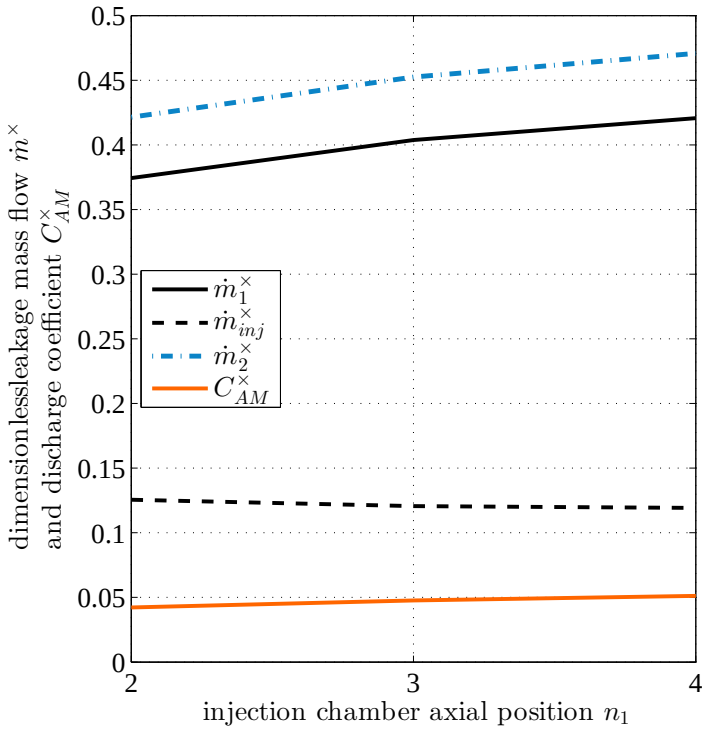

Figure 4.23: Dimensionless leakage mass flow $\dot{m}^{\times}$ and discharge coefficient for angular momentum $C^{\times}_{AM}$ against injection chamber axial position n_1.

5 Conclusion and Outlook

The method of reducing leakage in turbomachines by fluidic barriers has been studied extensively in literature. At the Institute for Energy Systems and Thermodynamics at the Technische Universität Wien the method of passive tip-injection has been presented and thoroughly researched. These investigations related to passive tip-injection for unshrouded turbine blades. Recently, numerical and experimental work has been done on shrouded and partially shrouded turbine blades. The focus of this research laid mainly on the tip-leakage mass flow reduction capabilities of passive tip-injection. Recently, analytical work [28] has been published relating to the impact of passive tip-injection on the generation of Thomas-Alford forces in unshrouded turbines. The influence of passive tip-injection on the cross force coefficients of shrouded axial turbine stages has not been investigated so far.

This work presents a two dimensional analytical model, which describes the flow through the tip gap of a shrouded axial turbine rotor with passive tip-injection. The model can be modified by simple adaptations to describe a shroud with and without fins, as well as to different forms of injections. The model especially considers the three dimensional aerodynamical effects of a swirled flow through the tip gap of an eccentric rotor. The model further covers the entire tip gap in circumferential and axial direction as well as the injection channel and the injection mass flow extraction at the turbine blade leading edge. This allows to determine the passive tip-injection mass flow for the given geometrical and operational parameters of the turbine. The model developed in this work allows to determine the streamlines and flow angles in the tip gap. This allows the investigation of the passive tip-injection on the flow turning in the tip gap cavity and the mixing conditions behind the blade row. The calculation of the pressure and leakage mass flow rate distributions in the tip gap in circumferential direction allows the determination of aerodynamically induced cross forces on the rotor. Both Thomas-Alford and pressure forces acting on the shroud surface can be determined. A variation of injection, geometry and operational parameters performed in this work provides substantial insight into the impact of passive tip-injection on the cross force generation in shrouded axial turbine stages.

5.1 Conclusions

It could be shown, that a pressure drop occurs in the injection chamber. This drop leads to elevated pressure levels upstream of the injection position and a reduced pressure gradient in the inlet section of the tip gap. This leads to a reduced mass flow entering the tip gap. This pressure

drop turns the momentum of the injection mass flow in the direction of the main tip-leakage mass flow, as stated in [2].

It is shown, that a reduction of the overall tip-leakage mass flow of 21% relative to the tip-leakage over a shroud with no passive tip-injection is possible. Ghaffari et al. [9] found a possible overall tip-leakage reduction through passive tip-injection for a similar setup of 13%. The higher value found in this work, is in part, due to the increased number of labyrinth fins and in part, due to the partial blockage of the injection channel in [9], which was not taken into account here. Ruiz et al. [15] predicted a reduction of the overall tip-leakage mass flow of 25%, but for the case of an active injection supplied by a higher driving pressure, than in the passive case presented here.

It could also be shown, that the angular momentum of the tip-leakage flow is reduced, when reentering the main flow channel downstream of the shroud through passive tip-injection. This reduction is achieved by reducing the overall tip-leakage mass flow, but also by the improved flow turning conditions in the tip gap with passive tip-injection. A reduction of angular momentum of approximately 38% compared to the case without passive tip-injection could be obtained. This leads to improved flow conditions considering the mixing of the tip gap flow with the main flow downstream of the shroud as also found by Ghaffari [10]. Considering the negative impact of an underturned tip gap flow on the mixing losses behind the blade row and on the incidence angle of the subsequent blade row [6] underlines the potential of the passive tip-injection method as presented here for increasing the turbomachinery efficiency.

The reduced pressure gradients upstream and downstream of the injection chamber lead to reduced amplitudes of pressure distributions in circumferential direction in the control planes. This increasing uniformity of the pressure in circumferential direction leads to a reduction of the pressure forces acting on the rotor, both perpendicular and against the direction of displacement. This also causes a reduced variation of the leakage mass flow rate in circumferential direction. Therefore the tangential forces on the turbine blades and the torque on the rotor are unbalanced to a lower extend. This in turn leads to a reduction of the Thomas-Alford forces acting on the rotor.

It could be shown, that passive tip-injection has the potential of reducing the cross force coefficient associated with the pressure force by 25% and the cross force coefficient associated with the Thomas-Alford force by up to 40%. Considering the stability analysis performed for a rotor under aerodynamically induced excitation forces in Sec. (3.1), this shows that passive tip-injection can have a considerable positive effect on the rotordynamic system.

Neither a reduction of the cross forces nor of the tip-leakage mass flow could be reached by increasing the inclination of the injection channel against the rotational direction of the rotor. It

could be shown, that the injection channel flow resistance increases with a stronger inclination due to the increased channel length. This reduces the injection mass flow and outweighs the advantageous effects of the injection channel inclination on tip gap flow turning. The negative effects of the longer injection channel are limited to the lower range of the inclination angle against the rotational direction. No significant impact of the inclination could be shown in the higher range. Therefore no recommendation can be made to change the inclination angle from the chosen 45° to a different value.

Further it could be shown that in order to obtain a maximum overall tip-leakage mass flow reduction, an injection position in the section close to the tip gap inlet has to be chosen. This increased effectiveness of passive tip-injection is also identified by Ghaffari et al. [9]. It was shown, that while increasing the overall tip-leakage mass flow, an injection position further downstream in the tip gap has an advantageous effect on the tip gap flow turning. This was also assumed by Auld et al. [2]. Due to the increased overall tip-leakage mass flow, this effect has no advantageous effect on the outflow angular momentum. Due to the pressure drop across the injection chamber, a position of the injection further upstream in the tip gap is shown to also have a positive effect on the reduction of pressure cross forces on the rotor. No significant impact of the injection position on the Thomas-Alford forces could be shown.

5.2 Limitations of the Model

Due to simplifications and general assumptions made when developing the model, certain effects known from literature could not be shown. Therefore these effects pose potential fields of interest for further research in the subject of passive tip-injection and its influence on the generation of aerodynamically induced cross forces in axial turbine stages.

In the model obtained in this work, no flow separation at sharp edges or contraction coefficient were considered. This effect potentially reduces the effective flow cross-sectional area at the tip gap entry edge, as well as at the leading edges of the labyrinth fins. Assuming a constant contraction coefficient, the effective tip gap width would shrink uniformly for the whole rotor under investigation. This would not lead to considerable changes in the dimensionless values calculated. However it is shown in literature [16], that the contraction coefficient depends on the tip gap width. This means, that taking into account a variable contraction coefficient for the flow over sharp edges would reduce the variety of the tip gap width of an eccentric rotor in circumferential direction. This would reduce the amplitude of the pressure and leakage mass flow rate distributions and ultimately reduce the cross forces acting on the rotor. In this sense, the cross forces shown in this work represent a conservative approach towards the tip excitation considerations.

Earlier work [9] showed, that flow separation also occurs at the upstream injection slot edge

directly before the injection mass flow enters the tip gap. This leads to a blockage of the injection channel and an undesired turning of the injection flow towards the tip gap flow direction. This negative impact on the effectiveness of the passive tip-injection could not be shown in this work, as the aerodynamic effects in the injection chamber were not modeled in detail.

The injection jet in the model developed for this work was designed to follow a straight streamline, when exiting the injection slot up to the radial position at the height of the labyrinth fin edges. No disadvantageous turning of the injection flow in axial direction was considered before it mixes with the main tip gap flow. Therefore the same advantageous conditions, otherwise found in a guided injection along an injection nozzle or labyrinth fin, were assumed for all considerations of this work.

The influence of one rotating sidewall (i.e. the rotor) and one stationary sidewall (i.e. the casing) on the flow in the streamtubes was not considered in this work. The rotation of the rotor has no influence on the tip gap flow, except on the injection velocity in circumferential direction, which is corrected for the rotational speed of the rotor. According to literature [2], the wall shear forces have a significant impact on the tip gap flow. It is further shown in literature [18], that the effect of rotation can have an disadvantageous impact on the sealing capabilities of see-through labyrinth seals.

Other factors that were not taken into consideration, but could potentially have a significant impact on the aerodynamically induced excitation cross forces for a shrouded turbine rotor with passive tip-injection are: Misalignment of the rotor relative to the casing, pressure forces on the sidewalls of the control volumes and radial inlet and outlet from the mainstream flow channel to the tip gap among others.

5.3 Recommendations for further Research

Based on the results presented in this thesis, further research could focus on the following aspects. It was shown, that passive tip-injection can reduce the cross force coefficients associated with the tip excitation of shrouded axial turbine stages. Further research could include a comprehensive rotordynamic analysis of a shrouded turbine rotor with passive tip-injection. By including the rotor shaft and the bearings with their characteristic rigidity and damping properties, actual rotor displacements and oscillations magnitudes could be accounted for. This could lead to information on whether the tip clearance can be further reduced as a result of reduced rotor vibration through the impact of passive tip-injection. This possible reduction in the nominal tip clearance could potentially have great impact on the tip-leakage behavior and the overall efficiency of the turbomachine. Further investigations could also include more detailed thermodynamics and a determination of the limit power output of the turbomachine with respect to rotordynamic instability caused by tip excitation.

The extensive possibilities and potential of computational fluid dynamics could also pose a wide field of further research on the influence of passive tip-injection on the aerodynamically induced cross force generation. A computational flow simulation of the tip gap of an eccentric turbine rotor under swirled flow conditions and under the influence of passive tip-injection could produce valuable information. Especially the flow conditions and pressure distributions in the injection chamber would be of great interest as they potentially influence the cross force generation. Further numerical investigations could also include an acoustic analysis.

The results from the proposed analytical and numerical investigations should be validated experimentally. Experiments could measure pressure and mass flow rate information for the tip gap with passive tip-injection. Earlier experiments [10] have shown the practical problems with establishing a through-blade tip-injection and realizing pressure and flow velocity measurements in a large number of positions in circumferential direction. This problem could be overcome by measuring the vibration and torque levels of an experimental turbomachine instead. Such experiments could validate the results obtained by more detailed analytical and numerical rotordynamic investigations of a shrouded turbine rotor with passive tip-injection.

Bibliography

[1] Alford, J. S.: Protecting Turbomachinery from Self-Excited Rotor Whirl. in: *ASME Journal of Engineering for Power* 87 (1965), pp. 333–343

[2] Auld, A. ; Hilfer, M. ; Hogg, S. ; Ingram, G. ; Messenger, A.: Application of an Air-Curtain Fluidic Jet Type Seal to Reduce Turbine Shroud Leakage. in: *ASME Paper GT2013-94198* (2013)

[3] Auyer, E. L.: Dynamic Sealing Arrangement for Turbomachines. in: *US Patent 2,685,429* (1954)

[4] Benoni, A.: *Einfluss von Geometrieparametern auf die Spaltverluste in axialen Turbinengittern mit passiver Einblasung*, Technische Universität Wien, PhD thesis, 2013

[5] Curtis, E. M. ; Denton, J. D. ; Longley, J. P. ; Rosic, B.: Controlling Tip Leakage Flow over a Shrouded Turbine Rotor Using an Air-Curtain. in: *ASME Paper GT2009-59411* (2009)

[6] Denton, J. D.: Loss Mechanisms in Turbomachines. in: *ASME Journal of Turbomachinery* 115 (1993), pp. 621–656

[7] Gasch, R. ; Nordmann, R. ; Pfützner, H.: *Rotordynamik*. Springer-Verlag, 2006

[8] Ghaffari, P.: *Einfluss des Schaufelkantenradius sowie der Einblasung auf den Spaltmassenstrom in axialen Turbinenbeschaufelungen*, Technische Universität Wien, Master's thesis, 2011

[9] Ghaffari, P. ; Willinger, R.: Impact of Passive Tip-Injection on the Performance of Partially Shrouded Turbines: Basic Concept and Preliminary Results. in: *ASME Paper TBTS2013-2038* (2013)

[10] Ghaffari, P. ; Willinger, R.: On the Impact of Passive Tip-Injection on the Downstream Flow Field of a Shrouded LP-Turbine: CFD and Experimental Results. in: *ASME Paper GT2016-56196* (2016)

[11] Ghaffari, P. ; Willinger, R. ; Bauinger, S. ; Marn, A.: Impact of Passive Tip-Injection on Tip-Leakage Flow in Axial Low Pressure Turbine Stage. in: *ASME Paper GT2015-42226* (2015)

[12] Grote, K. H. ; Feldhusen, J.: *Dubbel - Taschenbuch für den Maschinenbau.* Springer-Verlag, 2014

[13] Hamik, M.: *Einfluss von Ausblasung auf die Strömung in einem radialen Schaufelspalt*, Technische Universität Wien, Master's thesis, 2005

[14] Hamik, M.: *Reduktion der Spaltverluste in einem axialen Turbinegitter durch passive Einblasung*, Technische Universität Wien, PhD thesis, 2007

[15] Hogg, S. I. ; Ruiz, I. G.: Fluidic Jet Barriers for Sealing Applicaions. in: *ASME PAPER GT2011-45353* (2011)

[16] Kuhlmann, H. C.: *Strömungsmechanik.* Pearson Studium, 2007

[17] Martinez-Sanchez, M. ; Jaroux, B. ; Song, S. J. ; Yoo, S.: Measurement of Turbine Blade-Tip Rotordynamic Excitation Forces. in: *ASME Journal of Turbomachinery* 177 (1995), pp. 384–392

[18] Matthias, A.: *Das Durchflussverhalten von Labyrinthdichtungen bei unterschiedlichen Betriebsbedingungen*, Technische Universität Wien, PhD thesis, 2007

[19] Naljotov, O. ; Zitin, V.: Step of Pressure of the Steam and Gas Turbine with Universal Belt. in: *US Patent 6,632,069 B1* (2003)

[20] Neumann, K.: Zur Frage der Verwendung von Durchblickdichtungen im Dampfturbinenbau. in: *Maschinenbautechnik* 13 (1964), pp. 188–195

[21] Neumann, K.: Untersuchungen von Wellendichtungen für Dampfturbinen bei hohen Parametern. in: *Maschinenbautechnik* 15 (1966), pp. 27–31

[22] Song, S. J. ; Martinez-Sanchez, M.: Rotordynamic Forces Due to Turbine Tip Leakage: Part II - Radius Scale Effects and Experimental Verification. in: *ASME Journal of Turbomachinery* 119 (1997), pp. 704–713

[23] Thomas, H. J.: Instabile Eigenschwingungen von Turbinenläufern, angefacht durch die Spaltströmungen in Stopfbuchsen und Beschaufelungen. in: *Bull. de L.A.I.M.* 71 (1958), number 11/12, pp. 1039–1063

[24] Traupel, W.: *Thermische Turbomaschinen.* volume 1. Springer-Verlag, 1988

[25] Trutnovsky, K. ; Komotori, K.: *Berührungsfreie Dichtungen.* VDI - Verlag, 1981

[26] Turnquist, N. A. ; Bruce, K. L. ; Cerretelli, C. ; Tourigny, J. E.: Fluidic Sealing for Turbomachinery. in: *US Patent 2009/0297341 A1* (2009)

[27] Urlichs, K.: *Durch Spaltströmungen hervorgerufene Querkräfte an den Läufern thermischer Turbomaschinen*, Technische Universität München, PhD thesis, 1975

[28] Wiesche, S. aus d. ; Passmann, M. ; Willinger, R.: Reduction of Turbine Tip Leakage Losses and Excitation Forces by Passive Tip Injection. in: *ASME Paper IMECE2015-50120* (2015)

[29] Wohlrab, R.: *Experimental Determination of Gap Flow Conditioned Forces at the Rotors of Thermal Turbomachines*, Technische Universität München, PhD thesis, 1975